NORSAR

ROYAL NORWEGIAN COUNCIL FOR SCIENTIFIC AND INDUSTRIAL RESEARCH

Scientific Report No. 2-79/80

SEMIANNUAL TECHNICAL SUMMARY 1 October 1979—31 March 1980

By
A. Kr. Nilsen (ed.)

Kjeller, June 1980

SECURITY CLASSIFICATION OF THIS PAGE *(When Data Entered)*

REPORT DOCUMENTATION PAGE		READ INSTRUCTIONS BEFORE COMPLETING FORM
1. REPORT NUMBER F08606-79-C-0001	2. GOVT ACCESSION NO.	3. RECIPIENT'S CATALOG NUMBER
4. TITLE *(and Subtitle)* SEMIANNUAL TECHNICAL SUMMARY 1 October 1979 - 31 March 1980		5. TYPE OF REPORT & PERIOD COVERED 1 Oct 79 - 31 Mar 80 6. PERFORMING ORG. REPORT NUMBER Scientific Report 2-79/80
7. AUTHOR*(s)* A.Kr. Nilsen (ed.)		8. CONTRACT OR GRANT NUMBER*(s)* F08606-79-C-0001
9. PERFORMING ORGANIZATION NAME AND ADDRESS NTNF/NORSAR P.O. Box 51 N-2007 Kjeller, Norway		10. PROGRAM ELEMENT, PROJECT, TASK AREA & WORK UNIT NUMBERS NORSAR Phase 3
11. CONTROLLING OFFICE NAME AND ADDRESS		12. REPORT DATE June 1980 13. NUMBER OF PAGES
14. MONITORING AGENCY NAME & ADDRESS*(if different from Controlling Office)* VELA Seismological Center 312 Montgomery Street Alexandria, VA 22314 USA		15. SECURITY CLASS. *(of this report)* 15a. DECLASSIFICATION/DOWNGRADING SCHEDULE

16. DISTRIBUTION STATEMENT *(of this Report)*

17. DISTRIBUTION STATEMENT *(of the abstract entered in Block 20, if different from Report)*

APPROVED FOR PUBLIC RELEASE; DISTRIBUTION UNLIMITED:

18. SUPPLEMENTARY NOTES

19. KEY WORDS *(Continue on reverse side if necessary and identify by block number)*

20. ABSTRACT *(Continue on reverse side if necessary and identify by block number)*

This report describes the operation and research activities at the Norwegian Seismic Array (NORSAR) for the period from 1 October 1979 to 31 March 1980.

There has been a significant decrease in the performance of the NORSAR online DP system compared with the previous reporting period with average uptime of 83.7% compared to 95.5%. The SPS is the main trouble source accounting for 162 of the total 183 stops giving a mean-time-between-failures of 0.9 days

DD FORM 1 JAN 73 1473 EDITION OF 1 NOV 65 IS OBSOLETE

(2.5 days previous reporting period). The Event Processor operation has continued as before, the monthly bulletins have mostly been distributed in the first week of the following month. The average daily number of events is 8.9.

The array communications performance has been fair in the reporting period. Towards the end of the period 01B was used for testing of the Modcomp computer and disconnected from the Special Processing System (SPS) during the test periods. Also ARPA network communication has been satisfactory. Six institutions are now connected to the network via the NORSAR Terminal Interface Message Processor (TIP).

In October 1979 an experimental small-aperture subarray (NORESS) was set in operation in the 06C area, at first substituting the 06C short period (SP) data, and from 27 March substituting 01B Sp data. Horizontal SP seismometers were set in operation in the Long Period Vault of 06C 27 March 1980. The work with Modcomp-SPS substitution has continued during the period, and a satisfactory completion is expected in the near future. A study on a possible future computer upgrade at NORSAR has been conducted. This includes improvements specially of the detection processor and would require a modern high-capacity computer like the IBM 4341.

The research activities are summarized in eight subsections of the last chapter of this report. The first two subsections discuss research work on the small-aperture experimental subarray (NORESS), the third one deals with automatic arrival times for local and regional P and S waves. Subsection 4 describes mapping of upper mantle heterogeneities using data from local networks and ISC bulletins, and the next discusses structural complexities in ancient mountain ranges. Then follows a description of the final results of a microearthquake survey of the Svalbard region followed by seismicity evaluation of the Stiegler's Gorge area in Tanzania. The last subsection gives source parameters for the Melφy earthquakes.

AFTAC Project Authorization No.	:	VELA VT/0702/B/PMP
ARPA Order No.	:	2551
Program Code No.	:	0F10
Name of Contractor	:	Royal Norwegian Council for Scientific and Industrial Research
Effective Date of Contract	:	1 October 1978
Contract Expiration Date	:	30 September 1980
Contract No.	:	F08606-79-C-0001
Project Manager	:	Frode Ringdal (02) 71 69 15
Title of Work	:	The Norwegian Seismic Array (NORSAR) Phase 3
Amount of Contract	:	$1,233,000.-
Contract Period Covered by the Report	:	1 April - 30 September 1979

This research was supported by the Advanced Research Projects Agency of the Department of Defense and was monitored by AFTAC, Patrick AFB FL 32925, under contract no. F08606-79-C-0001.

NORSAR Contribution No. 282

TABLE OF CONTENTS

1. SUMMARY

This report describes the operation and research activities at the Norwegian Seismic Array (NORSAR) for the period from 1 October 1979 to 31 March 1980.

There has been a significant decrease in the performance of the NORSAR online DP system compared with the previous reporting period with average uptime of 83.7% compared to 95.5%. The SPS is the main trouble source accounting for 162 of the total 183 stops giving a mean-time-between-failures of 0.9 days (2.5 days previous reporting period). The Event Processor operation has continued as before, the monthly bulletins have mostly been distributed in the first week of the following month. The average daily number of events is 8.9.

The array communications performance has been fair in the reporting period. Towards the end of the period 01B was used for testing of the Modcomp computer and disconnected from the Special Processing System (SPS) during the test periods. Also ARPA network communication has been satisfactory. Six institutions are now connected to the network via the NORSAR Terminal Interface Message Processor (TIP).

In October 1979 an experimental small-aperture subarray (NORESS) was set in operation in the 06C area, at first substituting the 06C short period (SP) data, and from 27 March substituting 01B Sp data. Horizontal SP seismometers were set in operation in the Long Period Vault of 06C 27 March 1980. The work with Modcomp-SPS substitution has continued during the period, and a satisfactory completion is expected in the near future. A study on a possible future computer upgrade at NORSAR has been conducted. This includes improvements specially of the detection processor and would require a modern high-capacity computer like the IBM 4341.

The research activities are summarized in eight subsections of the last chapter of this report. The first two subsections discuss research work on the small-aperture experimental subarray (NORESS), the third one

deals with automatic arrival times for local and regional P and S waves. Subsection 4 describes mapping of upper mantle heterogeneities using data from local networks and ISC bulletins, and the next discusses structural complexities in ancient mountain ranges. Then follows a description of the final results of a microearthquake survey of the Svalbard region followed by seismicity evaluation of the Stiegler's Gorge area in Tanzania. The last subsection gives source parameters for the Meløy earthquakes.

Alf Kr. Nilsen

II. OPERATION OF ALL SYSTEMS

II.1 Detection Processor (DP) Operation

There have been 183 breaks in the otherwise continuous operation of the NORSAR Online system within the current 6 month reporting interval. This is an increase of 118 per cent in number of stops compared to last period. The DP downtime has increased with 11.6 per cent. As can be seen from Table II.1.1 most of the downtime is due to SPS problems, in fact of a downtime of 16.3 per cent the SPS alone stands for 15.4 per cent, only 0.9 per cent of the downtime is due to other reasons. Fig. II.1.1 and the accompanying Table II.1.1 both show the daily DP downtime for the days between 1 October 1979 and 31 March 1980. The monthly recording times and percentages are given in Table II.1.2.

The breaks can be grouped as follows:

a)	SPS malfunction	162
b)	Error on the multiplexor channel	5
c)	Stops related to possible program errors	0
d)	Maintenance stops	2
e)	Power jumps and breaks	4
f)	Hardware problems	6
g)	Magnetic tape and disk drive problems	0
h)	Stops related to system operation	1
i)	TOD error stops	3

The total downtime for this period was 717 hours and 7 minutes. The mean-time-between-failures (MTBF) was 0.9 days, as compared with 2.5 days of the previous reporting period.

J. Torstveit

LIST OF BREAKS IN DP PROCESSING THE LAST HALF-YEAR

DAY	START		STOP		COMMENTS
274	8	58	9	12	CE MAINTENANCE
277	2	30	3	25	SPS ERROR
278	19	11	24	0	SPS ERROR
279	0	0	10	29	SPS ERROR
280	16	8	20	22	SPS ERROR
280	22	39	24	0	SPS ERROR
281	0	0	6	51	SPS ERROR
281	7	44	8	58	SPS ERROR
283	2	23	3	17	CPU ERROR
283	21	53	24	0	SPS ERROR
284	0	0	0	9	SPS ERROR
284	0	49	14	49	SPS ERROR
288	1	40	2	40	SPS ERROR
288	11	57	12	4	SPS ERROR
288	22	43	23	16	SPS ERROR
289	10	10	10	21	SPS ERROR
291	12	6	12	24	POWER BREAK
292	7	54	8	14	MPX/LATE
297	12	13	12	20	CE MAINTENANCE
303	5	21	5	38	SPS ERROR
304	12	29	13	32	TOD ERROR
304	18	49	19	33	CPU ERROR
304	22	41	24	0	TOD ERROR
305	0	0	8	19	TOD ERROR
305	21	43	21	51	SPS ERROR
305	22	1	22	8	SPS ERROR
312	14	6	14	11	SPS ERROR
316	3	35	6	35	SPS ERROR
318	3	20	4	27	SPS ERROR
318	4	39	10	18	SPS ERROR
318	10	18	10	44	SPS ERROR
318	11	39	13	18	SPS ERROR
319	10	20	10	29	SPS ERROR
319	13	43	13	53	SPS ERROR
319	17	34	17	53	SPS ERROR
327	10	7	13	23	POWER BREAK
329	19	47	20	36	MPX/LATE
331	19	21	20	11	SPS ERROR

Table II.1.1

Breaks in DP Processing
October 1979 - March 1980

(Sheet 1 of 6)

LIST OF BREAKS IN DP PROCESSING THE LAST HALF-YEAR

DAY	START		STOP		COMMENTS
332	1	11	2	17	SPS ERROR
332	8	17	8	26	SPS ERROR
332	11	0	11	13	SPS ERROR
332	17	56	18	29	SPS ERROR
333	5	32	6	35	SPS ERROR
333	9	1	14	18	SPS ERROR
334	7	53	8	41	SPS ERROR
334	22	9	23	22	SPS ERROR
335	0	52	1	44	SPS ERROR
335	14	40	15	18	CPU ERROR
337	13	50	14	16	SPS ERROR
337	20	10	20	54	SPS ERROR
338	1	30	24	0	SPS ERROR
339	0	0	24	0	SPS ERROR
340	0	0	24	0	SPS ERROR
341	0	0	11	38	SPS ERROR
341	12	52	16	18	SPS ERROR
341	17	45	21	8	SPS ERROR
342	9	47	11	59	SPS ERROR
342	12	25	12	35	SPS ERROR
344	19	0	20	7	SPS ERROR
345	7	58	11	46	SPS ERROR
345	22	35	23	12	SPS ERROR
346	11	34	17	16	SPS ERROR
347	14	36	17	7	SPS ERROR
348	5	10	6	19	SPS ERROR
351	0	16	0	48	SPS ERROR
351	12	45	13	29	SPS ERROR
351	19	38	21	55	SPS ERROR
352	4	0	7	9	SPS ERROR
352	8	15	14	33	SPS ERROR
352	15	26	17	46	SPS ERROR
353	4	12	8	27	SPS ERROR
353	10	12	10	21	MPX/LATE
353	12	10	13	55	SPS ERROR
353	20	8	21	19	SPS ERROR
354	20	0	22	1	SPS ERROR
354	22	55	24	0	SPS ERROR

Table II.1.1

Breaks in DP Processing
October 1979 - March 1980

(Sheet 2 of 6)

LIST OF BREAKS IN DP PROCESSING THE LAST HALF-YEAR

DAY	START		STOP		COMMENTS
355	0	0	24	0	SPS ERROR
355	0	0	10	15	SPS ERROR
356	12	4	15	13	SPS ERROR
356	15	33	24	0	SPS ERROR
357	0	0	13	52	SPS ERROR
357	14	12	14	31	SPS ERROR
357	14	57	24	0	SPS ERROR
358	0	0	12	4	SPS ERROR
358	12	54	13	28	SPS ERROR
358	20	54	24	0	SPS ERROR
359	0	0	12	55	SPS ERROR
359	19	35	24	0	SPS ERROR
360	0	0	17	38	SPS ERROR
360	20	19	24	0	SPS ERROR
361	0	0	17	48	SPS ERROR
363	5	40	6	55	SPS ERROR
363	14	14	14	49	SPS ERROR
363	23	11	24	0	SPS ERROR
364	0	0	0	55	SPS ERROR
364	3	15	13	46	SPS ERROR
364	23	22	24	0	SPS ERROR
365	0	0	0	35	SPS ERROR
365	3	53	13	56	SPS ERROR
1	0	0	0	29	NEW YEAR
1	12	8	13	24	SPS ERROR
1	14	37	16	23	SPS ERROR
1	18	2	19	41	SPS ERROR
1	21	18	24	0	SPS ERROR
2	0	0	16	17	SPS ERROR
2	21	18	24	0	SPS ERROR
3	0	0	9	6	SPS ERROR
3	11	39	18	26	SPS ERROR
3	19	6	19	46	SPS ERROR
3	21	23	21	46	SPS ERROR
4	9	3	13	34	SPS ERROR
4	14	30	14	36	SPS ERROR
4	15	32	17	27	SPS ERROR
5	18	59	24	0	SPS ERROR

Table II.1.1

Breaks in DP Processing
October 1979 - March 1980

(Sheet 3 of 6)

LIST OF BREAKS IN DP PROCESSING THE LAST HALF-YEAR

DAY	START		STOP		COMMENTS
6	0	0	0	30	SPS ERROR
6	4	41	8	29	SPS ERROR
6	20	40	22	14	SPS ERROR
7	4	4	16	3	SPS ERROR
8	7	48	14	8	SPS ERROR
8	15	15	17	33	SPS ERROR
8	21	27	22	10	SPS ERROR
8	22	52	24	0	SPS ERROR
9	0	0	7	19	SPS ERROR
13	1	45	2	24	SPS ERROR
13	8	0	8	38	SPS ERROR
14	10	35	11	0	POWER BREAK
14	12	22	13	17	SPS ERROR
14	15	32	17	14	SPS ERROR
15	11	16	13	0	SPS ERROR
16	5	38	7	0	SPS ERROR
17	13	47	14	2	SPS ERROR
17	20	49	24	0	SPS ERROR
18	0	0	8	1	SPS ERROR
18	9	28	12	2	SPS ERROR
19	1	29	11	8	SPS ERROR
19	18	36	22	2	SPS ERROR
20	9	20	11	22	SPS ERROR
21	3	34	7	44	SPS ERROR
21	12	50	14	30	CPU ERROR
22	9	42	12	26	SPS ERROR
23	17	7	19	43	SPS ERROR
25	8	35	10	15	SPS ERROR
27	8	41	9	46	SPS ERROR
27	14	26	15	1	SPS ERROR
27	21	33	22	32	SPS ERROR
30	9	39	10	8	SPS ERROR
30	11	5	12	45	SPS ERROR
31	22	30	23	19	SPS ERROR
32	18	58	20	16	SPS ERROR
33	1	55	3	41	SPS ERROR
33	4	42	10	16	SPS ERROR
33	14	46	16	35	SPS ERROR

Table II.1.1

Breaks in DP Processing
October 1979 - March 1980

(Sheet 4 of 6)

LIST OF BREAKS IN DP PROCESSING THE LAST HALF-YEAR

DAY	START		STOP		COMMENTS
34	5	37	8	58	SPS ERROR
34	9	12	15	39	SPS ERROR
34	20	2	20	43	SPS ERROR
35	0	53	13	25	SPS ERROR
35	22	56	23	35	SPS ERROR
37	1	47	7	30	SPS ERROR
40	12	42	13	21	SPS ERROR
42	8	57	9	41	POWER BREAK
43	9	38	9	46	SPS ERROR
44	11	44	16	11	SPS ERROR
46	4	34	6	5	SPS ERROR
46	21	51	24	0	SPS ERROR
47	0	0	24	0	SPS ERROR
48	0	0	20	31	SPS ERROR
48	21	56	24	0	SPS ERROR
49	0	0	9	2	SPS ERROR
51	1	1	3	4	SPS ERROR
51	22	1	22	49	SPS ERROR
52	7	44	10	55	SPS ERROR
53	0	17	1	40	SPS ERROR
53	8	33	10	9	SPS ERROR
53	11	44	11	49	MPX/LATE
54	4	56	6	15	SPS ERROR
54	10	7	10	43	SPS ERROR
59	19	36	20	52	SPS ERROR
61	8	50	11	9	SPS ERROR
61	23	58	24	0	SPS ERROR
62	0	0	1	28	SPS ERROR
62	18	9	24	0	CPU POWER PROB_EM
63	0	0	14	44	CPU POWER PROB_EM
64	10	21	10	29	SPS ERROR
64	12	18	12	35	SPS ERROR
66	10	1	16	32	SPS ERROR
67	17	49	18	37	SPS ERROR
67	18	48	20	0	SPS ERROR
69	17	50	18	28	SPS ERROR
70	7	37	7	45	SPS ERROR
70	18	6	22	48	SPS ERROR

Table II.1.1

Breaks in DP Processing
October 1979 - March 1980

(Sheet 5 of 6)

LIST OF BREAKS IN DP PROCESSING THE LAST HALF-YEAR

DAY	START		STOP		COMMENTS
72	12	15	12	28	SPS ERROR
72	13	9	13	38	SPS ERROR
73	2	22	4	45	SPS ERROR
73	16	53	18	25	SPS ERROR
73	23	12	24	0	SPS ERROR
74	0	0	1	42	SPS ERROR
74	13	7	13	13	SPS ERROR
74	13	37	14	17	SPS ERROR
74	20	25	24	0	SPS ERROR
75	0	0	2	56	SPS ERROR
75	4	35	12	54	SPS ERROR
77	15	5	16	42	SPS ERROR
78	21	15	21	53	SPS ERROR
78	22	1	22	9	SPS ERROR
79	5	43	6	49	SPS ERROR
79	12	20	12	28	SPS ERROR
84	10	23	10	31	SPS ERROR
85	8	18	8	22	MPX/ LATE
88	8	48	8	55	SPS ERROR
89	18	5	19	27	SPS ERROR

*** NUMBER OF BREAKS = 180
*** MEAN TIME BETW. FAILURES = 0.8 DAYS
*** NUMBER OF UPTIME INTERVALS = 181

Table II.1.1

Breaks in DP Processing
October 1979 - March 1980

(Sheet 6 of 6)

Month	DP Uptime (Hrs)	DP Uptime (%)	No. of DP Breaks	No. of Days with Breaks	DP MTBF* (days)
Oct	690.74	92.8	20	15	1.4
Nov	683.58	94.9	23	11	1.2
Dec	444.73	59.8	41	28	0.5
Jan	599.02	80.5	44	24	0.6
Feb	577.63	83.0	26	19	0.9
Mar	679.18	91.3	29	20	0.9
Total Period	3674.88	83.7	183	117	0.9

* Mean-time-between-failures = (Total uptime/No. of Up Intervals)

Table II.1.2

Online System Performance

October 1979 - March 1980

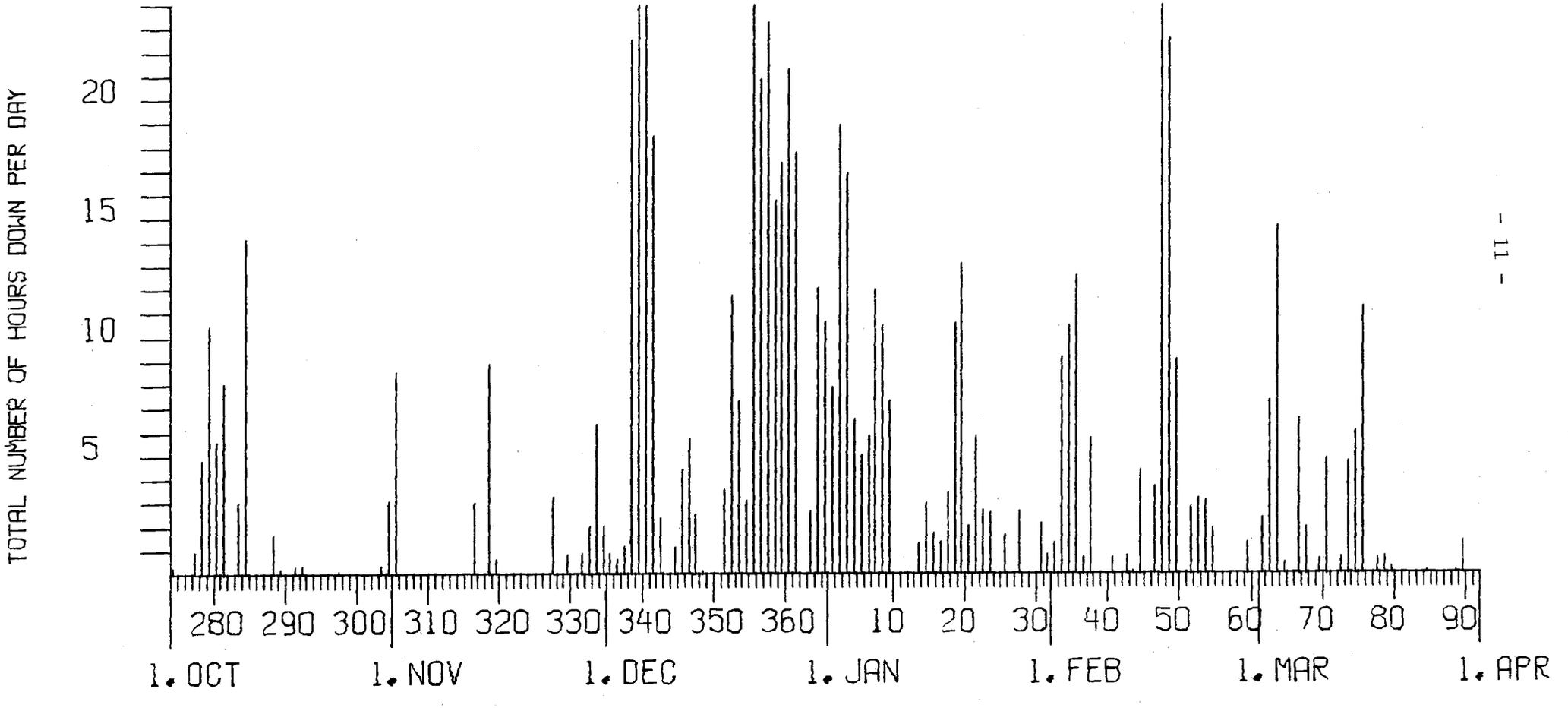

Fig. II.1.1 Detection Processor Downtime in the period September 1979 - March 1980.

II.2 Event Processor Operation

The Event Processor has been operated as before, and 4 of the 6 monthly bulletins in this reporting period were published in the first week of the next month. Some monthly statistics are presented in Table II.2.1.

	Teleseismic	Core Phases	Sum	Daily
Oct 1979	212	62	274	8.8
Nov 1979	214	58	272	9.1
Dec 1979	136	25	161	5.2
Jan 1980	239	26	265	8.5
Feb 1980	295	72	367	12.7
Mar 1980	238	58	296	9.5
	1334	301	1635	8.9

Table II.2.1

H. Bungum

II.3 NORSAR Data Processing Center (NDPC) Operation

Data Center

But for the numerous failures on the SPS which caused a lot of extra work in nights and weekends, the operation has been running smoothly. However, we still have a couple of students running jobs outside of office hours. They have both been at NORSAR for some time gaining experience, so also that part of the operation is going without serious problems.

J. Torstveit

II.4 Array Communication

General

In December 1979 and the first week of January 1980 our Special Processing System (SPS) was down most of the time and therefore we have no statistics pertaining to the subarray communications for these periods.

02C has frequently been infested with errors in the data stream toward the CTV. Although repaired quite a few times, the cable between Lillehammer and Hornsjø is most certainly the cause. Error rate is relatively low, and therefore data is not significantly affected.

Outages of long duration on individual subarrays have been caused by broken cables (by accident or prescheduled work, power or line trouble).

02B (faulty splicing after reorganization of Hamar Telestation, week 42, 43)
03C (prescheduled work, week 8)
02C (line failure, week 45) and power failure (week 48)
03C (week 52)
02B (week 52, resumed operation 10 Jan 80)

In connection with efforts to phase the Universal Communications subsystem of the Modcomp processor into the NORSAR system (in connection with SPS replacement) 01B (and partly 06C) communication circuits have rather frequently been routed to this computer.

On 27 March, 01B communication circuit was disconnected at Hamar. From the same day routing of data from an Experimental Subarray at 06C has taken place on the 01B circuit from Hamar to Kjeller (the new Experimental Subarray utilizes the 01B ID, and has its own data line from 06C).

Simultaneous Communication Outages, where groups or all subarrays have been affected

In the period thirty-four outages were observed.

October 79	4 outages (lasting 1-2 16-min periods)
November 79	None observed
December 79	SPS down therefore no observations
January 80	15 outages (lasting 1 to 9 consecutive 16-min. periods)
February 80	8 outages (lasting from 1 to 4 consecutive 16-min. periods)
March 80	7 outages (lasting from 1 to 5 consecutive 16-min. periods)

Individually affected communications circuits

Week/ Year	Subarray/Per cent outage						
	01A	01B	02B	02C	03C	04C	06C
40/79		20.5		5.0			2.8
41/79							14.5
42/79			89.2				
43/79			13.4		0.9		
44/79			1.2				
45/79			16.7				
47/79		0.6					
48/79				21.9			
2/80						0.5	
5/80				0.4			
6/80							1.6
7/80	0.9	3.2					
8/80				0.4	3.0		0.6
10/80		4.7					
11/80		72.7					0.9
13/80		44.0		0.9			4.0

TABLE II.4.1

Individual subarray outages. Figures in per cent of total time.

As previously mentioned in this report the majority of the outages have been caused by cables, either broken by accident or cut in connection with prescheduled work (Norwegian Telegraph Administration). Other reasons have been power failure and line trouble. The high figures pertaining to 01B must be seen in connection with routing of this circuit to the Modcomp Computer instead of the SPS.

SA	OCT (5) (1.10-4.11)		NOV (4) (5.11-2.12)		DEC (4) (3-31.12.79)		JAN (4) (7.1-3.2.80)		FEB (4) (4.2-2.3)		MAR (4) (3-30.3)		AVERAGE 5 Months	
	>20	>200	>20	>200	>20	>200	>20	>200	>20	>200	>20	>200	>20	>200
01A	0.2	0.1	-	-			0.5	0.9	0.3	0.4	0.1	0.5	0.2	0.4
01B	0.2	4.2	-	0.2			0.5	0.9	0.2	1.1	0.1	21.8	0.2	5.6
02B	2.8	21.2	-	4.3			0.8	4.9	0.2	0.3	0.3	0.6	0.8	6.3
02C	7.4	0.4	9.8	5.6			10.0	1.0	0.2	0.2	4.3	0.6	6.3	1.6
03C	0.2	0.3	-	-			0.5	0.9	0.2	1.0	0.1	0.5	0.2	0.5
04C	0.2	-	-	-			0.5	1.1	0.3	0.3	0.2	0.5	0.2	0.4
06C	0.1	3.4	-	-			0.4	0.9	0.1	1.3	-	1.7	0.1	1.5
AVER	1.6	4.2	1.4	1.4			1.9	1.5	0.2	0.7	0.7	6.6	1.1	2.3
LESS	02B 02C	01B 02B 02C	02C	02B 02C			02C	02B			02C	01B	02C	01B 02B 02C
	0.2	0.2	0.0	0.0			0.5	1.0			0.1	0.7	0.3	0.7

TABLE II.4.2

Communications (degraded performance >20/outages >200)
Figures in per cent of total time
Month four or five weeks, as indicated.

The ARPA subnetwork

The London communication circuit was disconnected week 40 and operation terminated.

The SDAC circuit

Reliable performance throughout the period. 24 October NCC reported our system isolated from the remaining network. Wanted line/modem checks. Also in January (11, 15, 16 and 17) our system was isolated due to cable work in the Kjeller area.

The Terminal Interface Message Processor (TIP)

Apart from a couple of restarts (29 Jan, 4 Feb), reliable performance. Preventive maintenance (PM) has been carried out.

TIP connections

The Central Institute for Industrial Research (SI) is now connected to TIP port 56 via 300 baud modems.

The following ports are now used:

Port 3	Dynasonic 390	NORSAR	(300 baud)
Port 4	Tele-Fec NFPA type2	NDRE	(300 baud)
Port 6	Tektronix	NORSAR	(300 baud)
Port 40	Terminet 300	NDRE	(300 baud)
Port 41	TI silent 700	NDRE	(300 baud)
Port 42	NEL spinwriter	NDRE	(300 baud)
Port 50	Tektronix	Univ. Olso	(300 baud)
Port 52	Display	NTA Research Institute (TF)	(300 baud)
Port 55	TI silent 700	Norsk Regne-sentral (NR)	(300 baud)
Port 56	TI Silent 700	SI	(300 baud)

III. IMPROVEMENTS AND MODIFICATIONS

III.1 NORSAR On-Line System

Fig. III.1.1 gives a schematic overview of the current NORSAR on-line computer configuration. No changes have been effected in the on-line system in the reporting period.

III.2 NORSAR Event Processor

No changes have been effected in the reporting period. Implementation of event processing on the new IBM 4331 research computer system, which has been funded by NTNF, is being investigated. Fig. III.2.1 gives an overview of the IBM 4331 processor and the associated peripheral equipment. Among the main features of this system, we mention

- Eight interactive terminals
- Large disk capacity (2000 Mbytes)
- Two Tektronix interactive graphics subsystems
- Shared peripherals with the IBM S/360 A and B computers
- Hardware and software compatibility with IBM S/360.

The system is intended to be used for research purposes only.

F. Ringdal

III.3 Array Instrumentation and Facilities

As of 16 October 1979 an experimental small subarray (NORESS - NORSAR Experimental Small-Aperture Subarray) in the area of subarray 06C (see Fig. III.3.1) was set in operation, replacing the SP data channels of 06C with the exception of channel 02, which is common for both subarrays (from 27 October with 8 Hz low pass filters on all SP channels). From 27 March 1980 NORESS data substituted the SP channels at 01B. An additional SLEM was connected to a new communication line from 06C CTV to Hamar and connected to the 01B line from Hamar to NDPC. No data is received from 01B from that time. The normal subarray 06C data was then transmitted on the 06C communication line with the exception of 06C02 and 04 which are used for horizontal NS and EW components using Geotech S-13 seismometers installed in the LPV. The vertical component is transmitted on NORESS 02 (standard HS-10 seismometer). The frequency response of the

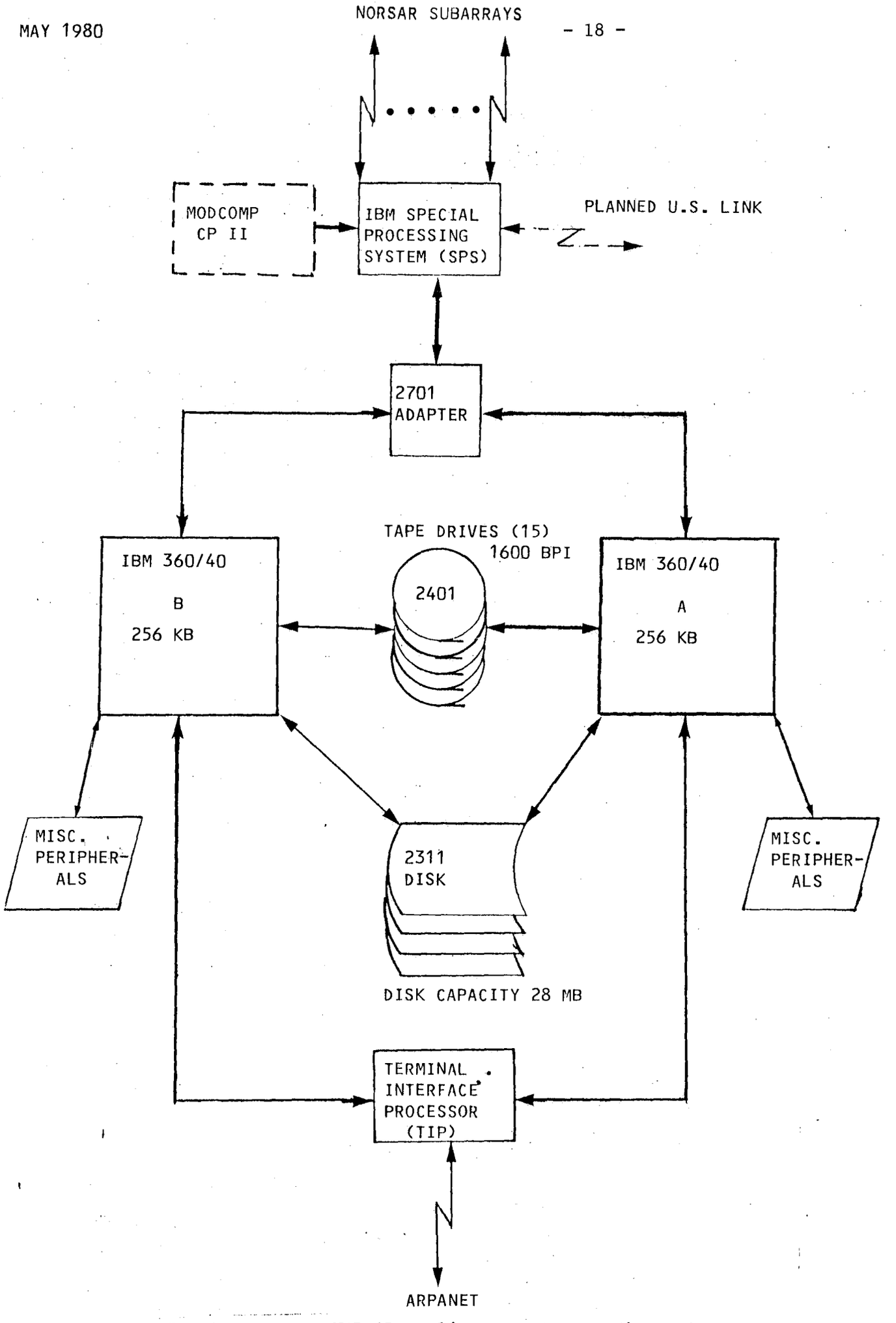

Fig. III.1.1 Current NORSAR on-line computer configuration.

NORSAR - IBM 4331 PROCESSOR

Installed April 1980

Cost: $400 000 - Funded by NTNF

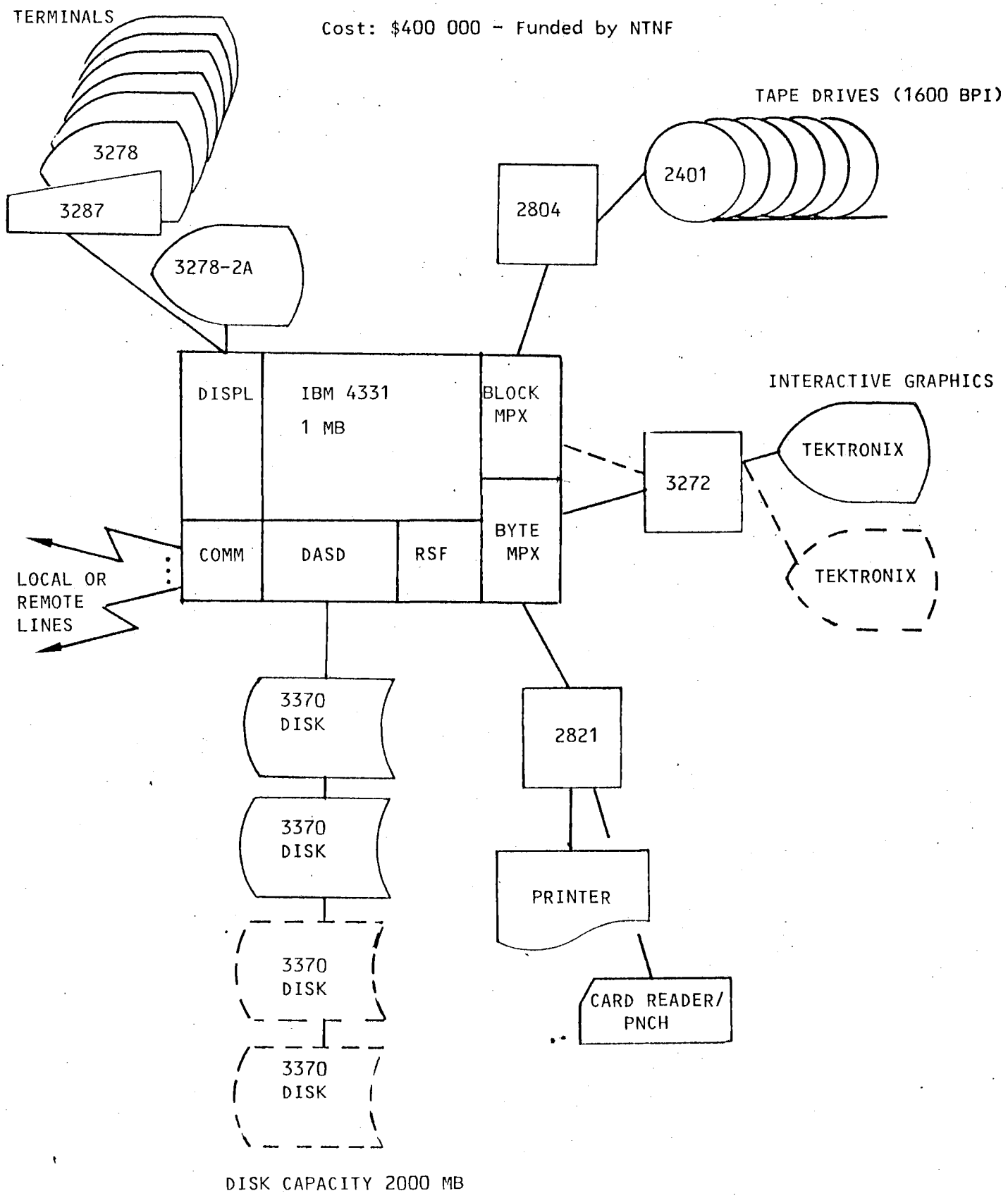

Fig. III.2.1 The IBM 4331 research computer system at NORSAR.

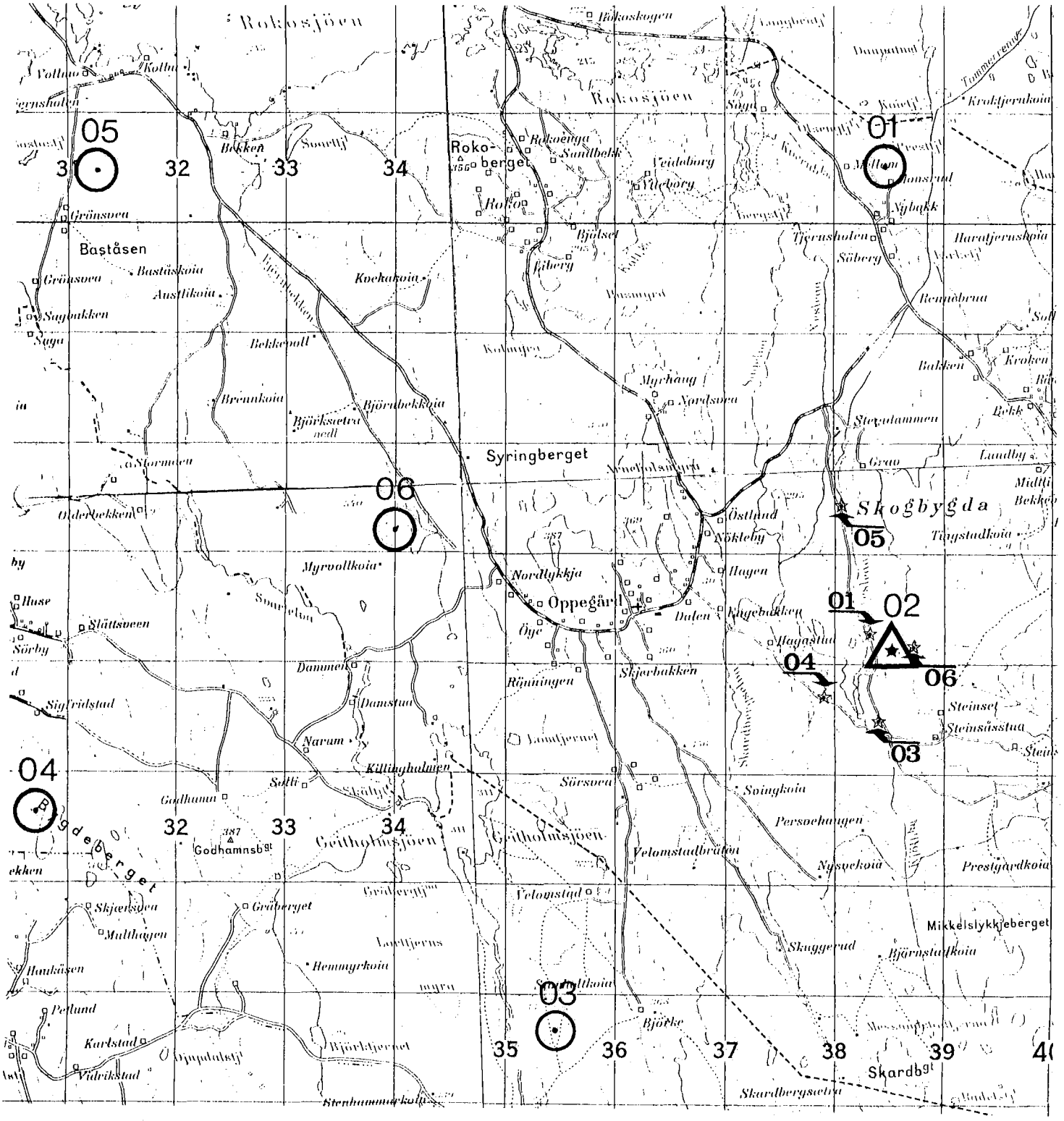

Fig. III.3.1 Configuration of subarray 06C including the experimental small subarray (NORESS - NORSAR Experimental Small-Aperture Subarray) marked with arrows. 06C02 (LPV) and NORESS 02 are common. In operation from 16 October 1979, substituting subarray 06C. From 27 March 1980 both subarrays are in operation, NORESS substituting 01B data.

S-13 horizontal seismometer is shown in Fig. III.3.2 and the corresponding numbers in Table III.3.1.

Frequency Hz	Channel Output QU peak-to-peak	Equivalent Earth Motion PM peak-to-peak	Channel Resolution PM/QU
0.2	1890	10000000	5291
0.3	2870	4444444	1549
0.4	3770	2500000	663
0.5	4590	1600000	349
0.6	5460	1111111	205
0.7	6070	816327	134
0.8	6390	625000	97.8
0.9	6720	493827	73.5
1.0	6800	400000	58.8
1.1	6720	330579	49.2
1.2	6560	277777	42.3
1.5	5900	177777	30.1
2.0	4920	100000	20.3
3.0	3110	44444	14.3
4.0	2300	25000	10.9
4.5	1970	19753	10.0
4.75	1470	17728	12.1
5.00	1150	16000	13.9

Table III.3.1

Frequency Response for the Horizontal Channels

Geotech S-13 Seismometer with standard coil, natural frequency 1.0 Hz and damping ratio 0.7.

Texas Instruments RA-5 amplifier gain 74.6 dB.

Line Terminating Amplifier low-pass filter with upper 3 dB point at 4.75 Hz.

Equivalent earth motion in picometers:

$$y = \frac{G_c \cdot i \cdot 10^{12}}{4\pi^2 \cdot f^2 \cdot m} \quad \text{where}$$

y = equivalent earth motion in picometers, peak-to-peak
G = calibration coil motor constant, newtons/ampere
i = current through the calibration coil, amperes peak-to-peak
f = frequency of calibration signal
m = weight of seismometer mass in kilograms

Channel resolution: $\frac{\text{Equivalent earth motion in picometers (PM)}}{\text{Quantum Units (QU) peak-to-peak at channel output}}$

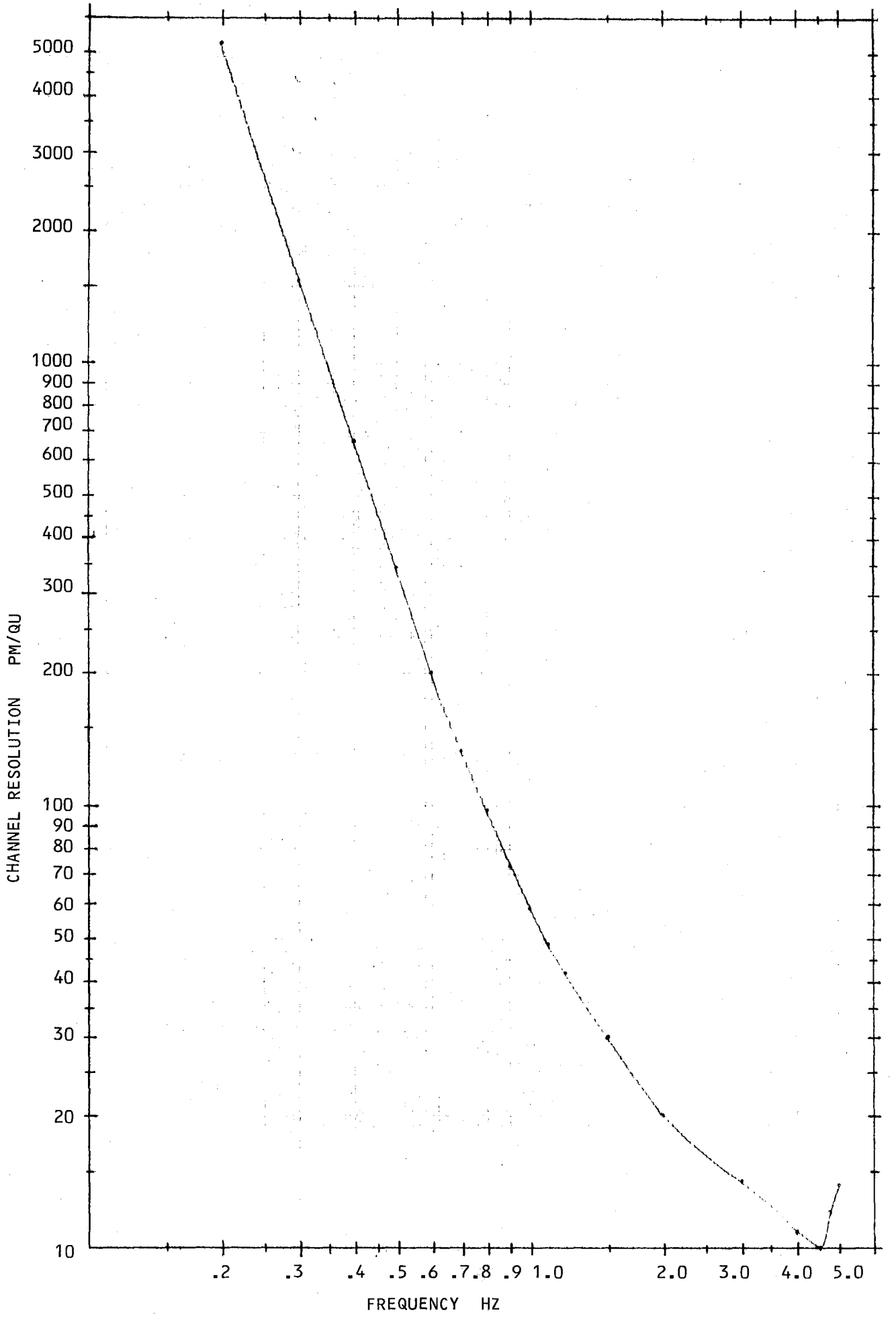

Fig. III.3.2 Frequency response of horizontal S-13 seismometers at 06C LPV with NORSAR standard seismometer and line termination amplifiers, 27 March 1980.

For the purpose of giving an easy overview of the NORSAR SP channel status at various points in time, a table is enclosed (Table III.3.2) summarizing the temporary changes in the array configuration that have been effected since 1 October 1976.

A.Kr. Nilsen

III.4 SPS Substitution

By the end of the reporting period, status on the MODCOMP interface was as follows:

- Data received by MODCOMP can be continuously read by IBM 360/40 and stored on magnetic tape in a backup mode. This transmission is now almost error-free, and it appears that the remaining problems are relatively minor ones.
- Two-way communication between MODCOMP and IBM 360/40 is still not satisfactory, but has been achieved in a test mode.
- The 230.4 kbps link between the two computers (via the 2701 unit) shows high reliability.
- The filtering and subarray beamforming tasks of the MODCOMP have been programmed and tested off-line, but will need some further refinement in order to be performed in real time. The reason is that the CPU load is fairly tight, so that optimizing of some of the time-critical code will be necessary.

A very intensive effort is now being undertaken to complete the MODCOMP development.

III.5 Future NORSAR Data Processing Center

A further study on a possible future computer upgrade at NORSAR has been conducted in the reporting period. This upgrade would address the on-line recording system, and would complement the recent NTNF-financed upgrade of the research computer at NORSAR.

STATUS OF NORSAR SP INSTRUMENTS RECORDED ON DATA TAPE

Subarray (Normally)	Instrument no. within SA	Channel no. on NORSAR data tape	Date and Time of Change									
			76/10/01	76/10/28	77/11/07 (Approx.)	78/03/15	78/04/05	78/04/12	79/08/28	79/10/16	79/10/23	80/03/27
01A (1)	1	1	Normal	-	-	-	S-13 (V)	-	-	-	-	-
	2	2	Normal	-	-	-	S-13 (NS)	-	-	-	-	-
	3	3	Normal	-	-	-	S-13 (EW)	-	-	-	-	-
	4	4	Normal	01A06 (30 dB down)	-	-	-	-	-	-	-	-
	5	5	Normal	-	-	-	-	-	-	-	-	-
	6	6	Normal	-	8 Hz filter (11/07)	-	-	-	-	-	Normal	-
01B (2)	1	7	Normal	-	-	-	-	-	-	-	-	NORESS(1) 8 Hz
	2	8	Normal	-	-	-	-	-	-	-	-	NORESS(2) 8 Hz
	3	9	Normal	-	-	-	-	-	-	-	-	NORESS(3) 8 Hz
	4	10	Normal	-	-	-	-	-	-	-	-	NORESS(4) 8 Hz
	5	11	Normal	-	-	-	-	-	-	-	-	NORESS(5) 8 Hz
	6	12	Normal	-	-	-	-	-	-	-	-	NORESS(6) 8 Hz
02B (3)	1	13	Normal	-	-	-	-	-	-	-	-	-
	2	14	Normal	-	-	-	-	-	-	-	-	-
	3	15	Normal	-	-	-	-	-	-	-	-	-
	4	16	Normal	-	-	-	-	-	-	-	-	-
	5	17	Normal	-	-	-	-	-	-	-	-	-
	6	18	Normal	-	8 Hz filter (11/07)	-	-	-	-	-	Normal	-
02C (4)	1	19	Normal	-	-	-	-	-	-	-	-	-
	2	20	Normal	-	-	-	-	-	-	-	-	-
	3	21	Normal	-	-	-	-	-	-	-	-	-
	4	22	Normal	-	-	-	-	-	-	-	-	-
	5	23	Normal	-	-	-	-	-	-	-	-	-
	6	24	Normal	-	8 Hz filter (11/03)	-	-	-	-	-	Normal	-

Table III.3.2 (page 1)

STATUS OF NORSAR SP INSTRUMENTS RECORDED ON DATA TAPE

Subarray (Normally)	Instrument no. within SA	Channel no. on NORSAR data tape	Date and Time of Change									
			76/10/01	76/10/28	77/11/07 (Approx.)	78/03/15	78/04/05	78/04/12	79/08/28	79/10/16	79/10/23	80/03/27
03C (5)	1	25	Normal	-	-	-	-	-	-	-	-	-
	2	26	Normal	-	-	-	-	-	-	-	-	-
	3	27	Normal	-	-	-	-	-	-	-	-	-
	4	28	Normal	-	-	-	-	-	-	-	-	-
	5	29	Normal	-	-	-	-	-	-	-	-	-
	6	30	Normal	-	-	-	-	-	-	-	-	-
04C (6)	1	31	Normal	-	-	-	-	-	-	-	-	-
	2	32	Normal	-	-	-	-	-	-	-	-	-
	3	33	Normal	-	-	-	-	-	-	-	-	-
	4	34	Normal	-	-	-	-	-	-	-	-	-
	5	35	Normal	-	-	-	-	-	-	-	-	-
	6	36	Normal	-	8 Hz filter (11/04)	-	-	-	-	-	Normal	-
06C (7)	1	37	Normal	-	-	-	-	-	-	NORESS(1)	8 Hz filter	Normal
	2	38	Normal	-	-	S-500 (8 Hz)	-	HS-10 (8 Hz)	Normal	Normal	8 Hz filter	06C02 NS
	3	39	Normal	-	-	-	-	-	-	NORESS(3)	8 Hz filter	Normal
	4	40	Normal	-	-	-	-	-	-	NORESS(4)	8 Hz filter	06C02 EW
	5	41	Normal	-	-	-	-	-	-	NORESS(5)	8 Hz filter	Normal
	6	42	Normal	-	8 Hz filter (11/03)	Normal	-	-	8 Hz filter	NORESS(6)	8 Hz filter	Normal

NOTE:
1) 'Normal' means standard HS/10, vertical, 4.75 Hz analog filter
2) ' - ' indicates no change from preceding status.
3) For information on NORESS (NORSAR small-aperture experimental subarray) we refer to the NORSAR Semi-annual report.

Table III.3.2 (page 2)

In our view, the basic requirements for a detection processor upgrade should be:

A. Capability for improved signal detection

- Implementation of new experimental detection algorithms
- Deploying additional beams steered to areas of special interest
- Optimizing bandpass filter selection on a regional basis
- Expanding and refining the on-line event processor (OEP) algorithms.

B. Extended data base support

- Obtaining sufficient on-line disk storage to retain an on-line buffer at any point in time covering
  - i) The last recorded 24 hours of raw data (~ 250 megabytes)
  - ii) The last 6 months of EPX files (about 5000 EPX executions) (~ 40 megabytes)
  - iii) The last 1 year of detection files (~ 2 megabytes)
  - iv) Complete raw data for the last 500 EPX executions (approximately 14 days) (~ 140 megabytes).
- Include on-line data obtained through exchange with other observatories
- Arrange for easy retrieval of all on-line data via Arpanet or other remote lines. No operator intervention at NORSAR should be required.
- If desired, establish the computer as a host computer within the Arpanet.

C. Improved research capabilities

- Support of an experimental on-line regional event detector based on high-resolution analysis of data from a closely spaced array
- Sufficient capacity for other large-scale research projects, related to real-time processing
- Obtain the capability to conduct off-line processing of very large data bases.

After looking carefully at various alternatives, we have now concluded that the best solution would be to replace the two S/360 Mod 40 computers with a new IBM compatible computer, which should have the capacity at least equivalent to an IBM 4341 processor. The main reason for staying with IBM compatible equipment would be to maintain hardware and software compatibility with the current system, and thereby ease system conversion. Moreover, with such a solution sharing of peripherals with the IBM 4331 would eliminate the need for purchasing costly new disk and tape drives.

In Fig. III.5.1 we give a schematic overview over how an upgraded NORSAR Data Processing Center could be configured. The cost of acquiring the necessary hardware has been estimated at approximately $400,000.

With respect to the time frame the equipment could be acquired during 1981 (based on information from the manufacturer). Complete software conversion would take approximately 1 year.

Note that the above cost estimate of $400,000 assumes data recording on 1600 bpi tapes as is presently done. It is desirable at some later date to upgrade the tape drives to 6250 bpi. This will reduce the size of the tape library at NORSAR and moreover make possible indefinite retention of all recorded data.

F. Ringdal

Approximate cost:

$400 000

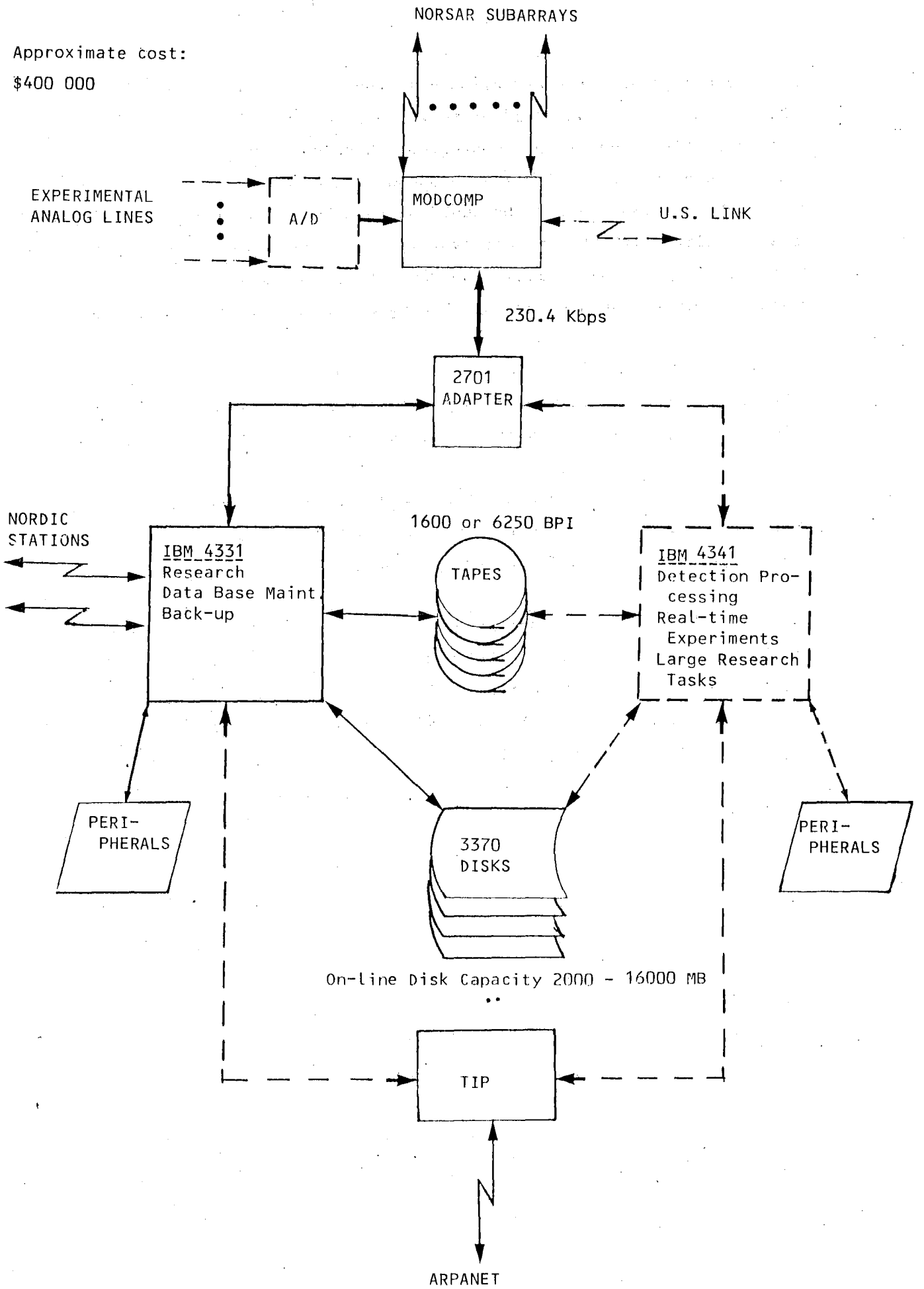

Fig. III.5.1 Suggested future NORSAR computer configuration.

IV. FIELD MAINTENANCE ACTIVITY

The maintenance activity at the subarrays has been low in the period, and the array instrumentation operation has been stable and satisfactory. There have been no major corrective or preventive projects during the period, but considerable time was spent on special projects and experiments.

Maintenance Visits

Table IV.1 shows the number of visits to the subarrays in the period. The average number of visits to each subarray is 3.7, except 06C: 1.5 visists, which is close to the same number as during the same period last year (1.7 times). The large number of visits to 06C is due to the establishment of the NORESS experimental subarray.

Subarrays	01A	01B	02B	02C	03C	04C	06C	Total
No. of Visits	2	1	2	1	2	1	17	26

Table IV.1

Number of visits to the NORSAR subarrays including NORESS in the period 1 Oct 79 - 31 Mar 80

Preventive Maintenance Projects

The preventive maintenance work in the array is described in Table IV.2. The adjustments are corrections of characteristics within the tolerance limits.

Unit	Action		No. of Actions
Seismometer	MP adjust (in field)		4
Line Terminator Amplifier	Adjustment of DC offset	SP	4
	Adjustment of channel gain	SP	6
	Adjustment of channel gain	LP	2
Emergency Power	Battery and charger check		6

Table IV.2

Preventive maintenance work in the period 1 Oct 79 - 31 Mar 80

Disclosed Malfunctions on Instrumentation and Electronics

Table IV.3 shows the number of accomplished adjustments and replacements of field equipment in the array with the exception of those mentioned in Table IV.2. There has been one power line fault requiring action by the field crew.

Unit	Characteristics	SP		LP	
		Repl.	Adj.	Repl.	Adj.
Seismometer	MP/FP (At NDPC)				57
	MP (in field)				1
	Damping				2
Seism. Amplifier RA-5/Ithaco	Distortion			1	
Line Termination Amplifier	Channel gain		1		
	Ripple	1			
	DCO		3		
	CMR		1		
	TC	1			
	8 Hz filter replacement	4			
SLEM	Test generator	1			
	RSA/ADC		3		
	Mux card	1			

Table IV.3

Total number of required adjustments and replacements in the NORSAR data channels and SLEM electronics in the period 1 Oct 79 to 31 Mar 80

Array Status

The status of the array instrumentation characteristics is close to normal with little change from previous periods. As of 31 March 1980 there are three channels with out-of-tolerance conditions (01A 02,03 and 02B NS). Channels with nonstandard conditions are:

01A	04	Attenuated 30 dB	01A 06	data
01B	01-06	Used for NORESS data		
	LP	Down, disconnected		
06C	02	NS SP horizontal		
	04	EW -"-		

A.Kr. Nilsen

ABBREVIATIONS

ADC	-	Analog-to-digital converter
CMR	-	Common mode rejection
CTV	-	Central Terminal Vault
DC	-	Direct current
DCO	-	Direct current offset
FP	-	Free period
LP	-	Long period
MP	-	Mass position
NDPC	-	NORSAR Data Processing Center
NORESS	-	NORSAR Experimental Small-Aperture Subarray
RSA	-	Range switching amplifier
SLEM	-	Seismic short and long period electronics module
SP	-	Short period
TC	-	Time constant

V. DOCUMENTATION DEVELOPED

Bungum, H., and Y. Kristoffersen (1979): A microearthquake study of the Svalbard Region, NORSAR Tech. Rep. No. 1/79.

Bungum, H., and F. Ringdal (1979): Stiegler's Gorge Power Project. Reevaluation of the seismic risk analysis, Phase I, NORSAR Tech. Rep. 2/79, NTNF/NORSAR, Kjeller, Norway.

Bungum, H., S. Pirhonen and E.S. Husebye (1980): Crustal thicknesses in Fennoscandia, Geophys. J.R. astr. Soc., in press.

Gjøystdal, H. (ed.) (1979): Semiannual Technical Summary, 1 April - 30 September 1979, NORSAR Scientific Report 1-79/80, NTNF/NORSAR Kjeller, Norway.

Husebye, E.S., and H. Bungum (1980): New crustal thicknesses for Fennoscandia, Geol. Fören Stockholm Förh., in press.

Nilsen, A.Kr. (1979): Operation Checklist for Stiegler's Gorge Seismic Network, NORSAR Internal Rep. 1-79/80, NTNF/NORSAR, Kjeller, Norway.

VI. SUMMARY OF TECHNICAL REPORTS/PAPERS PREPARED

VI.1 An Experimental Small Subarray within the NORSAR array: Crustal Phase Velocities and Azimuths from Local and Regional Events

In October 1979, NORSAR subarray 06C was modified to a small aperture array - NORESS - with station distances in the range 125 - 2051 m. Fig. VI.1.1 gives the former and present configuration of 06C. All six sensors are now equipped with 8 Hz lowpass filters.

The purpose of the NORESS experiment is to obtain data from closely spaced sensors in order to

- Investigate noise and signal coherencies at high frequencies
- Identify P, S and Lg phases from regional seismic events
- Detect and locate regional events.

The first two items above are the subject of this contribution.

Fig. VI.1.2 shows a map of seismic events in Fennoscandia that occurred during the first half year of operation of the experimental array. These events are located by the regional seismic network with typical location uncertainties of 10-30 km.

Both signal and noise coherencies have been evaluated for the 'new' array. An example of how the records of NORESS compare with those of an ordinary subarray at NORSAR is given in Fig. VI.1.3. For this Lg phase the waveform changes rather drastically from sensor to sensor within a 'normal' NORSAR subarray (6 top traces from subarray 02B) with a diameter about 10 km and typical sensor spacings of 3-4 km. The NORESS array proves to offer a significant improvement in this respect, as can be seen from the lower 6 traces. The epicentral distance is the same for the two subarrays.

For both signal and noise, coherencies are given in Figs. VI.1.4 and VI.1.5 for 2 and 4 Hz, respectively, for all station combinations within NORESS. The noise data set consists of 20 blocks each of 512 samples of 20 Hz data, amounting to a total of 8.53 minutes. This time interval was carefully selected to avoid detectable signals within it. The signal is a 12 seconds interval (1 block of 240 samples), of an Lg phase for

an event about 200 km away and in appearance very similar to the one in Fig. VI.1.3. Fig. VI.1.5 shows that coherency at 4 Hz is maintained at a level above 0.5 out to about 1 km and then drops to a random level. This point should serve to illustrate the need for small station separations in the study of regional Lg waves. For lower signal frequencies the coherency is maintained at a relatively high level throughout the range of NORESS station distances.

For the processing of NORESS data the high-resolution frequency-wavenumber analysis has been applied to all distinct phases for the events in Fig. VI.1.2. The single frequency theoretical response pattern of the NORESS array is shown in Fig. VI.1.6. For slow phases (phase velocity in the order of 3.5-4.0 km s^{-1}) and high frequencies (say 5 Hz), the corresponding wavenumber is larger than 1 km^{-1} and side lobe effects due to array response might become important. On the other hand, P phases of all frequencies (8 Hz lowpass filters aplied to all channels) should have a fair chance of being correctly determined by such an array.

Fig. VI.1.7 shows records from the 6 NORESS sensors for event no. 1 (earthquake) in Fig. VI.1.2. For each of the phases P_n, P and Lg in this figure, high-resolution frequency-wavenumber plots were produced for 5 different frequencies and all for 100 samples (5 sec) of each phase. For the P_n phase the results are shown for three frequencies in Fig. VI.1.8. According to the reporting agency (UPP), the 'true' azimuth from NORESS to the epicenter is 104^o, while the three frequencies displayed give values of 98^o, 97^o and 103^o. All wavenumber grids consist of 31 x 31 points, yielding an azimuth resolution of about $3\text{-}4^o$ for this phase. The phase velocity values fluctuate around 8 km s^{-1} but could not be attributed to anything else than a P phase of some kind. In the following analysis, for each phase analyzed we will select the frequency or equivalently the azimuth and phase velocity corresponding to the largest power. For the Lg phase of the same event, the corresponding results are given in Fig. VI.1.9. The analysis of this phase serves to illustrate the side lobe problems encountered in a few cases. The frequency (3.5 Hz) corresponding to the largest power gives a maximum power in k-space which obviously results from spatial aliasing and the azimuth

and phase velocity values are thus misleading. The other 4 frequencies analyzed, like 4.5 Hz (shown in Fig. VI.1.9) give, however, 'correct' values both for phase velocity and azimuth.

Event 2 of Fig. VI.1.2 is a mining blast at Titania Gruber, Hauge i Dalane. The NORESS records in Fig. VI.1.10 show only one clear phase (Lg), while the P phase is hardly detectable by eye. However, a 5-sec interval including the expected P-arrival time is processed with the result given in Fig. VI.1.11 for the frequency corresponding to the largest power. The analogous result for the Lg phase is also given in Fig. VI.1.11. The 'true' azimuth in this case is 233^{o}, i.e., the Lg and P results are both 'wrong' by about 10^{o}.

With the exception of a few cases for which spatial aliasing effects are easily identified, all phase velocities are plotted in Fig. VI.1.12 for the events in Fig. VI.1.2. All measurements correspond to the one frequency out of five that has the maximum power. With the k-space grid that has been used, the phase velocity resolution is typically 0.3-0.4 km s^{-1}. Where more than one P phase is available, only the strongest (in terms of power) is included in this figure. On the basis of this figure, the following conclusions are readily reached.

- The P and Lg phases separate into nonintersecting phase velocity bands and a discrimination between P and Lg is possible from NORESS data.
- It is hardly possible to separate Lg from S (the S phases here are believed to be S_n) on the basis of phase velocity measurements alone.

The evaluation of the NORESS array continues and will include the following items:

- Processing of new events as they become available.
- Alteration of the array geometry to remove all side lobes from the part of the k-space corresponding to $|k| < 2$ km^{-1} to eliminate all spatial aliasing problems.
- Do high-resolution frequency-wavenumber analysis with a denser grid in wavenumber space for more detailed phase velocities.

S. Mykkeltveit, F. Ringdal & H. Bungum

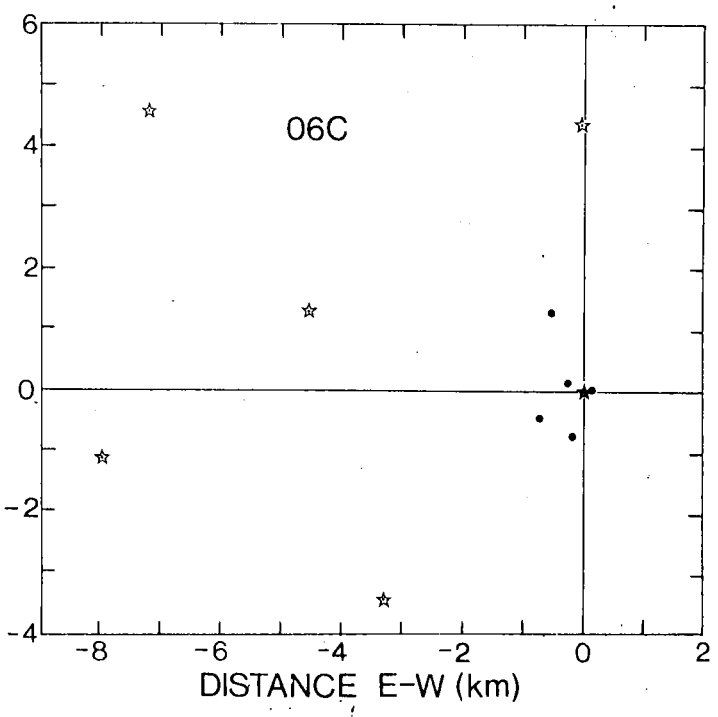

Fig. VI.1.1 Geometry of the 06C subarray before (stars) and after (dots) the change in October 1979. NORESS location is given by the star.

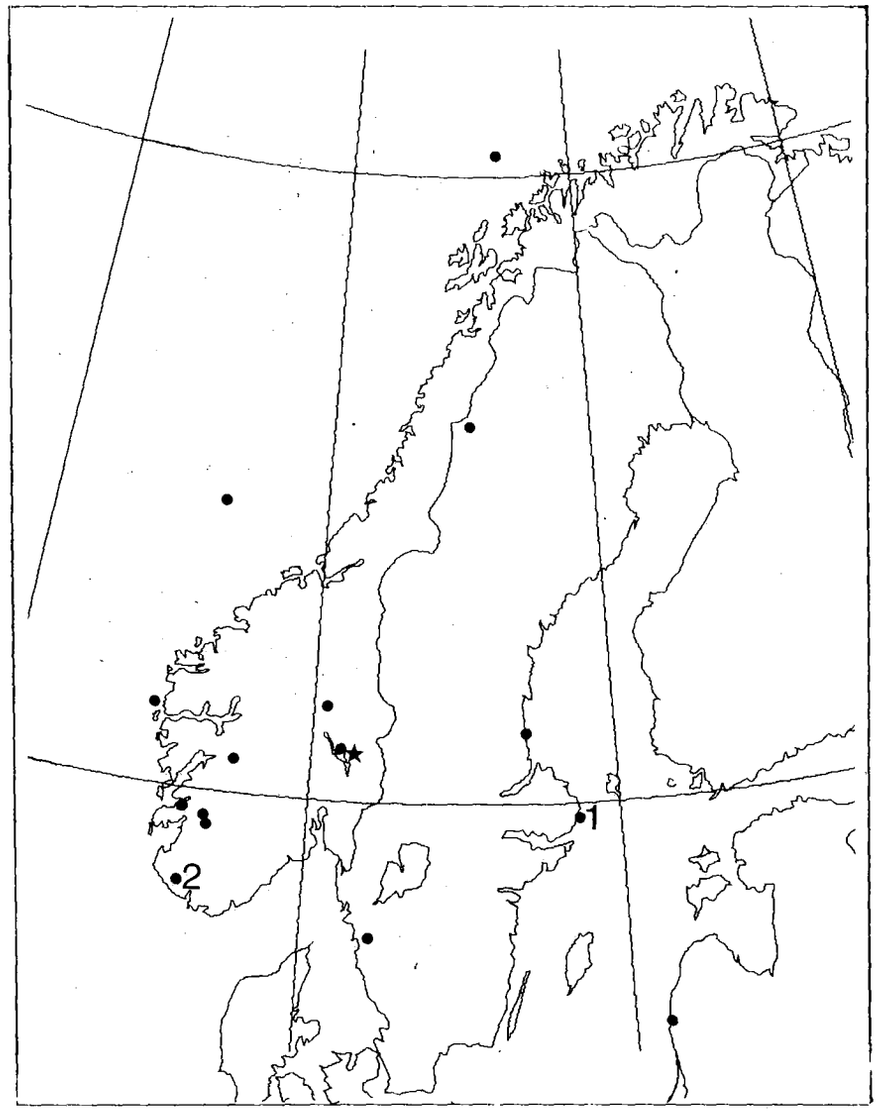

Fig. VI.1.2 Seismic events in Fennoscandia for the period October 1979-April 1980 as located by various agencies on the basis of the regional station network.

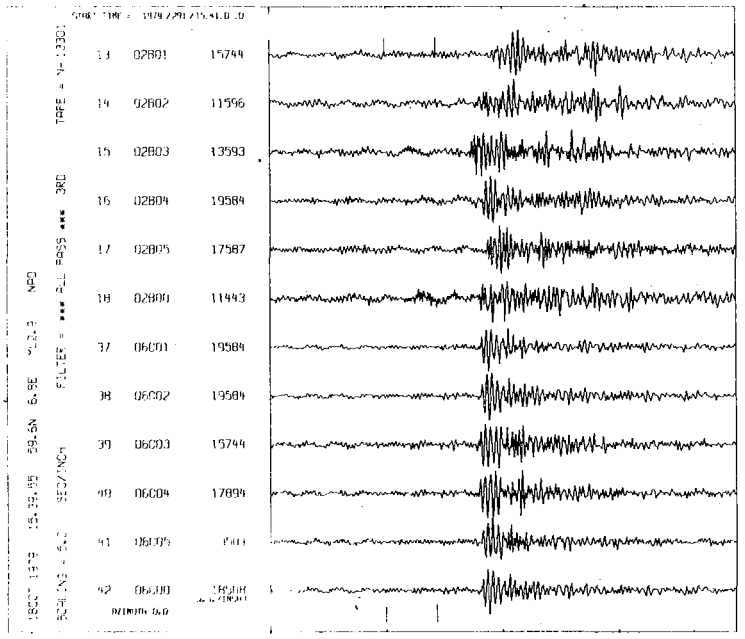

Fig. VI.1.3 Lg waves from an explosion about 300 km away. The top six traces are from standard subarray 02B, the lower six traces from NORESS. The time interval covered is 40 sec.

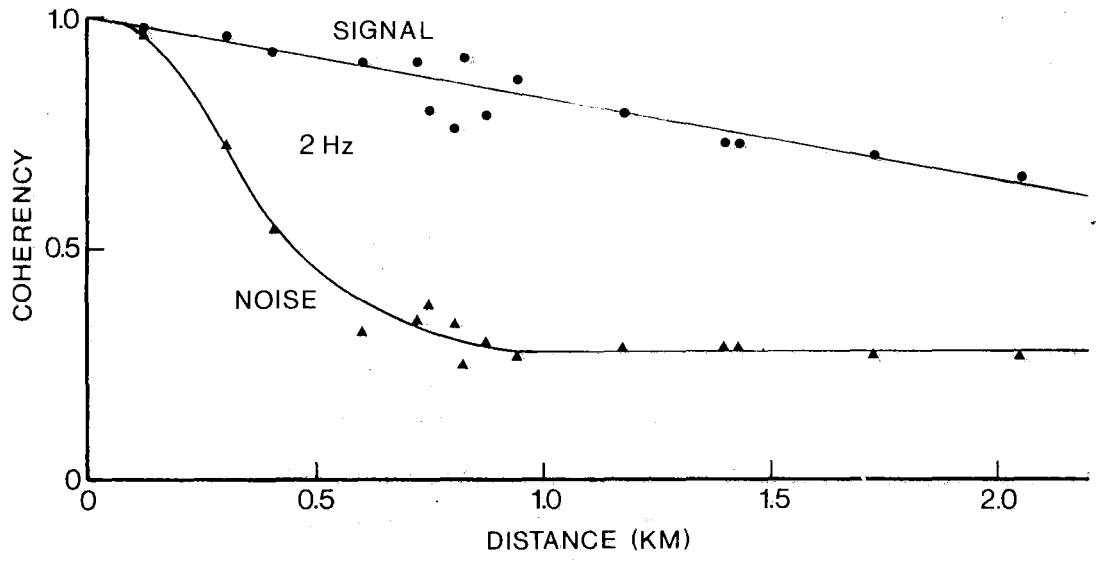

Fig. VI.1.4 Signal and noise coherencies at 2 Hz as a function of sensor distances within NORESS.

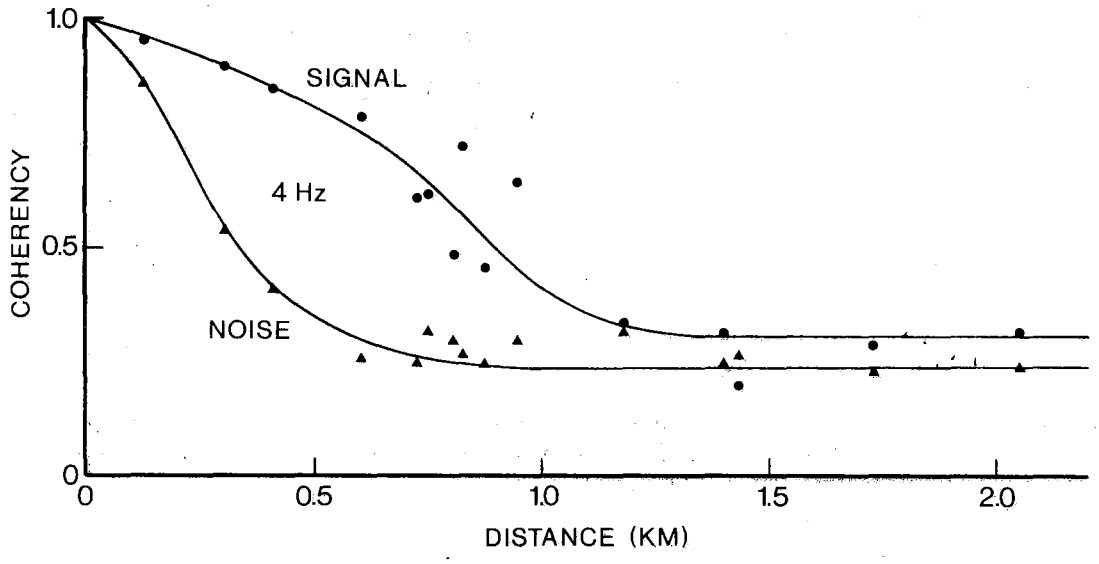

Fig. VI.1.5 Same as Fig. VI.1.4, for 4 Hz.

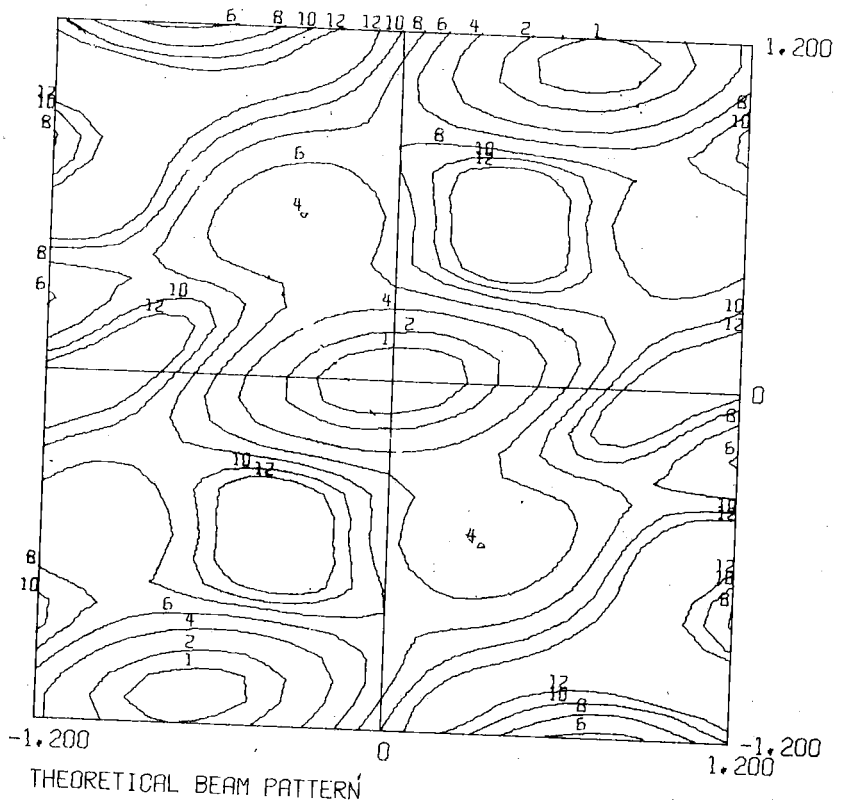

Fig. VI.1.6 Single frequency theoretical response pattern for NORESS.

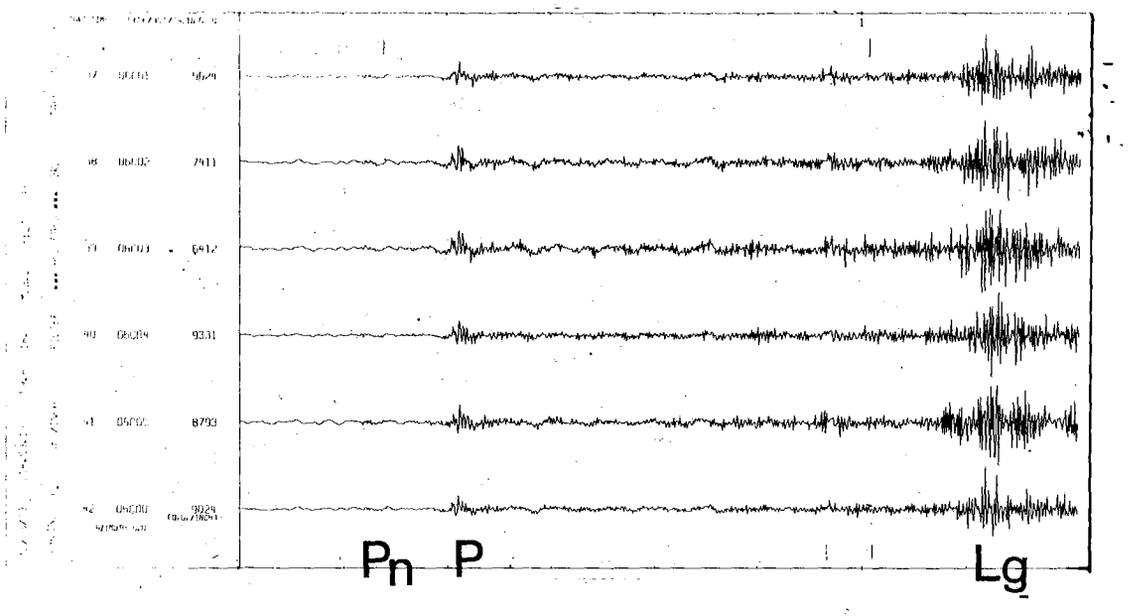

Fig. VI.1.7 NORESS records for event 1 in Fig. VI.1.2. The epicenter information is as reported by Uppsala. The time window covers 80 sec.

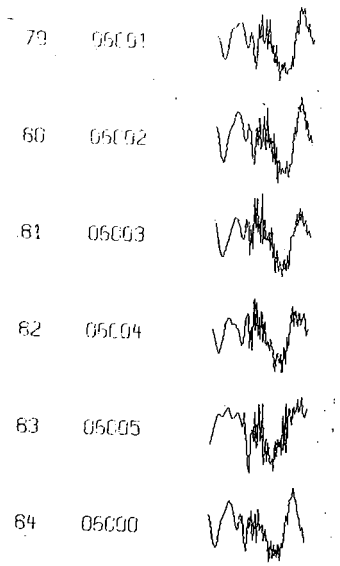

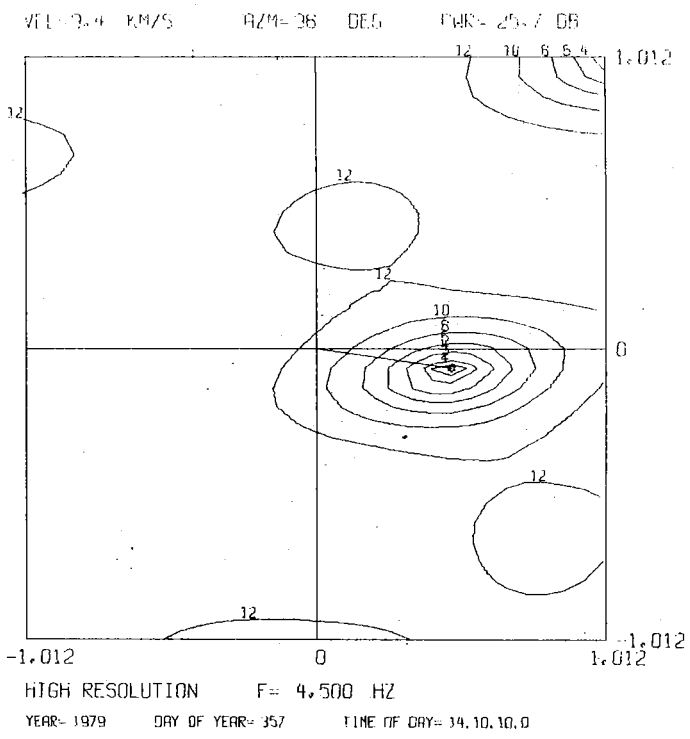

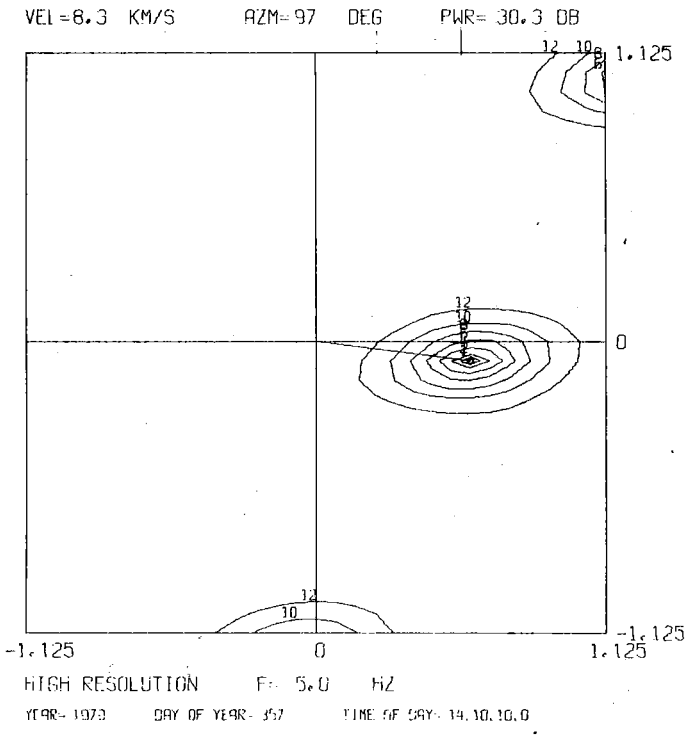

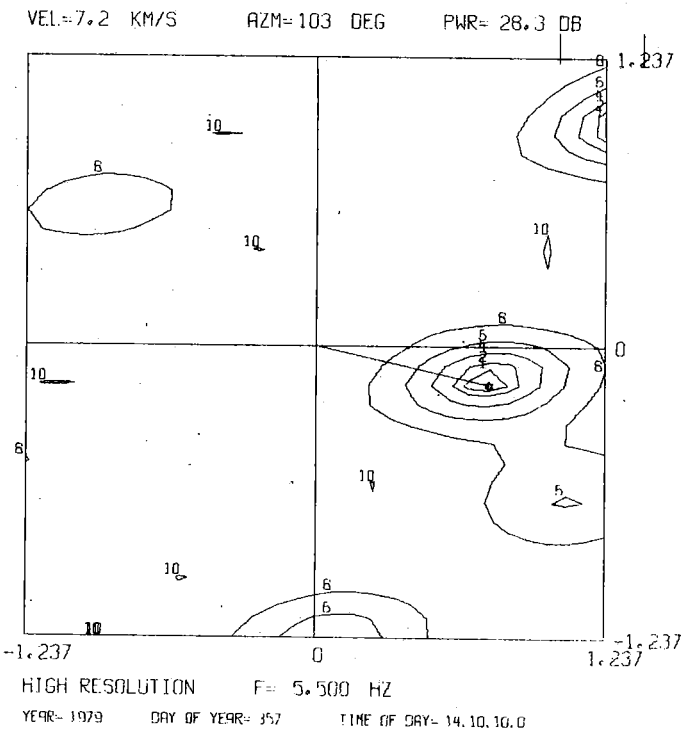

Fig. VI.1.8 High-resolution frequency-wavenumber plots at three frequencies for the 5 sec of the P_n phase shown in upper left corner.

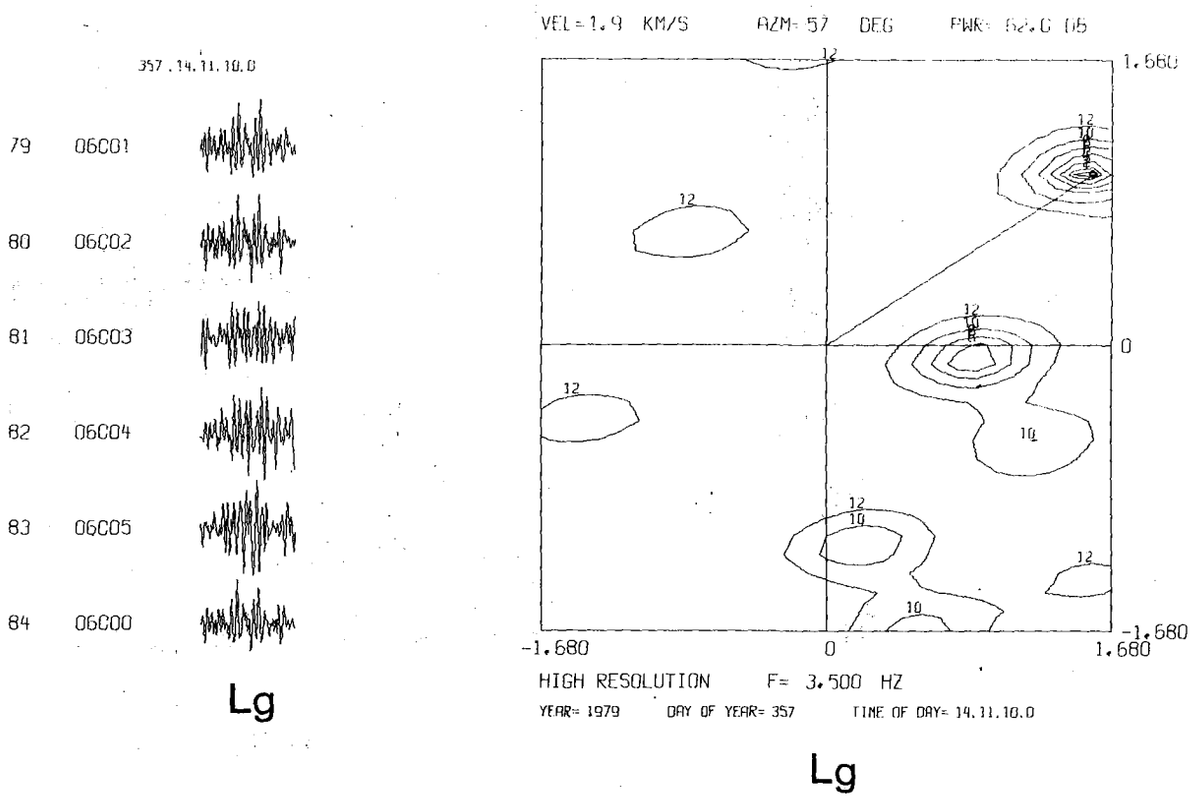

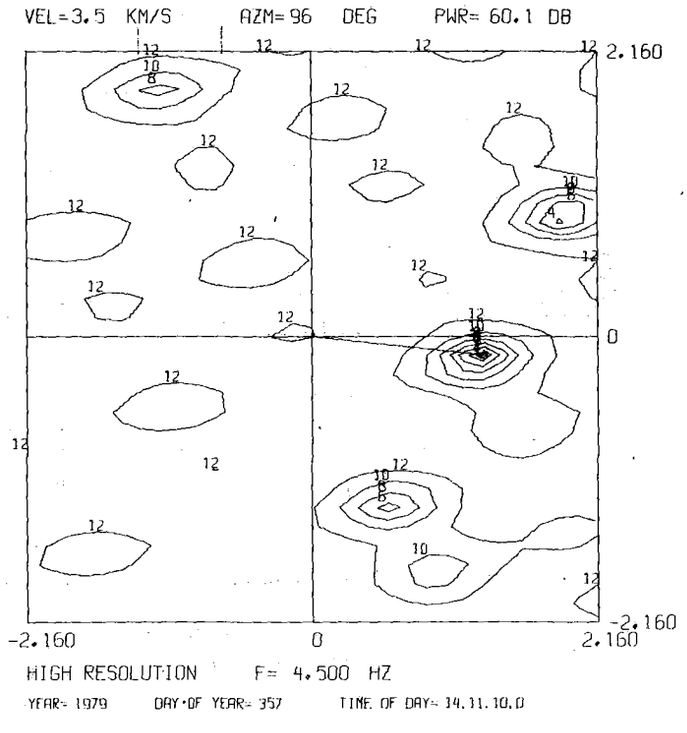

Fig. VI.1.9 Same as Fig. VI.1.8 for two frequencies for the Lg phse.

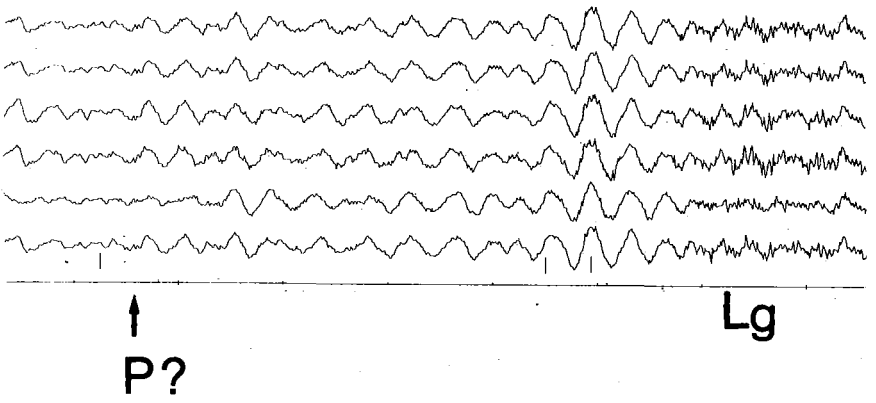

Fig. VI.1.10 NORESS records for event 2 in Fig. VI.1.2 (explosion at Titania Gruber). The time window covers 80 sec.

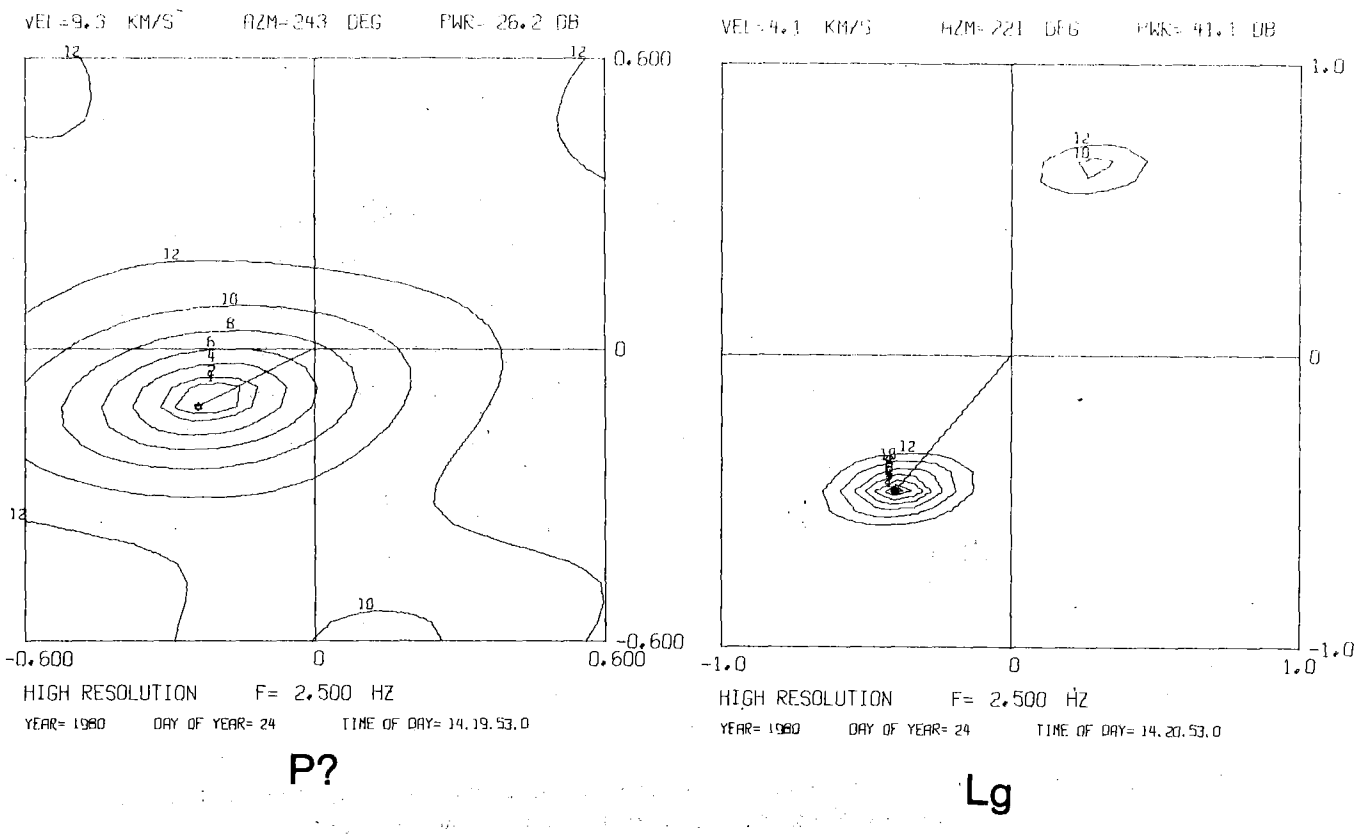

Fig. VI.1.11 High-resolution frequency-wavenumber plots for the P and Lg phases (5 sec of each) from event 2 in Fig. VI.1.2.

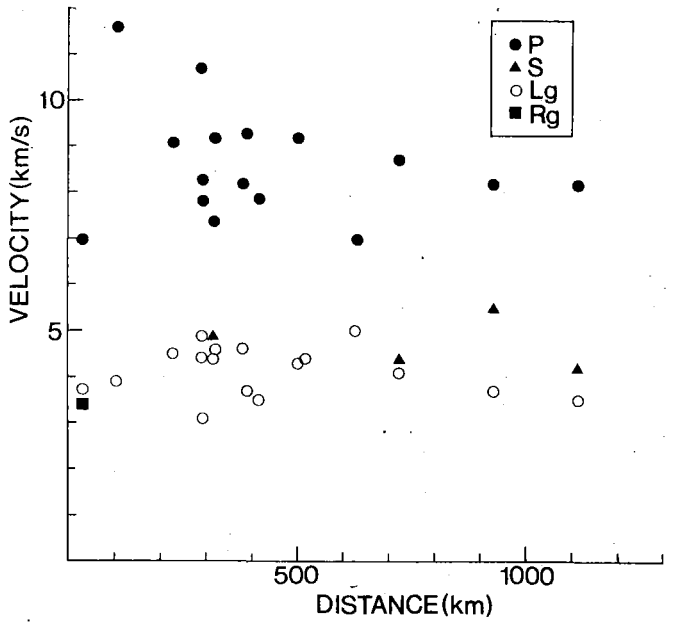

Fig. VI.1.12 Phase velocities as determined by processing of NORESS data from the events of Fig. VI.1.2.

VI.2 An Experimental Small Subarray within the NORSAR Array: Location of Local and Regional Events

Since November 1979 one of the NORSAR subarrays (6 seismometers, each with an 8 Hz lowpass filter) has been operated with station distances from 125 to 2051 meters. The purpose of this NORSAR Experimental Small-Aperture Subarray (NORESS) has been to obtain SP data from closely spaced sensors in order to

- Investigate noise and signal coherencies at high frequencies
- Identify P, S and Lg phases from regional seismic events
- Detect and locate regional events.

This paper describes a location procedure that has been developed for local and regional events, using NORESS. Briefly, the location algorithm consists of the following steps:

1. Identification of the P and Lg phases for each event using high-resolution frequency-wavenumber analysis
2. Manual pick of onset times for P and Lg
3. Epicenter azimuth determination based on the high-resolution analysis results
4. Epicenter distance determination using Lg-P travel time differences and a standard crustal model.

The efforts at this stage have been focused at obtaining a very simple procedure, with no attempt made to optimize location accuracy, e.g., by using azimuth-dependent travel time tables. The crustal model used for determining P wave travel times has been as follows:

Depth	P_n Velocity
0-16 km	6.20 km/s
16-40 km	6.70 km/s
40-95 km	8.15 km/s
95- km	8.25 km/s

The group velocity of Lg has been set to 3.5 km/s, which is consistent with earlier results obtained for Fennoscandia.

The data base for the study has consisted of:

- 16 regional events from Fennoscandia
- Distance range from NORESS 200-1200 km
- Magnitude range (M_L) 2.0-3.5

Note that 15 of the events have been located independently using the Fennoscandian seismograph network. These location estimates have subsequently been used to evaluate the accuracy of the developed location procedure.

The first step of the location procedure, the high-resolution analysis of recorded waveforms, has been conducted as follows:

- Each phase processed at 5 frequencies: 1, 2, 3, 4 and 5 Hz
- For each phase: azimuth and phase velocity is obtained from the frequency with largest signal power
- Phase (P or Lg) is then identified from the estimated phase velocity.

For further discussion of the results here, it is referred to subsection VI.1. We note only that the 'side lobe' problem discussed there implies a need for further refinement of the sensor deployment.

With respect to the third step of the location procedure, azimuth determination, we have investigated and assessed several alternatives:

a) P_n azimuth from high-resolution analysis
b) Azimuth from 'best' P phase (P_n og P_g)
c) Lg azimuth
d) Average of P and Lg azimuths.

The results of the location evaluation are shown in Figs. VI.2.1-VI.2.4 for various alternative ways of azimuth determination. The dots on each figure correspond to the epicenter determined via the Fennoscandian network, while the end of each arrow indicates the location obtained using NORESS alone. Best result (Fig. VI.2.2) is achieved using the azimuth computed from the largest P phase.

In Figs. VI.2.5 and VI.2.6 we compare the NORESS estimated azimuth with those corresponding to the network determinations. Similarly, in Fig. VI.2.7, the respective epicenter distance estimates are plotted against each other.

In summary, our main conclusions are:

Phase Identification

- Accurate separation has been achieved between P and secondary phases (S, Lg)
- It is difficult to distinguish S from Lg based on phase velocity alone.

Distance Estimates

- Median 'error' is 11 km using Lg-P times
- No clear azimuth-dependent effect is apparent

Azimuth Estimates

- From Lg phase: Median 'error' is 6^{o}
- From largest P phase: Median 'error' is 3^{o}

Location Estimates

- Using Lg azimuth: Median 'error' is 45 km
- Using P azimuth: Median 'error' is 30 km.

It should be noted that the above 'errors' are relative to the location results from the Fennoscandian network, and that these locations are uncertain by typically 10-30 km or more. Thus the majority of the processed events can be located with a difference from the network location that is within the uncertainty limits of the latter.

Our future plans for the small aperture array developments include:

- Design array to minimize the side lobe problem
- Develop criteria for automatic identification of S and Lg phases
- Automate the picking of phase arrival times
- Refine the techniques for computing distance and azimuth from a NORESS type array
- Obtain an extended data base for evaluation
- Compare the results to those obtained using three-component location procedures, and possibly combine the two approaches.

F. Ringdal & S. Mykkeltveit

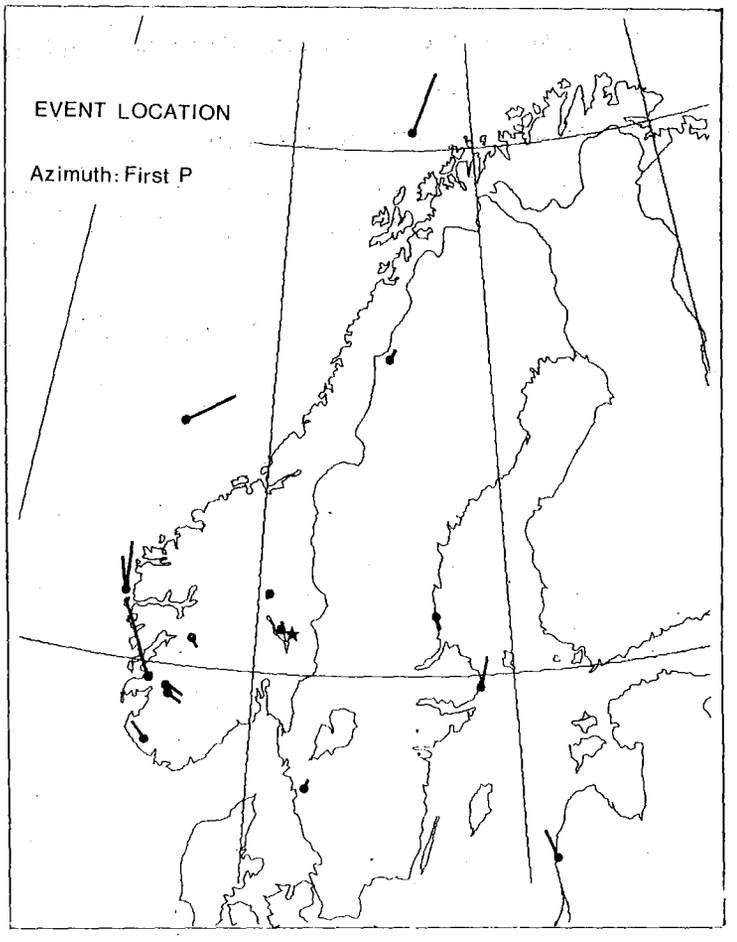

Fig. VI.2.1 'Location errors' using NORESS (with azimuths determined from the first P phase) for regional event location. Dots indicate epicenters determined by the Fennoscandia station network, while the end of the arrows indicate locations from NORESS processing.

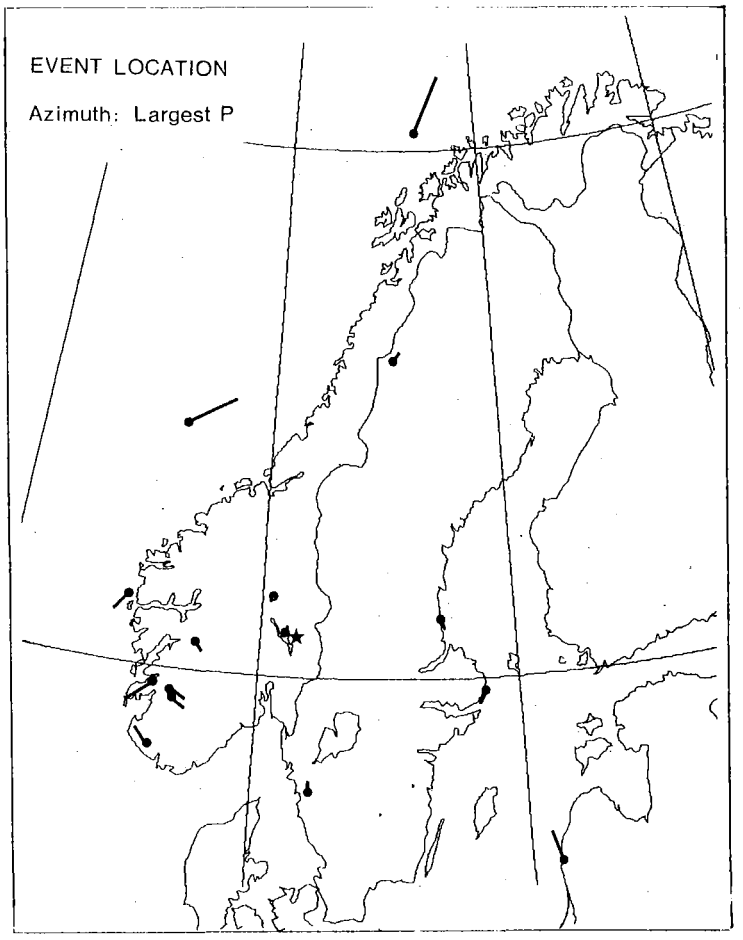

Fig. VI.2.2 Same as Fig. VI.2.1, but with NORESS azimuths determined from the largest P phase.

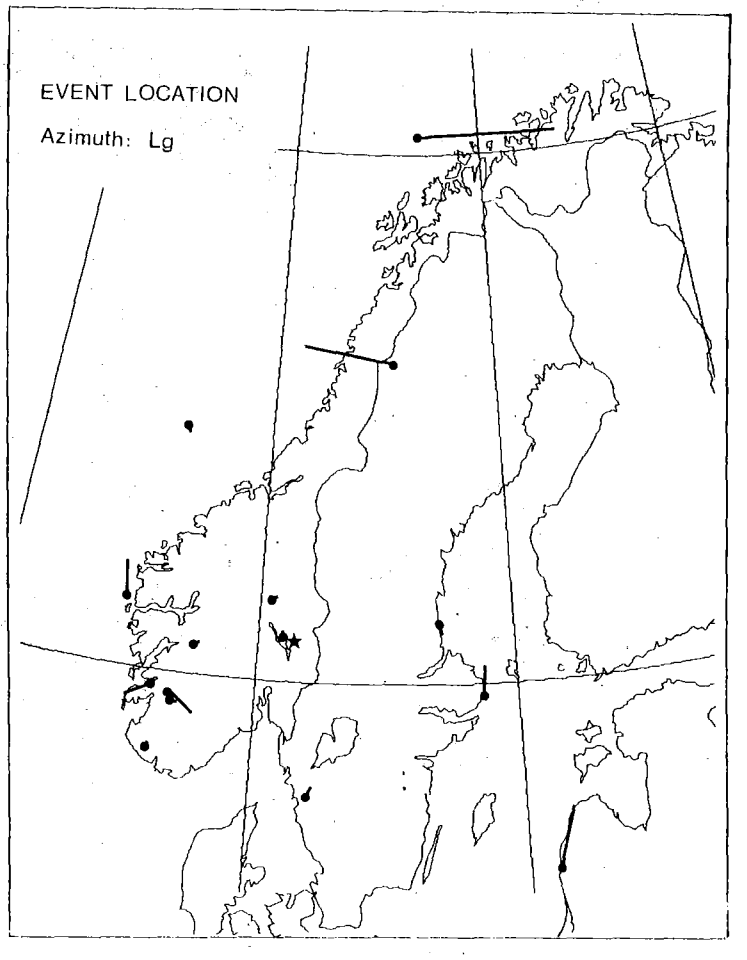

Fig. VI.2.3 Same as Fig. VI.2.1, but with NORESS azimuths determined from the Lg phase.

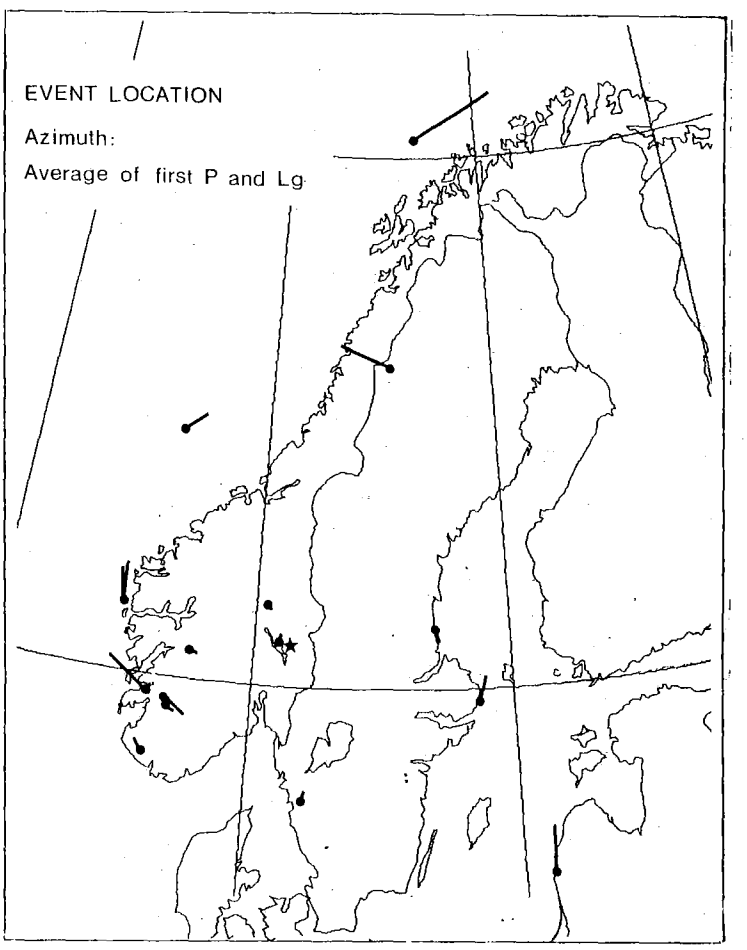

Fig. VI.2.4 Same as Fig. VI.2.1, but with NORESS azimuths determined from averaging the azimuths of the first P and the Lg phases.

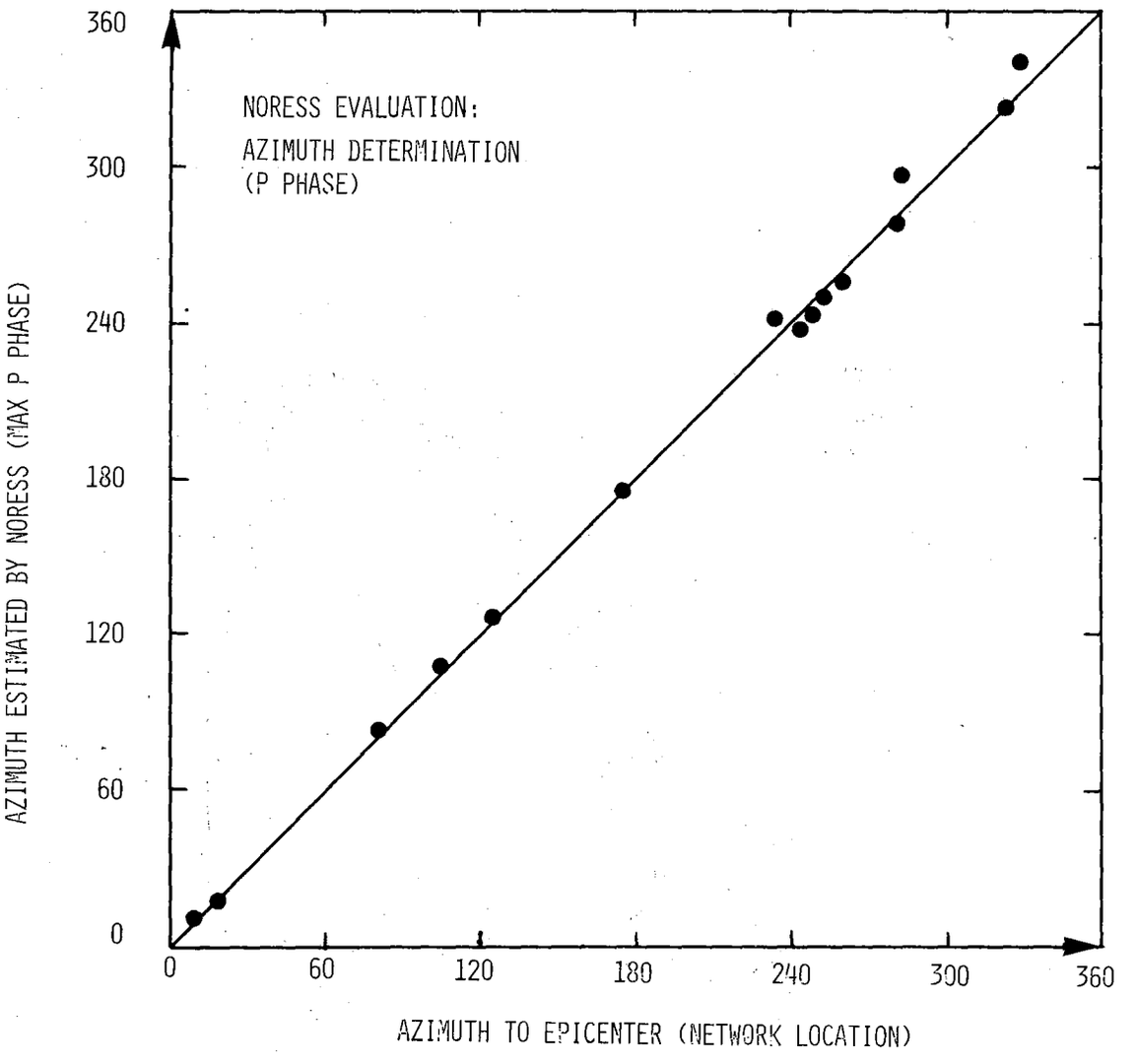

Fig. VI.2.5 Comparison of azimuths determined from NORESS processing (largest P phase) with those based on Fennoscandian network locations.

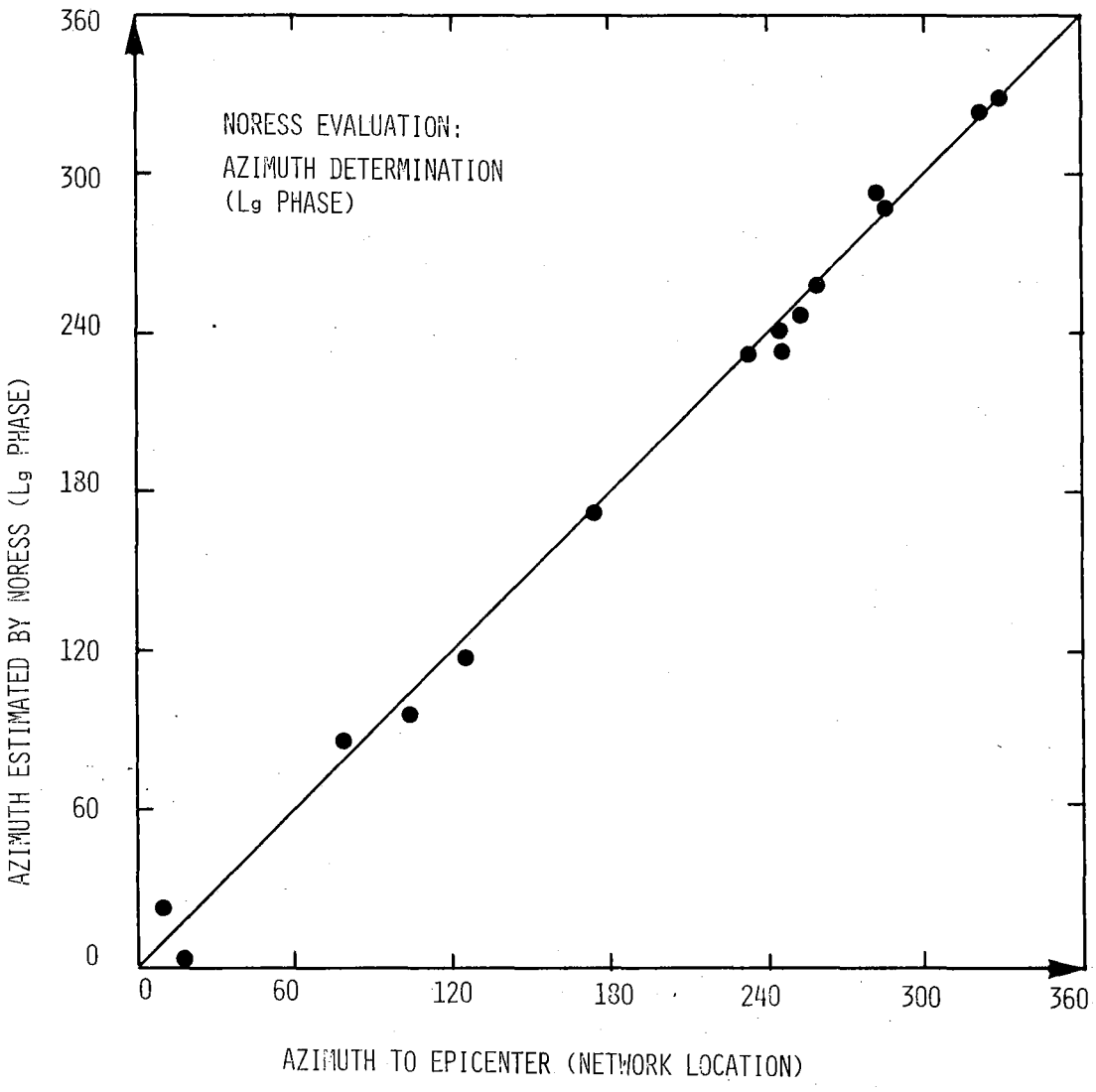

Fig. VI.2.6 Comparison of azimuths determined from NORESS processing (Lg phase) with those based on Fennoscandian network locations.

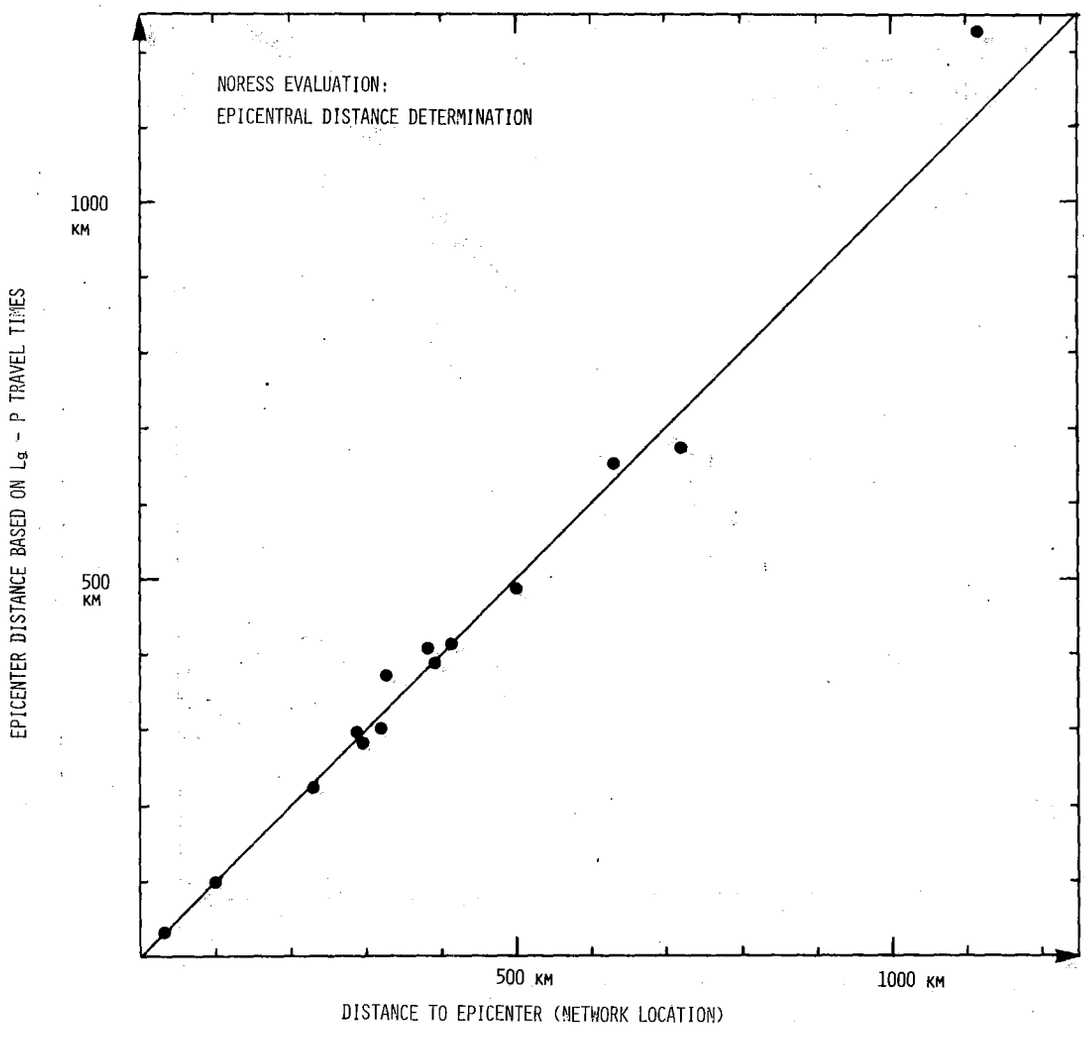

Fig. VI.2.7 Comparison between epicentral distance estimates using NORESS Lg-P travel time differences and the distance based on Fennoscandian network locations.

VI.3 Automated Arrival Time Determination for Local and Regional P and S Waves

Microearthquake arrays quite often have a detectability down to zero or below in local magnitude (cf. Section VI.6). This means that even for intermediately active areas the number of recorded earthquakes may be substantial, quite often many thousand in a single year. The routine work connected to the analysis of such data may therefore be substantial, with large potential gains if the procedure can be automated.

Our approach to the problem has been to compute signal envelopes following a procedure outlined by Levshin et al (1972). After an initial inverse Fourier transform a bandpass filter is applied (in frequency domain), and the envelope is computed as the absolute value of a complex function where the real part is the output of the filter and the imaginary part is its Hilbert Transform. The time of computation is speeded up significantly by a folding procedure by which the sampling rate of the initial Fourier transform is reduced n times, the effect on the envelope being to avoid oversampling and to introduce smoothing.

Given the envelopes covering a certain time interval for each trace, the next step is to detect signal arrivals. This is done by computing STA/LTA ratios, where we initially have used window lengths of 0.2 and 1.67 sec, respectively (30 Hz sampling rate). This is followed by an iterative detection procedure in which the following parameters have been used, and where a detection is declared if P out of Q values of STA/LTA exceed the given threshold:

Iteration	Threshold	P/Q
1	1.55	5/9
2	2.00	3/5
3	3.50	2/4

These parameter values have been chosen for the following reasons:

In iteration 1, the threshold is low in order to be sensitive to first arrivals, and P and Q are large in order to avoid spike detections. Also, in this iteration it usually takes a long time to leave detection state, and until then a new detection cannot be declared. This means that only very strong and late second arrivals can be picked up, illustrated by the bottom event in Fig. VI.3.1. We see that all the S arrivals for this event are correctly determined, and note especially that we have been able to avoid the large secondary P arrival for Channel 5.

Iterations 2 and 3 are only entered if for a given channel only one detection has been declared in previous iterations. In this case we start the search following detection 1. This means a higher sensitivity for events with short S-P times, which is the case for the two top events in Fig. VI.3.1. Some of the S phases there are determined in the second, and some in the third iteration. For Event 1 one of the S phases is incorrectly determined (Ch. 6) and one is not found (Ch. 3). For Event 2 one S is possibly wrong (Ch. 3), one S has not been found (Ch. 7), and since P is not seen on Ch. 6 the S phase has been called P by the automatic procedure.

It is of course necessary that a procedure like this is followed by manual control and editing. However, provided that data files with the appropriate format are established in the automatic analysis for each event, the editing time can be very short compared to a manual analysis from scratch. A procedure like that is under establishment for our data from the Stiegler's Gorge Seismic Network, and we plan to use it also for data from the microearthquake network now under establishment in Southern Norway. So far, the procedure has not been tested on a larger number of events, and it is quite likely that this will lead to changes in the parameter values given above, maybe also to the procedure as such.

H. Bungum

References

Levshin, A.L., V.F. Pisarenko and G.A. Pogrebinsky, 1972: On a frequency-time analysis of oscillations. Ann. Geophys., 28, 211-218.

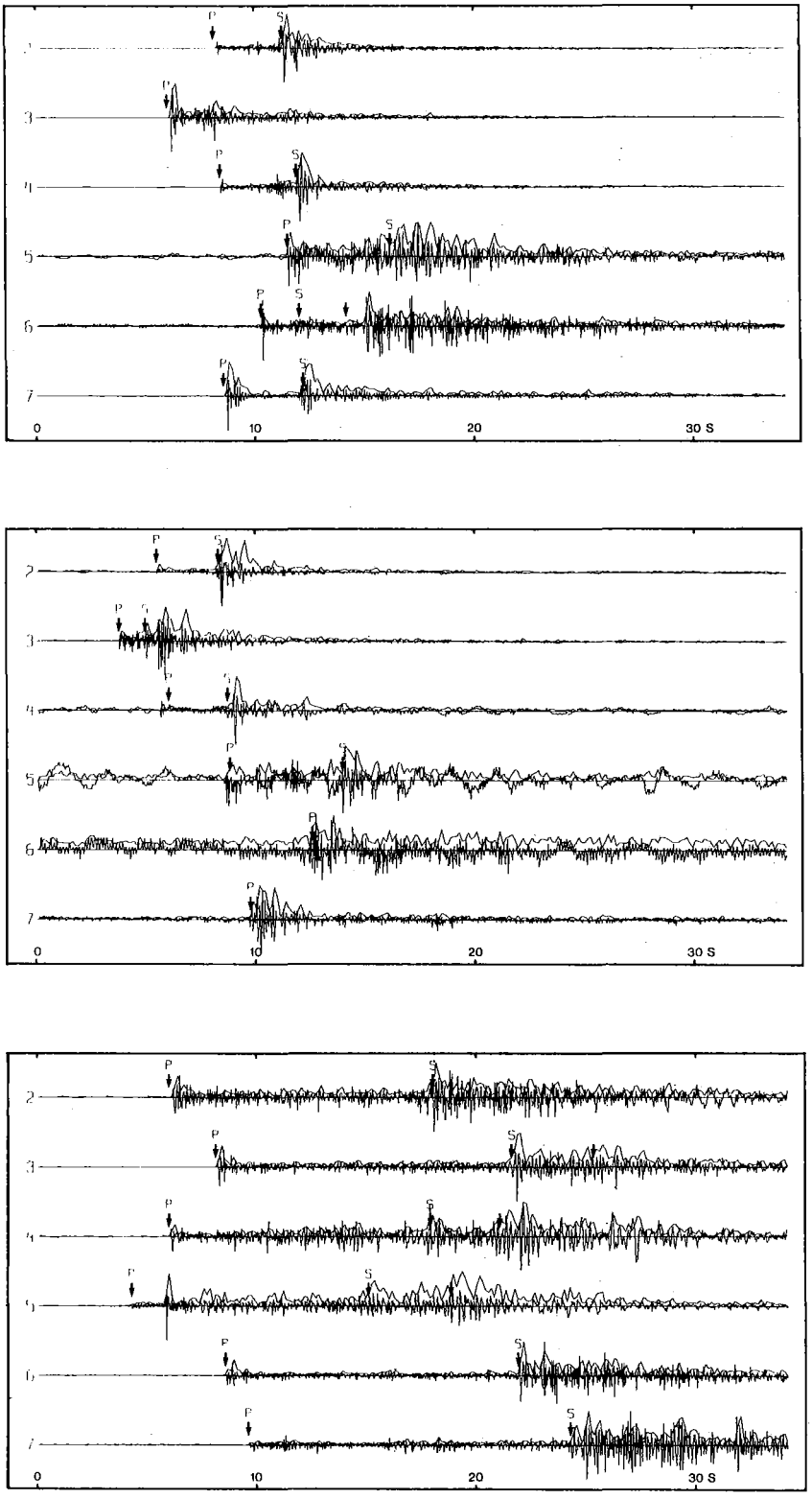

Fig. VI.3.1 Automatically determined P and S waves for three local events recorded at the Stiegler's Gorge Seismic Network. The data traces are unfiltered while the plotted envelopes are based on data filtered between 2 and 8 Hz.

VI.4 Mapping of Upper Mantle Heterogeneities

The method developed by Aki, Christoffersson and Husebye (1977) - denoted the ACH method in the following - for 3-dimensional inversion of P-wave residuals from a 2-dimensional network of stations has been successfully applied in studies of crustal and upper mantle heterogeneities in various parts of the world. The network data used have mainly been extracted from local networks and thus not generally available. The only exception in this regard is the ISC bulletins containing P-residuals for all those stations regularly reporting to ISC. In certain regions like Central Europe the distribution of ISC-reporting stations is sufficiently dense so as to motivate an adaption of the ACH method for analysis of this kind of data. Such an experiment is to be described in this section.

Method of analysis

The method used for analysis of P residuals from subset of ISC-reporting stations is essentially an adaptation of the ACH method to arrays of continental dimensions. A brief description of this modified inversion approach is given in the following.

The travel time residuals are related to velocity anomalies via the integral:

$$\delta T_i = \int_{A_i}^{B_i} \delta s \, d\ell \qquad \text{(VI.4.1)}$$

over the ray path in the original medium or initial earth model. Fermat's principle of least time shows that changes in the ray path caused by changes in velocity (ds) will be of second order and thus small.

The input data for each event are the focal parameters (except origin time) and a series of J-B time residuals for those stations in the network reporting the event in question. Ray parameters and azimuth (p_o and z_o) are computed from the event location to a reference station near the network center, while p and z for other receivers are estimated by the linear formulae:

$$p = p_o + \frac{\partial p}{\partial \Delta}\,\delta\Delta \qquad \text{with} \qquad \delta\Delta = -D\cos(z_o-\theta)$$

and

$$z = z_o - \frac{D\sin(z-z_o)}{\Delta}$$

where Δ is the distance from event to center station and D,θ are the relative distance and azimuth to another station within the network. Knowing p and z the ray paths are traced through the spherically symmetric starting model using an appropriate upper mantle velocity distribution. The velocity structure was represented by a smooth cubic interpolation between slowness values on a three-dimensional grid of 'knots', which in turn requires that the first and second slowness derivatives be known.

To obtain a linear relationship between observed time residuals and the velocity structure formalism above (Smith et al, 1979), we proceeded in the following manner. Let $\{f_i\}$, $\{f_i'\}$ be the values of a function f(x) and its derivative on a grid of points (i=1,2...N) with equal spacing Δx. A Hermite interpolation can be written as:

$$f(x) = \sum_{i=1}^{N} f_i H(dx^{-1}x-i) + f_i'\,\Delta x H'(dx^{-1}-i) \qquad \text{(VI.4.2)}$$

where

$$H(x) = \begin{cases} (x+1)^2(1-2x) & -1\le x\le 0 \\ 2x^3-3x^2+1 & \text{for} \quad 0\le x\le 1 \\ 0 & \text{otherwise} \end{cases}$$

$$H'(x) = \begin{cases} x(1+x)^2 & -1\le x\le 0 \\ x(1-x)^2 & \text{for} \quad 0\le x\le 1 \\ 0 & \text{otherwise} \end{cases}$$

The cubic functions have the property that they and their derivatives vanish at all points except the ith, where $H_i(x)$ is unity and its derivative is zero, and $H_i'(x)$ is zero and its derivative is unity. We do not know the $\{f_i'\}$ and so they must be estimated. Invoking continuity of second derivatives

of f(x) gives the usual spline representation where the $\{f_i'\}$ are all related to all the $\{f_i\}$. This non-local representation was rated too expensive to compute and was replaced by an estimate of $\{f_i'\}$ in which they are related only to f_{i-2}, f_{i-1}, f_i and f_{i+1} through the equation:

$$f' = G\, f \qquad \text{(VI.4.3)}$$

where

$$G = \begin{pmatrix} -2 & 1 & 2 & -1 \\ -1 & 0 & 1 & 0 \\ 0 & -1 & 0 & 1 \\ 1 & -2 & -1 & 2 \end{pmatrix}$$

Now equation (xx.2) can be written:

$$f(x) = \sum_{i}^{N} f_i\, C_i(x) \qquad \text{(VI.4.4)}$$

where

$$C_i(x) = H(dx^{-1}x-i) + \sum_{j=0}^{3} G_{ji}\, dx\, H'(dx^{-1}x-j)$$

In practice $C_o(x)$ is computed for 300 values in the range (0,1) and these are stored. The values of the $\{C_i(x)\}$ can then be 'looked up' in this table with considerable savings in computer time.

The generalization to three dimensions is obvious, namely:

$$ds(x,y,z) = \sum_{i,j,k} ds_{ijk}\, C_k(x)\, C_j(y)\, C_k(z) \qquad \text{(VI.4.5)}$$

First and second derivatives are computed by storing the corresponding derivatives of $C_o(x)$, as in the one-dimensional case.

Substituting equation (VI.4.5) into the travel time integral (VI.4.1) gives:

$$\delta T_i = s_{pqr} \int_{B_i}^{A_i} C_p(x)\, C_q(y)\, C_r(z)\, d\ell \qquad \text{(VI.4.6)}$$

The integral in eq. (xx.6) is calculated by the trapezoidal rule from known points along the ray path.

Eq. (VI.4.6) is in the form of a standard linear inverse problem for s_{pqr} and the method of solution by least squares follows that of Aki et al (1977) except on two major points. Firstly, because p and z vary slightly across the array, the assumption that the average velocity on any horizontal surface will be completely undetermined is only approximately valid. The second difference lies in the spectrum of the normal equations matrix which in turn made the stochastic inverse type of solution the obvious choice. For further details on this method and comutational schemes for associated parameters like resolution, standard errors and variance improvements, reference is made to Hovland et al (1980).

Choice of network and data used in analysis

The Central Europe seismograph network (see Fig. VI.4.1) appeared to be an appropriate one for testing the inversion scheme outlined in the previous section. The data used were, as mentioned above, P-time residuals for teleseismic events as listed in the ISC-bulletins for 1971-1974. The following station and event screening procedures were used; stations with poor detectability (Ringdal et al, 1977) were excluded as such stations appear to report systematically too late arrival times and besides they have very few observations. As regards events to be used, they were initially grouped in 10 deg azimuth/distance areas, out of which the one or two best in the sense of many and consistent observations were selected. The above screening procedure left us with 167 events out of an initial total of 1314. The final number of observations was 5807. The data base epicenters are plotted on an azimuthal equi-distant projection, centered on station BSF, in Fig. VI.4.2.

Results

The region covered by the network of stations is from 41.5°N to 54.5°N and from 4.5°W to 18.5°E, a square of side approximately 1400 km. The network data are expected to be sensitive to anomalies down to depths

comparable with the radius of its aperture. The thickness of the anomalous zone was set at 600 km, which conveniently includes the whole of the upper mantle. The grid acopted had 4 (in depth) x7x7 knots. Each interpolation coefficient affects to some extent the slowness at all depths and to a horizontal distance of 4 times the knot spacing. The slowness in the depth range 0-100 km is dominated by the values at the top level of knots, for 100-300 km the second level, 300-500 km the third level and 500-600 km by the bottom level.

The choice of the smoothing parameter θ^2 in the stochastic inverse solution is always subjective to some extent. If θ^2 is too small, the derived model will exhibit large anomalies that fluctuate rapidly between adjacent knots. Increasing θ^2 reduces the RMS of the slowness perturbations versus the reduction in RMS travel time residual for various choices of the smoothing parameter gives a trade-off curve from which one can decide at what point a decrease of θ^2 will drastically alter the model without improving the fit. Such a curve, based on the data discussed here, is displayed in Fig. VI.4.3. The overall reduction in residuals achieved by our model (Fig. VI.4.5) is 11%, from an RMS of 0.72 s for the raw data to 0.64 s. This is less than for NORSAR, which is closer to a 60% reduction. The total time variance reductions are respectively around 20% and 70%. The difference reflects a difference in the quality of the data and the larger area and correspondingly coarser grid in the Central European inversion. However, the RMS residual explained by the laterally varying models is the same for NORSAR as for the present model and is about 0.2 s.

In Figs. VI.4.4 and VI.4.5 the estimated resolution and standard errors for the velocity perturbations associated with the knots of all 4 levels are displayed. In the following detailed comments upon observed anomalous velocity features will be presented.

Level 1 (Fig. VI.4.5a) is representative of the uppermost 100 km and corresponds roughly to the lithosphere. The low velocity in the southern North Sea appears to be a real phenomenon required by the observations. However, its apparent extension northeastwards is poorly resolved by

data and thus should be given very little weight. There is a broad area of high velocity centered over Eastern Germany and comprising the Bohemian Massif and the eastern part of the Ardennes. The whole of the Paris Basin is low velocity while another high velocity region stretches from the Armorican Massif in Brittany to the Central Massif in Southern France. The Po Plain-N. Adriatic Sea exhibit a marked velocity high, but the area is poorly resolved which may reflect a lack of stations in Switzerland and N. Italy. Finally, other interesting though poorly resolved areas are the Pannonian Basin in the east and parts of the Pyrenees in the west.

Levels 2 and 3 show features that are broadly similar to each other (Figs. VI.4.5b&c), though the anomalies are somewhat smaller than for levels 1 or 4. Resolution is good except near the corners of the region, and the standard error estimates are again about 1%, larger near the edges. In level 2 the dominant feature is a velocity high covering the Paris Basin and SE-France and a velocity low over most of the German-Polish Depression. As before, parts of the Pannonian Basin and (eastern) Pyrenees remain low, while the N. Adriatic Sea now is definitely high. The Paris Basin high of level 2 becomes more dominant in level 3, encompassing also the Alps, Pannonian Basin, Po Plain and the Appennines. Further north the German-Polish depression area of velocity low appears to have been shifted slightly westward. Also Brittany and adjacent areas remain mostly low and the same applies to the eastern Pyrennees.

The anomalies in level 4 (Fig. VI.4.5.d) are with few exceptions well resolved because there are many intersecting ray paths contributing to the values at most of the knots. The picture is very different from that in the shallower levels with pronounced highs in the German-Polish Depression, Sudetes and Southern France, and similar pronounced lows in the Paris Basin and Appeninnes-Sardinia area.

Interpretation

Three possible influences on the P wave velocity will be discussed: temperature, differences in composition of the underlying mantle and sedimentary thickness at the surface.

Level 1

The velocity anomaly map for the uppermost 100 km (Fig. VI.xx.5a) shows a remarkabel correlation with both available heat flow data and the tectonic features of Central Europe. The most prominent feature is the large high in northern Germany and Poland. This region coincides with low heat flow and the Bohemian Massif and the Ardennes which are Hercynian folded units.

Consider first the effect of thermal anomalies. The heat flow in this region is on average 60 $mW \cdot m^{-2}$ with a low of 40 $mW \cdot m^{-2}$. Taking the thermal conductivity of igneous rocks to be 2.5 $W \cdot m^{-1} K^{-1}$ gives a geotherm of 24 $K \cdot km^{-1}$ for the average figure. 70 $mW \cdot m^{-2}$ gives a geotherm of 28 $K \cdot km^{-1}$. Assuming the geotherm to be constant for the whole of the 100 km thick lithosphere gives average temperature differences of 200 K for each 10 $mW \cdot m^{-2}$ change in heat flux. A typical estimate for the change of P velocity with temperature is:

$$\frac{\partial v_p}{\partial T} = -5.0\ 10^{-4}\ km \cdot s^{-1} K^{-1}$$

(Christensen 1979) giving a lateral change in v_p of 0.1 $km \cdot s^{-1}$ for 200 K or 1.2% fast for each 10 $mW \cdot s^{-2}$ low in the heat flux. The observed velocity anomalies of 2-5% fast can therefore, by this rough calculation, be explained by thermal anomalies going down to 100 km which cause the variations in heat flow from 40 $mW \cdot m^{-2}$ to 70 $mW \cdot m^{-2}$.

Another possible explanation for high velocity anomalies is that the rocks comprising the mentioned massifs have a higher velocity than elsewhere. An anomaly of 5% over 100 km produces a travel time anomaly of half a second. However, the Hercynian granites are probably only a few km thick and thus cannot account for such a large travel time residual. Between the two major high areas (see Fig. VI.4.5a) is a low velocity region over the Paris Basin and southern North Sea. The correlation with heat flow is good. There are very few stations in the Paris Basin and so it is unlikely that the time delays are caused by the sediments, which are several kilometers thick in places, because no ray paths pass through them. The sharp low in the southern North Sea also coincides with high heat flow and besides the south end of the Central Graben. The low

velocity associated with the Paris Basin may indicate a southward extension of this thermal anomaly. We mention in passing that there is low velocity over the German-Polish Depression, where there are also thick sediments and high heat flow, but these anomalies are not well resolved.

Levels 2 and 3

The anomalies in these two levels are very similar to each other and are smaller than those in level 1, and also than those in level 4 deeper down (see below). This finding agrees with the general view that the material below the lithosphere lid is more homogeneous because of its lower strength. The broad high ridge trending NW-SE across the continent cannot be explained in terms of known thermal or compositional anomalies and is plausibly accounted for by variations in the depth to the phase change at about 400 km. This phase change gives rise to a P wave velocity increase of about 5% from 8.7 to 9.2 $km \cdot s^{-1}$. For a velocity anomaly Δv in a layer of thickness x, a change in depth of the phase boundary d is given approximately by:

$$\frac{d}{x} = \frac{\Delta v}{\delta v}$$

where δv is the velocity change associated with the phase change. For level 3, $\frac{\Delta v}{v}$ = 2% and x = 200 km leading to a depth change of 80 km. For anomalies throughout level 2 and 3 of about 1% give the same result. The anomalies are therefore consistent with a shallow ridge of the olivine-spinel phase transition running NW-SE across France.

Level 4

The anomalies in level 4 are different from those in 2 and 3 and are larger. The resolution is good, and the anomalies may be related to variations in the depth of the 650 km discontinuity, where the P wave velocity increases by 10% from 10.2 to 11.2 $km \cdot s^{-1}$. For 3% anomalies in a 100 km thick layer this give a depth variation of 30 km or so for the phase boundary.

Final remarks

We have shown that it is possible to use ISC-reported travel times to obtain meaningful models of lateral variations in P wave velocity in the mantle beneath Europe. In particular, the correlation between the obtained P wave velocity anomalies exhibit a remarkably good correlation with dominant tectonic features and heat flow data. Also, the detectability estimates of Ringdal et al (1977) for Central European stations also reflect roughly the same features, and the same is likely to apply to surface wave propagation efficiency.

Studies similar to that described above are now in progress for south-east Europe and parts of Central Asia.

J. Hovland
D. Gubbins (Univ. of Cambridge, U.K.)
E.S. Husebye

References

Aki, K., A. Christoffersson and E.S. Husebye (1977): Determination of the three-dimensional seismic structure of the lithosphere, J. Geophys. Res., 82, 277-296.

Christensen, N.I. (1979): Compressional wave velocities in rocks at high temperatures and pressures, critical thermal gradients, and crustal low velocity zones, J. Geophys. Res., 84, No. B12.

Hovland, J., D. Gubbins and E.S. Husebye (1980): Upper mantle heterogeneities beneath Central Europe, Geophys. J.R. Astr. Soc., in press.

Ringdal, F., E.S. Husebye and J. Fyen (1977): Earthquake detectability estimates for 478 globally distributed seismograph stations, Phys. Earth Planet. Inter., 15, P24-P32.

Smith, M.L., B.R. Julian, E.R. Engdahl, D. Gubbins and R. Cross (1979): Linearised inversion of travel times for three dimensional earth structure, Abstract EOS Trans. Am. Geophys. Union, 59, 12.

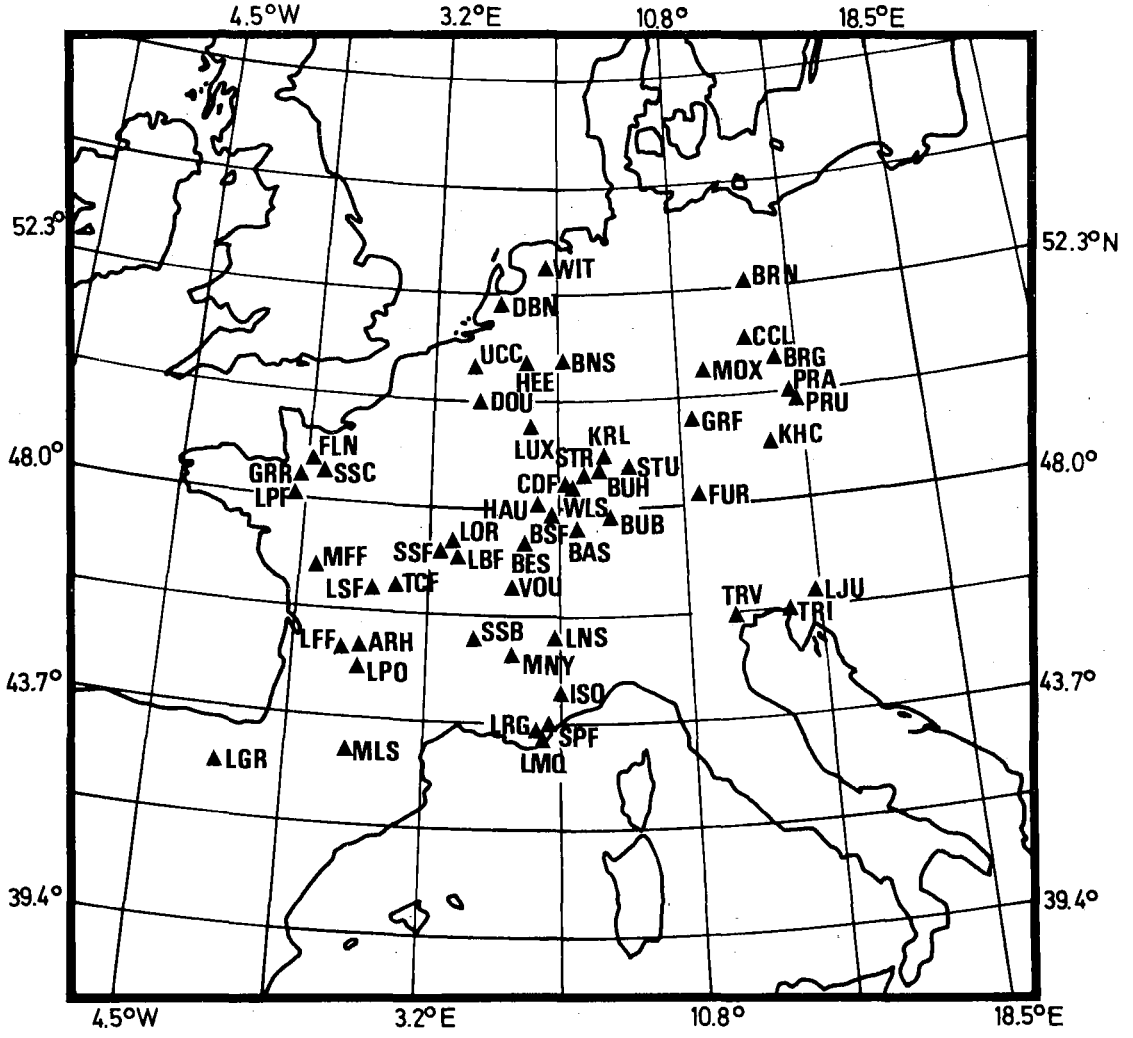

Fig. VI.4.1 Central European seismograph station network used in analysis. The intersections of the latitude/longitude grid system correspond to the nodes in the time residual inversion described in the text.

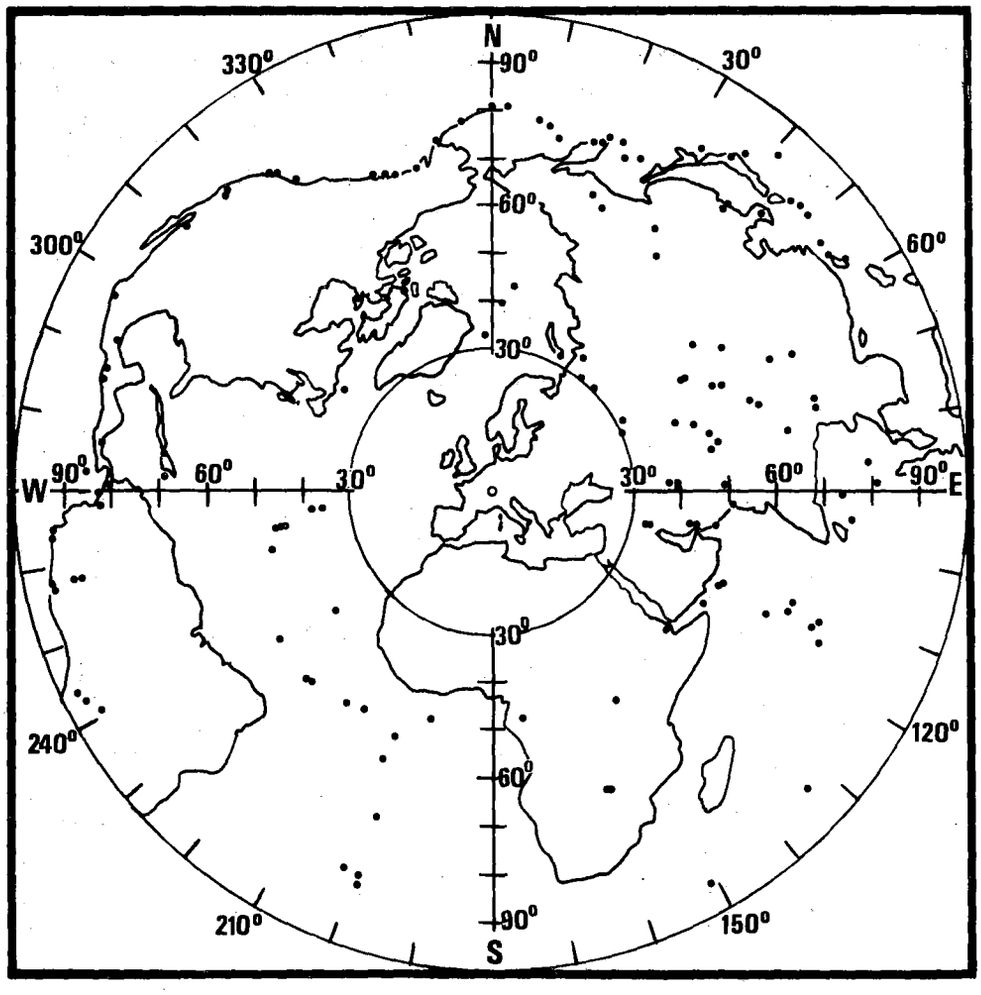

Fig. VI.4.2 Epicenter map of the 167 events used in analysis.

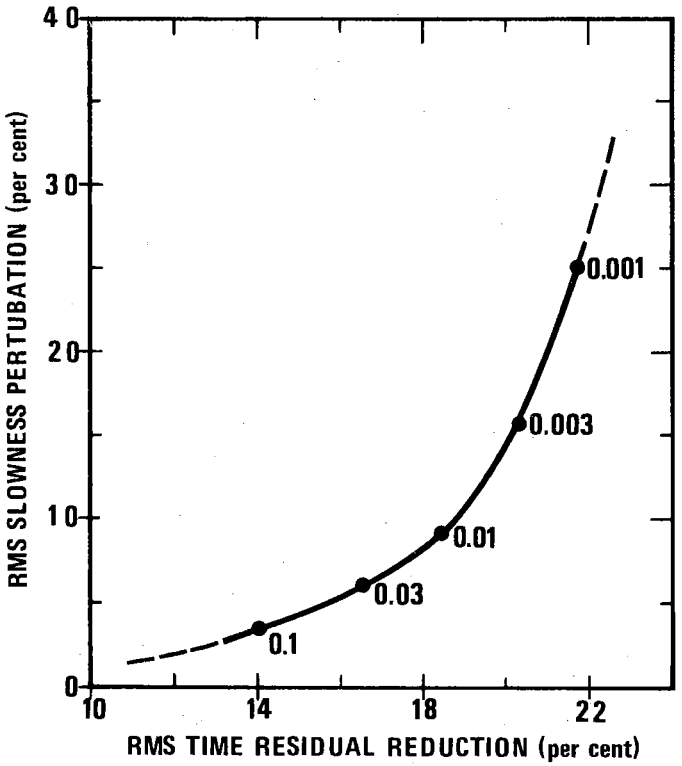

Fig. VI.4.3 RMS slowness (velocity) perturbation versus RMS time residual reduction for various values of the smoothing parameter.

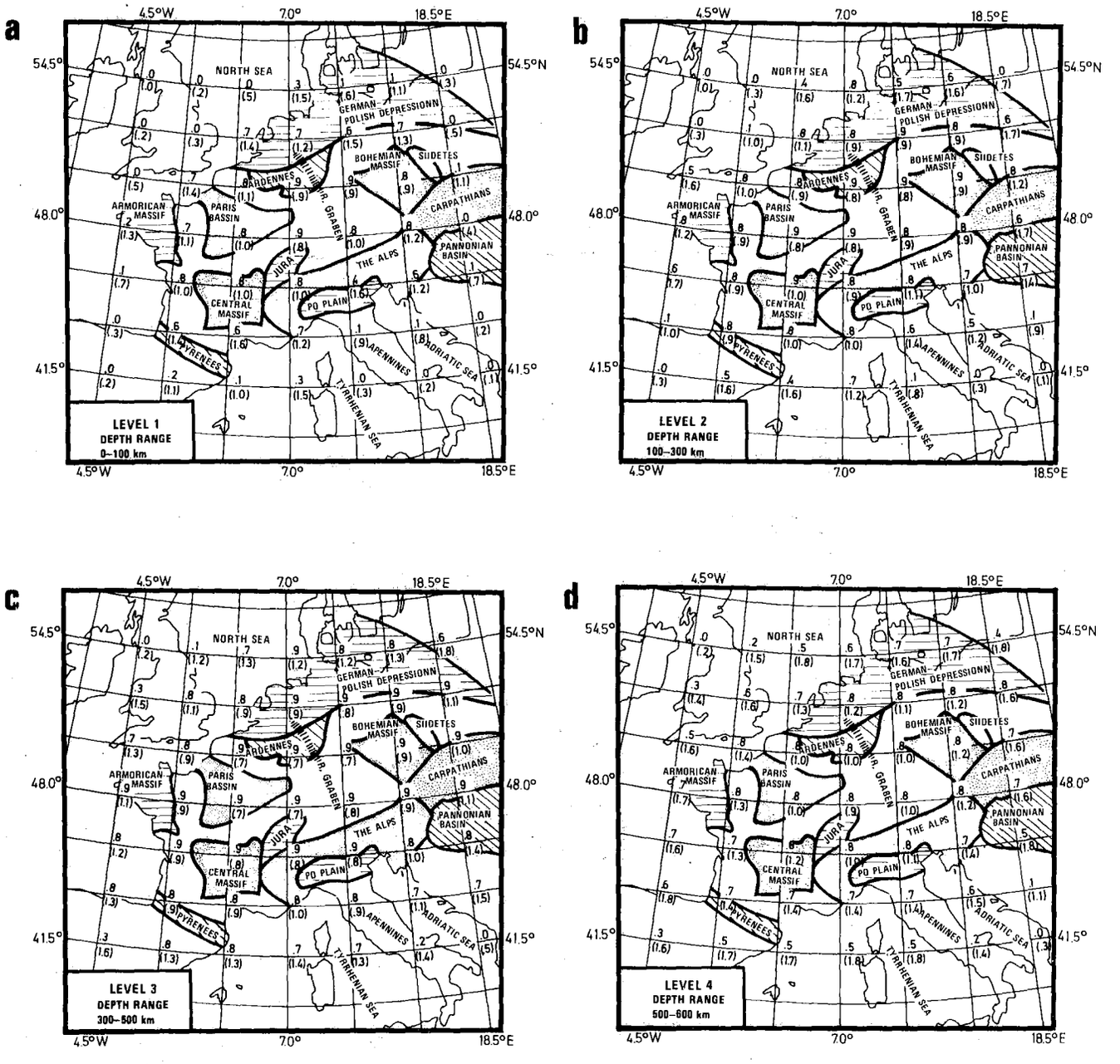

Fig. VI.4.4a Resolution and standard error (in brackets) estimates for all level 1 nodes. Geographical locations referred to in the text are also indicated.

b Resolution and standard error (in brackets) estimates for all level 2 nodes.

c Resolution and standard error (in brackets) estimates for all level 3 nodes.

d Resolution and standard error (in brackets) estimates for all level 4 nodes.

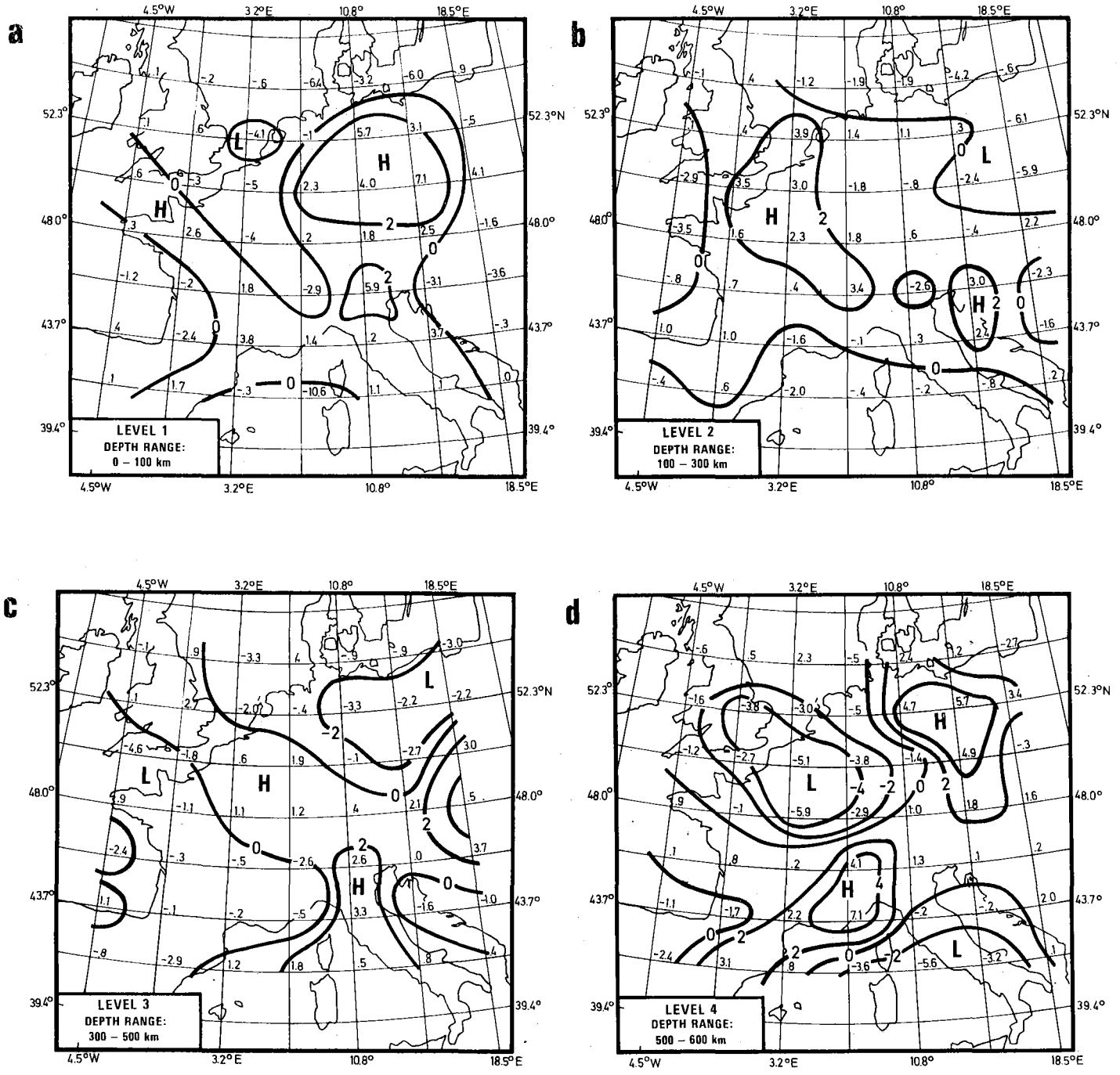

Fig. VI.4.5a Velocity perturbations (in per cent) for level 1. Areas of high and low velocities are indicated by capital letters H and L. Resolution and standard errors for all nodes are displayed in Fig. VI.4.4a.

b Velocity perturbations (in per cent) for level 2. Otherwise as for Fig. VI.4.5a.

c Velocity perturbations (in per cent) for level 3. Otherwise as for Fig. VI.4.5a.

d Velocity perturbations (in per cent) for level 4. Otherwise as for Fig. VI.4.5a.

VI.5 Structural Complexities in Ancient Mountain Ranges

Lg propagation efficiency in Central Asia is apparently strongly path dependent and thus not easily related to gross tectonic features. However, such effects must have a structural origin and thus imply the preservation over a considerable period of time of small-scale imprints of past tectonic processes. In order to actually map such heterogeneities high-frequency data are needed, preferably of the seismic profiling type. Although we do not have access to such observations from parts of Central Asia, data from a refraction/wide angle reflection profile across parts of the Caledonides of western Norway (Mykkeltveit, 1980) will in the following be used to illustrate the potential tectonic complexities of plate collision manifestations like mountain ranges.

The refraction/wide angle reflection seismic profiling line is indicated on the map of Fig. VI.5.1, together with the two shot point locations I and II. Five 3-component seismometers were moved along the profile using an interspacing of 2.5 km on the average, while charges in the range 25-300 kg of explosives were fired at water depths of approx. 20 m at the shot points. Altogether 145 seismic field records were obtained, but many of them were not appropriate for detailed digital analysis. Many records of poorer quality, however, were used for extracting first arrival travel times.

After the necessary elevation corrections, etc., had been introduced, a Herglotz-Weichert inversion procedure was applied to the first arrival observations (see Fig. VI.5.2a). The continuously increasing velocity distribution obtained (Fig. VI.5.2b) was truncated at 12-14 km depth because the pronounced offset in the Fig. VI.5.2a travel time curves suggests the existence of a low velocity zone (LVZ) in the upper crust. It should be added that strong lateral inhomogeneity effects are ruled out when detailed comparison of records from the 2 shot points is undertaken.

The outstanding feature of the velocity model obtained is the roughly 4 km thick low velocity zone in the upper crust. Being aware of objections to such a feature on the grounds of both realistic heat generation mechanisms and limited resolving power of the data at hand, extensive synthetic

seismogram analyses were undertaken. These experiments demonstrated that the appropriate model for reconciling discontinuous travel time data and amplitude distributions of primary and secondary phases in fact involved the introduction of a low velocity zone. Fig. VI.5.2c shows an extract from both the real record section (shot-point I) and a synthetic section calculated from the model in Fig. VI.5.2b, covering the distance interval over which the LVZ reflections are observed. The corresponding branches are well modelled, as seen in the synthetic section.

The nature and significance of low velocity zones are still not well understood, though the main prerequisite for such phenomena is either anomalously high temperatures and/or profound compositional changes. Within the Møre gneisses there is no evidence of high heat flow, so the postulated LVZ must be tied to velocity reversals associated with compositional changes. We note in passing that further to the north near Mo i Rana a trans-Scandinavian profile also gives evidence of upper crustal velocity reversal under the Caledonides only. In the following, two hypotheses will be examined as regards these rather unique observational data, namely, i) the Gneiss Region is allocthonous and represents an overthrust of the American block over the Eurasian, or ii) a double overthrust where serpentinized mantle/lowermost ocean crust has become 'sandwiched' between continental rocks from two opposite continents.

The geologists working with the basement/cover relations of the Caledonides in southern Norway mostly favor the view that the Møre gneisses represent an autochthonous area above which Caledonian nappes to the east have been thrust from a westerly location in the once proto-Atlantic ocean. Special support for this hypothesis is found in Råheim's (1977) work. The alternative i) above is tied to the general features of the Bergen-Namsos area which exhibits a lithologic and structural development clearly different from that of southeastern Norway. In this context, the Bergen-Namsos area may be classed as a separate Precambrian block or may represent an overthrusting part of the American block over the Eurasian one. In this case we cannot decide decisively between a serpentinite or a trench sediment origin for the Møre LVZ. However, the latter alternative seems the most attractive according to the literature on subduction tectonics. A favored mechanism imagining a

Himalaya-type doubling of the crust for the mid-Scandinavian Caledonides is illuminated in Fig. VI.5.3.

Finally, a recent Fennoscandian study supports the idea of a relatively thick crust (~ 40 km) in the coastal areas of western and particularly northern Norway as opposed to southeastern Norway (Oslofjord) with a Moho depth of around 30 km only.

The above explanations are speculative, but may on the other hand serve to illustrate that continental collision zones like the Urals and the Himalayas (in the wide sense) may exhibit localized barriers to efficient Lg propagation.

S. Mykkeltveit
E.S. Husebye

Reference

Mykkeltveit, S. (1980): A seismic profile in southern Norway. Pure and Applied Geophysics, 118, 1308-1323.

Råheim, A. (1977): Norsk Geol. Tidsskr., 57, 193-204

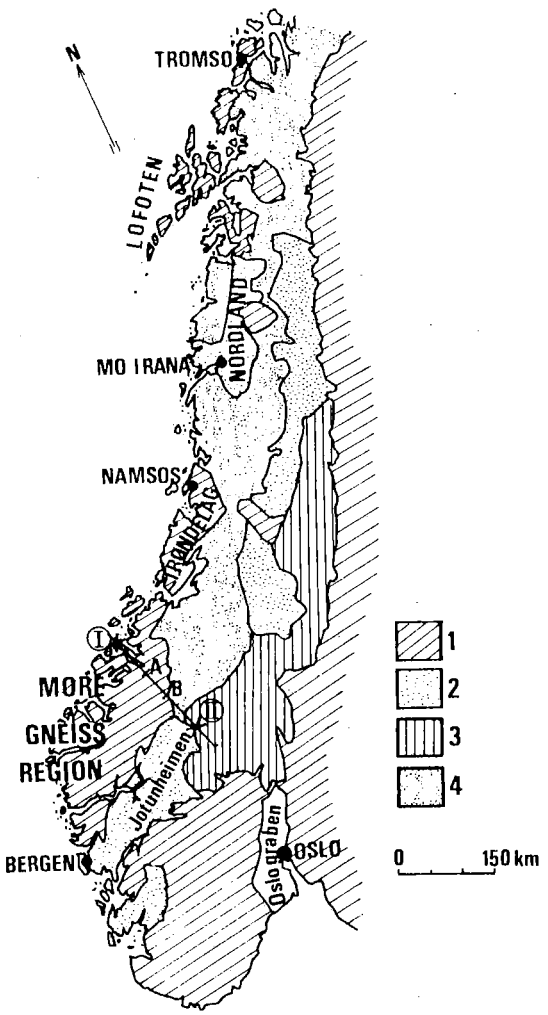

Fig. VI.5.1 Simplified tectonic map of Norway redrawn after Reymer, including shot points I and II for the seismic profile transecting the Møre Gneiss Region. Legend markings are as follows: 1) Precambrian basement, including the generally presumed autochtonous Møre Gneiss Region, with radiometric age determinations in the range 1900-1200 Ma, 2) Mostly Precambrian nappes (1200-850 Mz) also including structures of Caledonian ages, 3) Lower Palaeozoic elements, (par)-autochtonous-allochtonous structures of mostly Cambrian-Silurian ageas, 4) Lower Palaeozoic elements, typical nappe substructures having a presumed southeastern direction of thrusting.

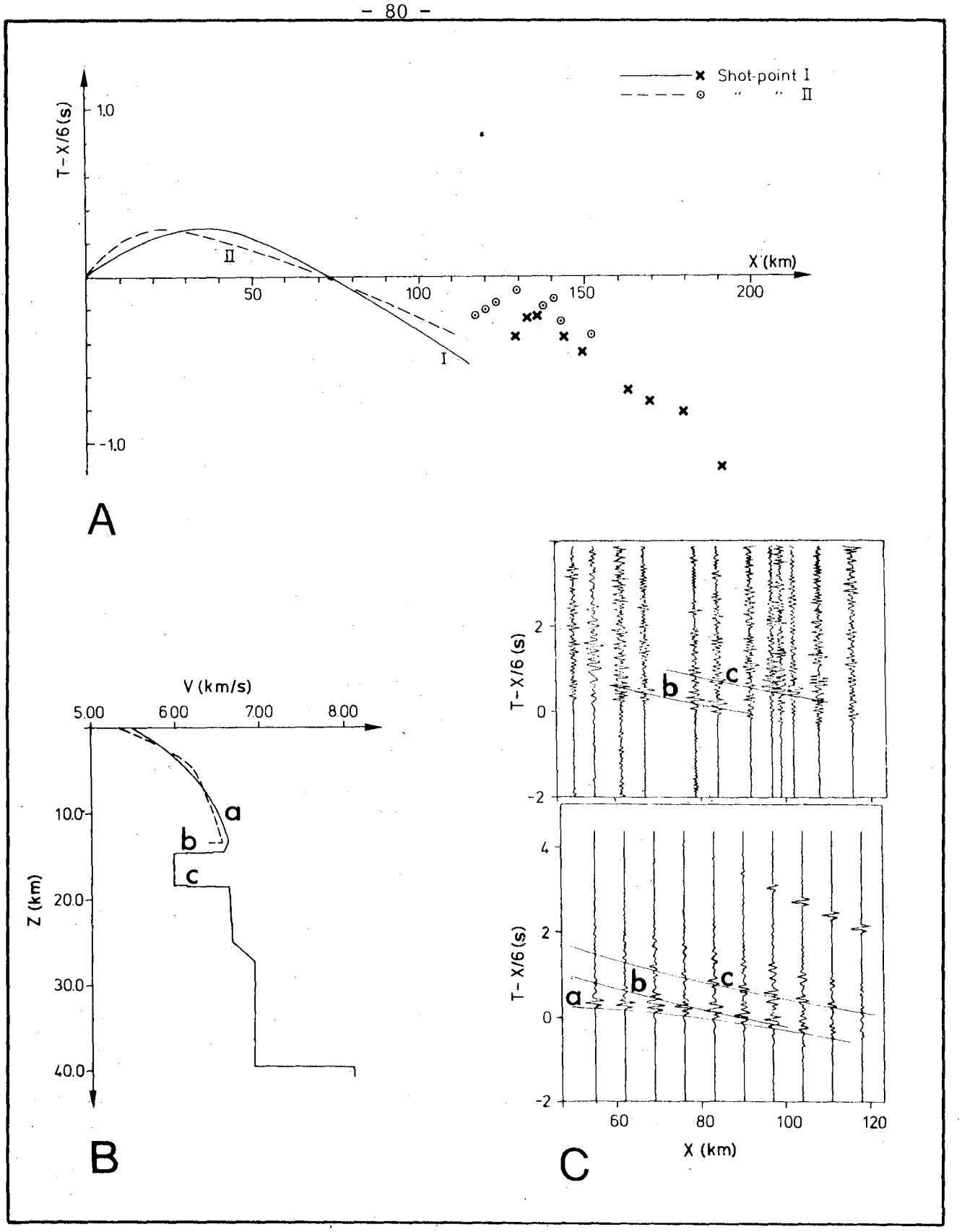

Fig. VI. 5.2 A) First arrival travel times for both shot points. The continuous curves represent a slight smoothing of travel time observations. B) Velocity-depth distribution derived from shot point I data. The dashed curve corresponds to shot point II data. C) Detail of record section (top) for shot point I and corresponding synthetic section (bottom). Selected segments of the travel time curves as computed from Fig. VI.xx.2b are inserted.

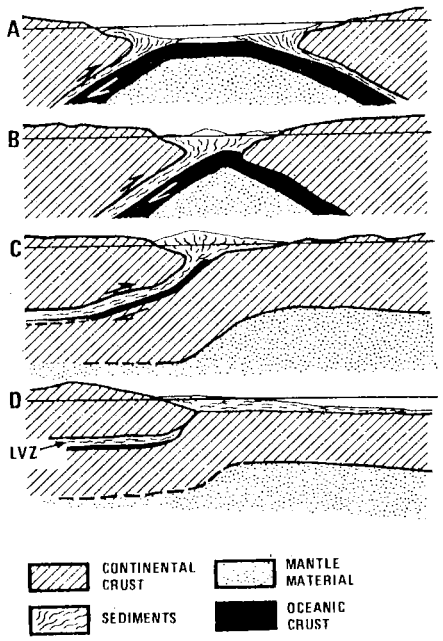

Fig. VI.5.3 Schematic and simplified cross sections of the closing of the Iapetus ocean displayed to illuminate our alternative ii) for explaining the low velocity zone (LVZ) beneath the Møre Gneiss Region. A) Late stage in the closing of the Iapetus ocean. B) Situation before the continents collide, with a westerly dipping subduction zone along which orogenic sediments are dragged down. C) The continental collision resulting in crustal doubling with sediments and remnants of oceanic crust - constituting the hypothesized LVZ - sandwiched between the two crustal blocks. D) From isostatic uplift a westerly Himalayan chain off which the nappes glide to the east.

VI.6 A Microearthquake Survey of the Svalbard Region, Final Results, Phase I

A program for mapping of the seismicity of the Svalbard region was conceived jointly by Norsk Polarinstitutt and NTNF/NORSAR in 1977 as a step by step effort to acquire an improved data base for the seismicity of the area relevant to future evaluation of the related environmental hazard. The objectives of Phase I, the results of which are reported here, were to monitor the frequency of occurrence of microearthquakes and locate the seismic active areas using portable microearthquake instruments operating in the mining settlements between December 1977 and October 1978.

In order to reduce possible biased errors in epicentral locations, crustal models were derived for the Svalbard area. For the continental model we used data from a refraction profiling survey conducted in 1978 by the University of Bergen in cooperation with the University of Hamburg, the Polish Academy of Sciences and the Saint Louis University (M.A. Sellevoll, Bergen, personal communication). We used only data from our stations with travel times as shown in Fig. VI.6.1. The derived model, which explains reasonably well the first arrivals and partly the later ones, has P-velocities of 5.7, 6.7 and 8.2 km/s, with interfaces at 16 and 32 km. For events from the mid-ocean ridge west of Svalbard, a model with a constant P-velocity of 7.5 km/s was derived, based on travel times from teleseismically recorded and located earthquakes.

The Svalbard network has a very good detectability for local events, with most of them coming from the Heer Land earthquake zone. In addition to this zone, a large number of events are recorded from the mid-oceanic ridge west of Svalbard. A total of 1320 events have been analyzed, and of these are about 70% local earthquakes from the Svalbard area. A breakdown of detectability on stations and type of events shows that the three microearthquake stations BBG, PRD and LYR (equipped with Sprengnether MEQ-800 seismographs) are about equal in terms of number of events. Not surprisingly, the WWSSN station KBS is best on teleseismic events, and relatively poor on local events. Epicenters have been estimated for about 75% of the local events, the criterion for locating being that both P- and S-wave readings are available from at least two stations.

Epicenter solutions are presented here in terms of maps in Figs. VI.6.2-3, with data subjected to various precision requirements. In Fig. VI.6.2 the number of locations have been reduced to 339 by requiring at least 3 stations, 4 phases, a 95% error radius of less than 30 km, and a residual Root Mean Square (RMS) level (when calculated) of less than 5.0 seconds. In Fig. VI.6.3 the number of events have been reduced to 241 by the additional requirement that all solutions should involve KBS. It is clear from Figs. VI.6.2-3 that the seismicity in the Svalbard region is dominated by the activity in the Heer Land zone. The size of this zone is only slightly larger than the location uncertainty, so a breakdown of the structure of this zone cannot be obtained from the data at hand. We note from Fig. VI.6.3 that the westernmost epicenters on the map extend out to and beyond the Knipovich Ridge and the Spitsbergen Fracture Zone. Although the location errors remain fairly large, they are certainly not large enough to account for all of the dispersion of the epicenters along the ridge axis.

The complex geologic history of the area around the northern Knipovich Ridge and the Spitsbergen Fracture Zone has probably created large zones of weakness where the present tectonic stress is being released in terms of earthquakes. The most significant factors here are probably (1) the transition from a sheared to a rifted margin with reactivization of old faults, (2) the eastward migration of the spreading axis as late as in early Pliocene, and (3) the unique location of this young spreading center near the passive continental margin north of 77.5^{o}N. With the latter point in mind, we note that this is also the area where the seismicity extends from the rift and more or less continuously into the continental crust. The earthquake activity on the continental shelf north of 77.5^{o}N seems to extend northward to the Yermak Plateau and the northern slope. This feature exhibits some resemblance to what is being observed also further south, i.e., along the Norwegian continental shelf.

The main reason for the present interest in the seismicity of Svalbard has been the Heer Land zone activity. Earthquakes up to m_b 5.5 have been reported from this area, and a recurrence study shows that an m_b 4.2

event occurs roughly every 4 years. A magnitude formula which has been developed for our microearthquake data gives about the same recurrence relationship for the Heer Land earthquakes, and with a b-value of -1.4.

H. Bungum

Y. Kristoffersen, Norsk Polarinstitutt

References

Bungum, H., and Y. Kristoffersen, 1980: A microearthquake survey of the Svalbard region. Final Report, Phase I. NORSAR Technical Rep. No. 1/80, 28 pp.

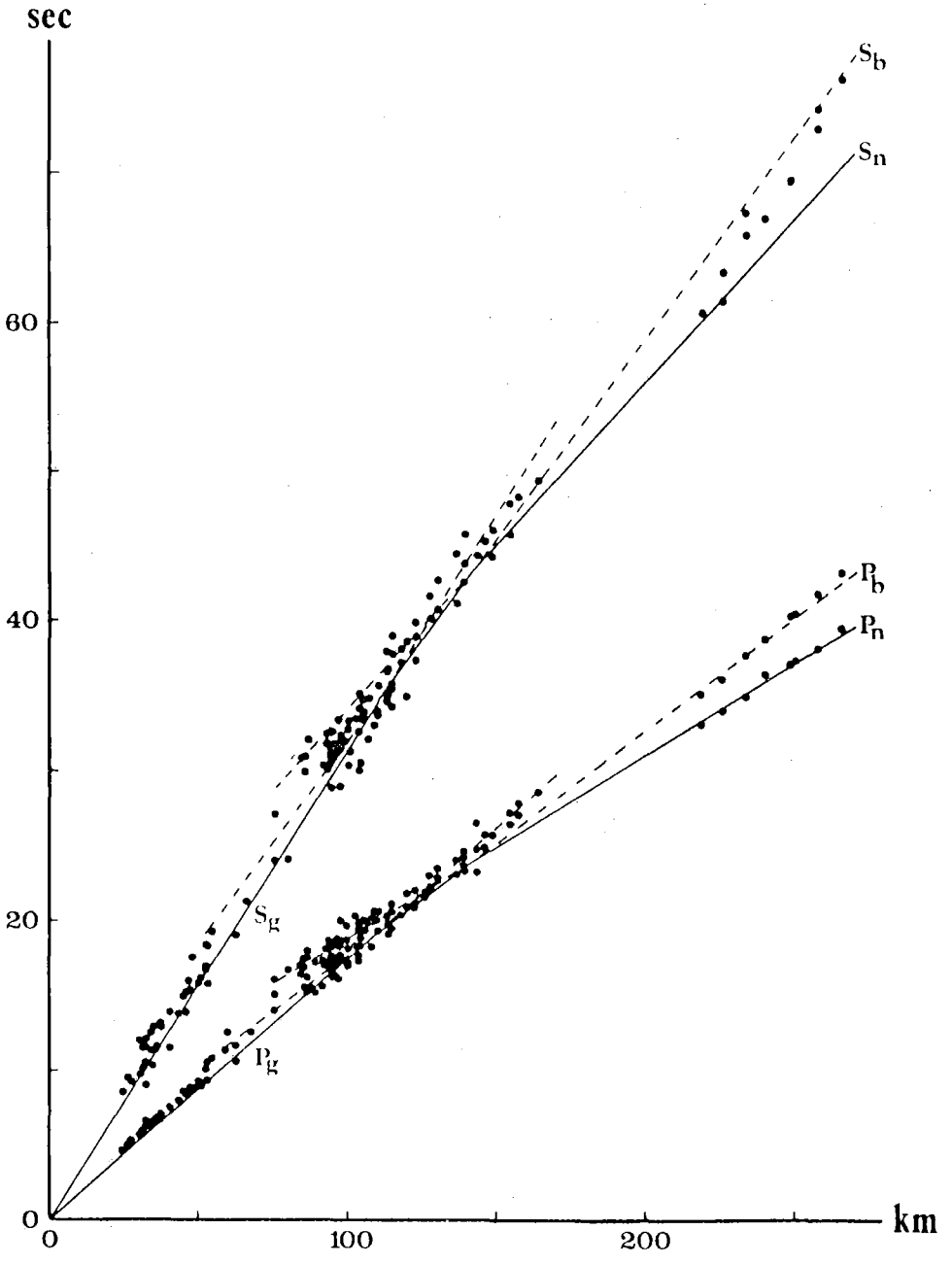

Fig. VI.6.1 Continental travel times for Svalbard, with dots giving travel times (vs distance) for explosions, and straight lines travel times computed from the derived model. Most of the readings are from PRD, some from KBS and a few from SWE.

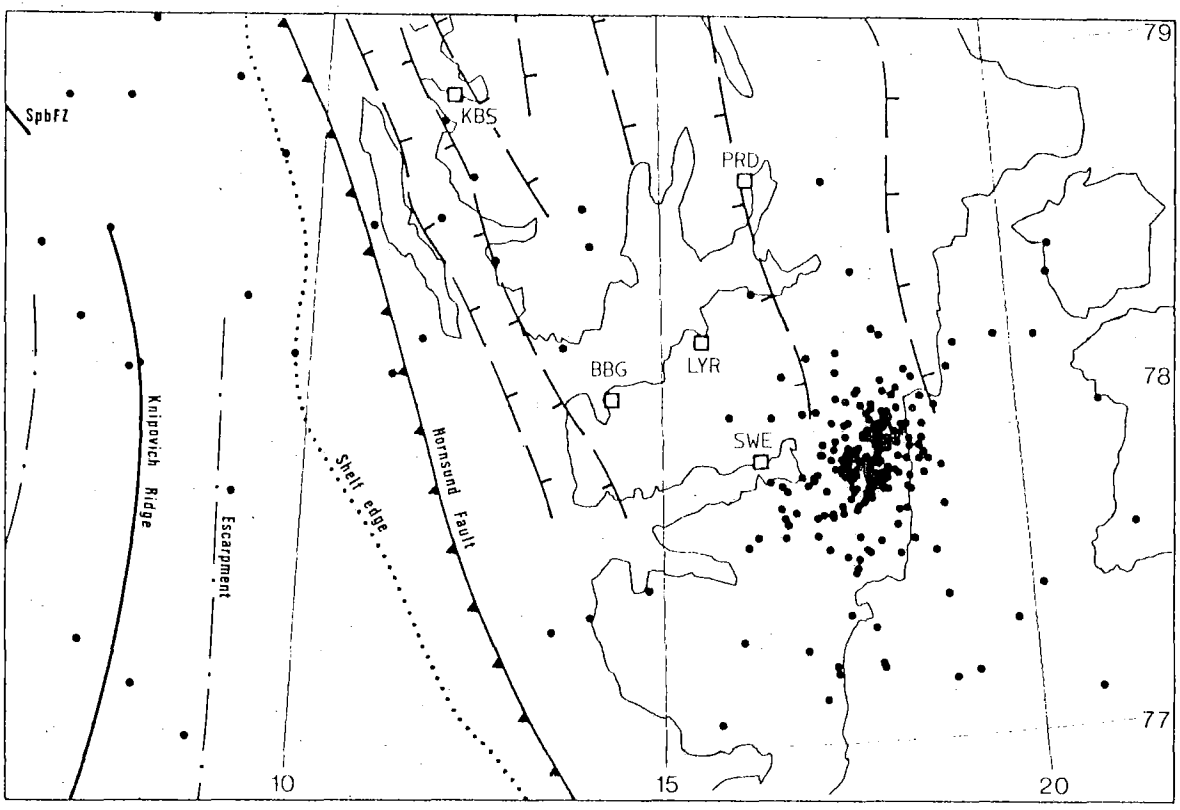

Fig. VI.6.2 Epicentral distribution for earthquakes recorded at 3 stations or more, with a minimum of 4 phases. Each epicentral solution has a 95% error radius of less than 30 km and an RMS error of less than 5.0 sec (if the latter estimate is available). 339 events satisfied these criteria, with 290 inside the area covered by the map. The station locations are shown as squares.

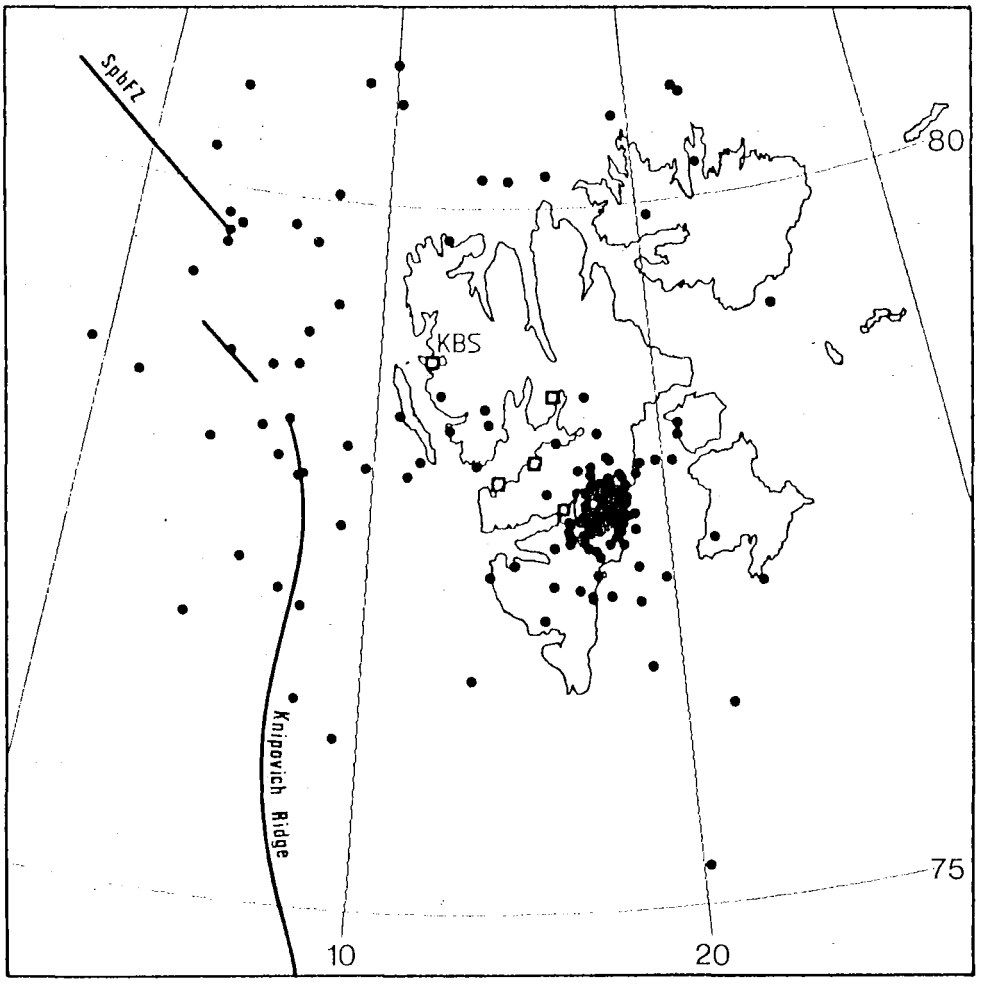

Fig. VI.6.3 Epicentral distribution of earthquakes with acceptance criteria identical to those for Fig. VII.xx.2, but with the additional requirement that station KBS is used in all the solutions. 241 events satisfied these criteria, with 237 inside the area covered by the map.

VI.7 The Seismicity of the Stiegler's Gorge Area, Tanzania

This project has been described and a few results have also been presented in previous Semiannual Technical Summaries. A substantial amount of new data from the Stiegler's Gorge Network (SGSN) has now been analyzed, and a total of 1450 events are now on file covering the time period September 1978 - January 1980. Hypocentral solutions are computed for about 750 of these, while in Fig. VI.7.1 we have reduced this number to 475 by requiring an RMS time residual value less than 0.75 sec, and standard errors (both horizontally and vertically) of less than 5.0 km. Typically, the RMS value is 0.1-0.4 sec and the standard error 1-3 km. We have moreover required that at least 5 P phases and 2 S phases are used in the hypocentral calculations; this requirement is particularly essential for events outside of the array.

It is seen from Fig. VI.7.1 that there is a high concentration of events near the dam site; this is real enough although somewhat exaggerated because of the decreasing sensitivity of the network to detect events as the distance increases. It is also seen that the activity is confined to two major zones, (i) a NW-SE lineation of events near the dam site and not far from a prominent fault system (Tagalala), and (ii) a SW-NE lineation near stations 5 and 6.

A more detailed seismicity map is presented in Fig. VI.7.2, where also two vertical cross-sections are shown, at directions of N30^{o}E and N120^{o}E. It is seen there that the activity near the dam site is concentrated along a plane dipping about 45^{o} to the NE, striking the surface about 10 km SW of the dam with a direction near N120^{o}E. This is in good agreement with focal mechanisms derived from first motion directions, showing that normal faulting takes place along the plane defined above, with extensional movements in the east-west direction. This is moreover consistent with what we know about the regional tectonics in the area (the east African rift zone).

A problem of great importance for the interpretation of these measurements is the establishment of a reliable magnitude scale for the local earthquakes.

In this case we have developed a scale based on signal duration, and applicable to local as well as regional earthquakes. Only one Stiegler's Gorge earthquake recorded at SGSN has so far been recorded elsewhere, this quake (from 9 June 1979) has been set at a magnitude of 4.2, and the scale has moreover been calibrated against some regional events (distances 11^{o}-19^{o}) recorded at SGSN. The formula reads

$$M = -1.0 + 1.8 \log \tau + 0.1(\log \tau)^2 + 0.002 \cdot \Delta$$

where τ is signal duration in sec (measured from analog recordings) and Δ is epicentral distance in km. This has given a recurrence relationship for Stiegler's Gorge earthquakes as shown in Fig. VI.7.3, where it is seen that the second largest earthquake has a magnitude of 3.1. It is therefore fair to say that the large number of events shown in Fig. VI.7.2 first of all is a result of the high sensitivity of the instruments used, and that the sizes of the earthquakes have so far been quite moderate.

H. Bungum

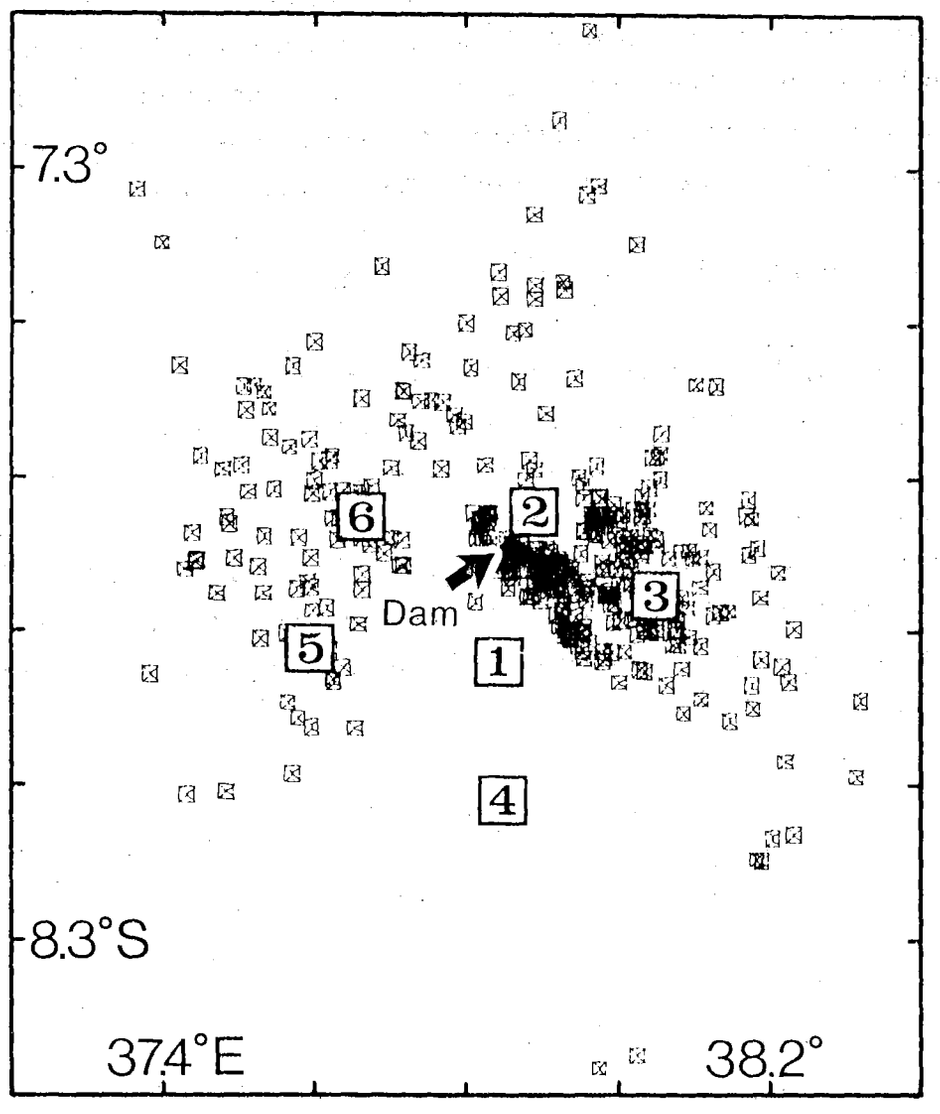

Fig. VI.7.1 Precisely located earthquakes in the Stiegler's Gorge area between 14 Sep 1978 and 16 Jan 1980. The locations of the seismic stations (SGSN) are given as boxed numbers.

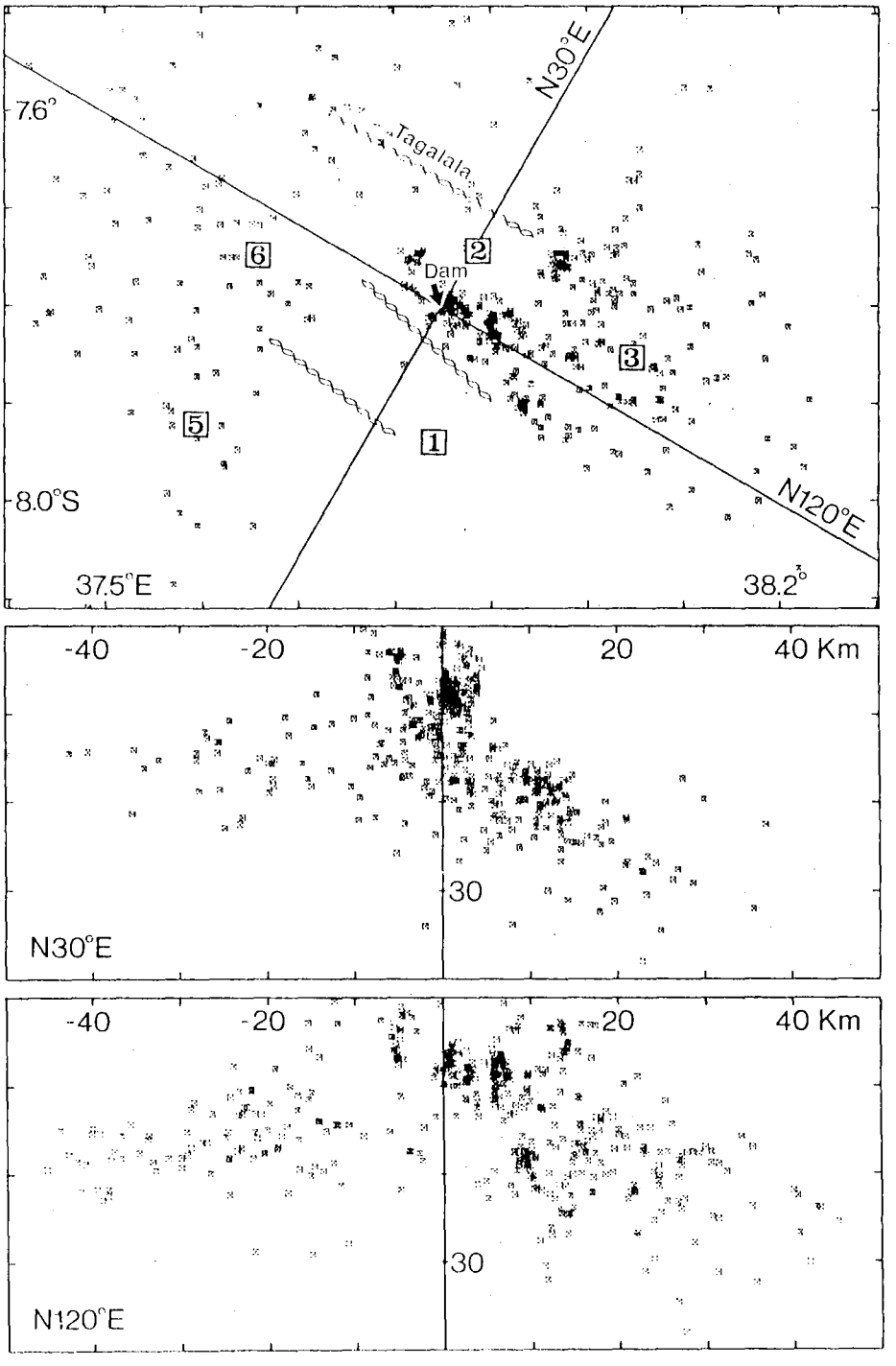

Fig. VI.7.2 Earthquakes in the Stiegler's Gorge area between 14 Sep 1978 and 16 Jan 1980. The epicenter distribution at the top is a blowup of what is shown in Fig. VI.7.1, with additional indication of the three most prominent faults in the area including Tagalala. Below are given two vertical cross-sections, centered at the dam site and along the directions N30°E and N120°E, respectively. The cross-sections extend 100 km across and 40 km in depth, and very few of the more precisely located earthquakes are found outside the volume covered by this figure.

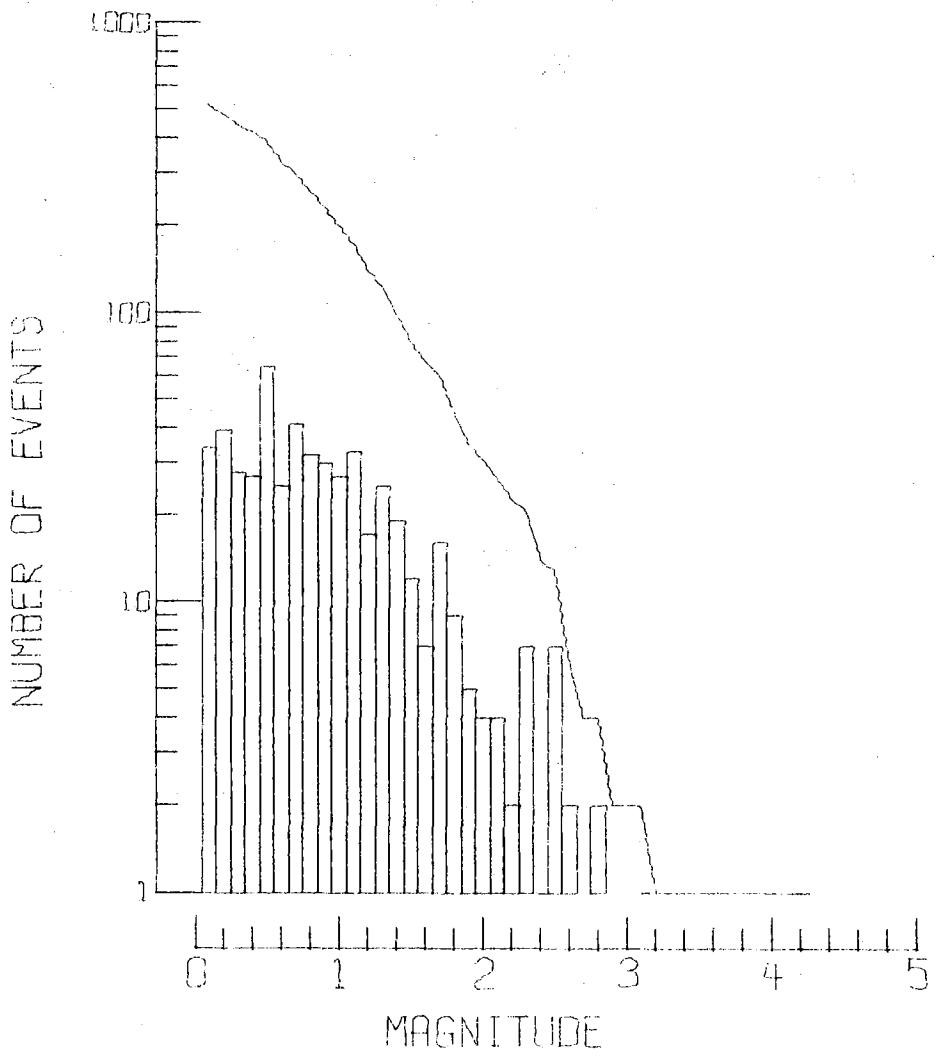

Fig. VI.7.3 Frequency-magnitude distribution for local earthquakes recorded by SGSN. Corresponding epicenter locations are given in Fig. VI.7.1.

VI.8 Earthquake Spectrum Scaling Law - Source Parameters for the Melφy Earthquakes

The prime motivation for deployment and operation of regional seismic networks is that of detecting and locating small events which otherwise are very seldom reported by stations in the teleseismic distance range. The design of such networks in terms of sampling frequency and station spacing is critically dependent on the 'expected' source spectra for the events in question, say, in the M_L magnitude range 0-3. Surprisingly, adequate spectral data here are available for very few areas, notably California and Japan (Aki & Chouet, 1975), while to our knowledge hardly any from typical shield areas like Fennoscandia and Western Russia. The reason for this appears to be a lack of digital, high-frequency recording capabilities and/or that the standard analog recording equipment used have not been suitable for subsequent digitalization.

During the height of the Melφy, N. Norway, microearthquake activity in November/December 1978 (Bungum et al, 1979; Bungum and Husebye, 1979), the Seismological Observatory, University of Bergen, deployed in short time intervals a set of 3 seismometers (3-comp.) having a flat response in the 5-100 Hz frequency range (Vaage, 1980). The data were recorded on analog tape and subsequently digitized at a 500 mHz sampling rate. Preliminary results from studies relevant to source spectra and its scaling with magnitude (or moment) are depicted in Fig. VI.8.1. The seismic moment corresponds to the zero frequency value of the source-displacement spectrum (Bakun and Lindh, 1977)

$$M_\omega = 4\pi \rho R \beta^3 P_s^{-1} R_s^{-1} \Omega(s) \qquad \text{(VI.8.1)}$$

where ρ = density, R = hypocentral distance, β = shear wave velocity, P_s = path correction (involving Q among other factors), R_s = radian pattern coefficient, and $\Omega(s)$ = S-wave displacement spectrum. For the Melφy earthquakes the hypocentral distance R is near 10 km, and with proper assumptions for the rest of the coefficients, we find seismic moment values in the range 10^{18} to 10^{20} dyne-cm. By comparing with local magnitudes in the range 0-2 M_L units calculated from signal duration we find the following M_0/M_L relationship (see Fig. VI.8.2):

$$\log M_0 = 18.7 + 0.85\, M_L \qquad \text{(VI.8.2)}$$

which implies a larger a-value (18.7) and a smaller b-value (0.85) than what is observed at least from California (Suteau and Whitcomb, 1979).

Now, assuming a simple circular source, we can calculate source radius (r), stress drop ($\Delta\sigma$) and average displacement ($\bar{u}$) from the following relationships (Hanks and Wyss, 1972; Brune, 1970, 1971)

$$r(S) = \frac{2.34\beta}{2\pi f_c} \qquad \text{(VI.8.3)}$$

$$\Delta\sigma = \frac{7}{16} \cdot \frac{M_0}{r^3} \qquad \text{(VI.8.4)}$$

$$\bar{u} = \frac{M_0}{\pi r^2 \cdot \mu}$$

where μ = shear modulus and f_c = corner frequency.

The critical parameter is clearly the corner frequency f_c, to be obtained from the set of displacement spectra in Fig. VI.8.1. The most probable interpretation of those curves leads to the following (i) corner frequencies are very high, probably in the range 18-30 Hz, (ii) the corner frequency rolloff is very steep, i.e., the frequencies increase only slightly with decreasing moment, and below 10^{19} dyne-cm the curve is almost vertical. Using the above formulae, with appropriate parameters, we find source parameters as given in Table VI.8.1. We see there that the largest events (for which spectra are estimated) have a source radius of about 70 m, a stress drop of about 100 bars, and an average displacement across the fault of about 1.2 cm. These numbers look reasonable for events this size, while a stress drop of 100 bars is typically observed for intraplate areas (Kanamori and Anderson, 1975; Richardson and Solomon, 1977). It is important to note here, however, that in order to keep

M_0 (dyne-cm)	M_L	f_c (Hz)	r(s) (m)	$\Delta\sigma$ (bars)	$\bar{u}$ (cm)
10^{20}	1.5	19	68	99	1.2
10^{19}	0.4	26	50	28	0.3
10^{18}	-0.8	31	42	5	0.04

Table VI.8.1

Relations between seismic moment (M_0), local magnitude (M_L), corner frequency (f_c), source radius (r), stress drop ($\Delta\sigma$) and average displacement (u) for the Melϕy earthquakes.

the stress drop within reasonable limits for larger events, it is necessary that the rolloff of the corner frequency curve approaches a ω^{-3} relationship as the moment values go above 10^{20} dyne-cm. Even though the largest Melϕy event recorded on tape had a magnitude of about 2.0, the largest one in the sequence had an M_L value of 3.2, corresponding to a seismic moment $M_0 = 2.6 \times 10^{21}$ dyne-cm. The stress drop for that event would then be in the range 100-250 bars if we assumed a corner frequency in the range 6-8 Hz.

In conclusion, we have found for the Melϕy earthquakes that (i) the M_0/M_L relationship has a lower slope than usually observed, (ii) for events in the moment range 10^{18}-10^{20} dyne-cm corner frequencies are in the range 20-30 Hz, (iii) for a seismic moment of about 10^{20} dyne-cm (corresponding to $M_L = 1.5$) we have calculated a source radius of about 70 m, a stress drop of about 100 bars, and an average displacement of about 1.2 cm, (iv) for decreasing magnitudes, the corner frequency curve falls off steeply, implying decreasing stress drops.

H. Bungum
S. Vaage, University of Bergen
E.S. Husebye

References

Aki, K., and B. Chouet, 1975: Origin of coda waves: Source, attenuation and scattering effects, J. Geophys. Res., 80, 3322-3342.

Bakun, W.H., and A.G. Lindh, 1977: Local magnitudes, seismic moments and coda durations for earthquakes near Oroville, California. Bull. Seism. Soc. Amer., 67, 615-630.

Brune, J.N., 1970: Tectonic stress and the spectra of seismic shear waves from earthquakes, J. Geophys. Res., 75, 4997-5009.

Brune, J.N., 1971: Correction, J. Geophys. Res., 76, 5002.

Bungum, H., B.K. Hokland, E.S. Husebye and F. Ringdal, 1979: An exceptional intraplate earthquake sequence in Melφy, Northern Norway, Nature, 280, 32-35.

Bungum, H., and E.S. Husebye, 1979: The Melφy, northern Norway, earthquake sequence - a unique intraplate phenomenon, Nor. Geol. Tidsskr., 59, 189-193.

Hanks, T.C., and M. Wyss, 1972: The use of body-wave spectra in the determination of seismic-source parameters, Bull. Seism. Soc. Amer., 62, 561-589.

Kanamori, H., and D.L. Anderson, 1975: Theoretical basis for some empirical relations in seismology, Bull. Seism. Soc. Amer., 65, 1073-1095.

Richardson, R.M., and S.C Solomon, 1977: Apparent stress and stress drop for intraplate earthquakes and tectonic stress in the plates, Pure and Appl. Geophys., 115, 317-331.

Suteau, A.M., and J.H. Whitcomb, 1979: A local earthquake coda magnitude and its relation to duration, moment M_0, and local Richter magnitude M_L, Bull. Seism. Soc. Amer., 69, 353-368.

Vaage, S., 1980: Seismic evidence on complex tectonics in the Melφy earthquake area, Nor. Geol. Tidsskr., in press.

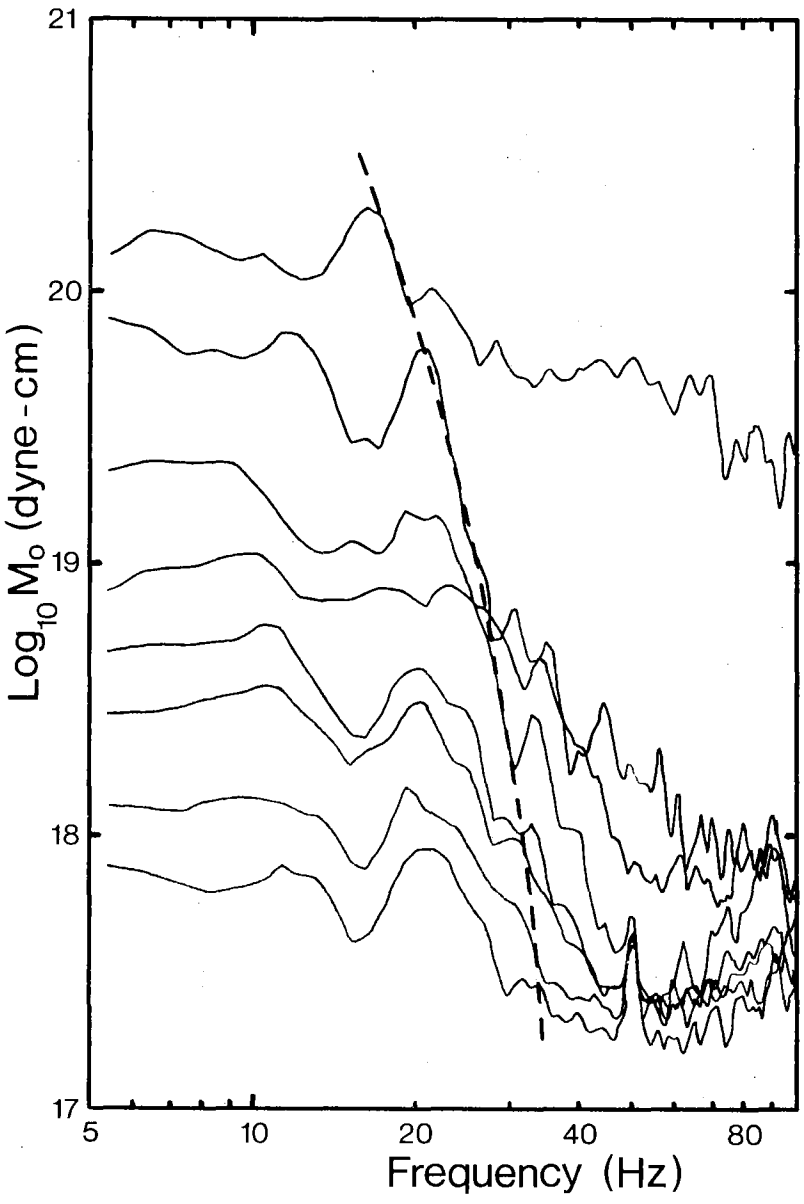

Fig. VI.8.1 S-wave displacement spectra for the Melφy earthquakes. The spectra are scaled with respect to seismic moment (M_0), and each curve represents data from 5 events in average (altogether 40 events). The dashed line indicates the corner-frequency curve.

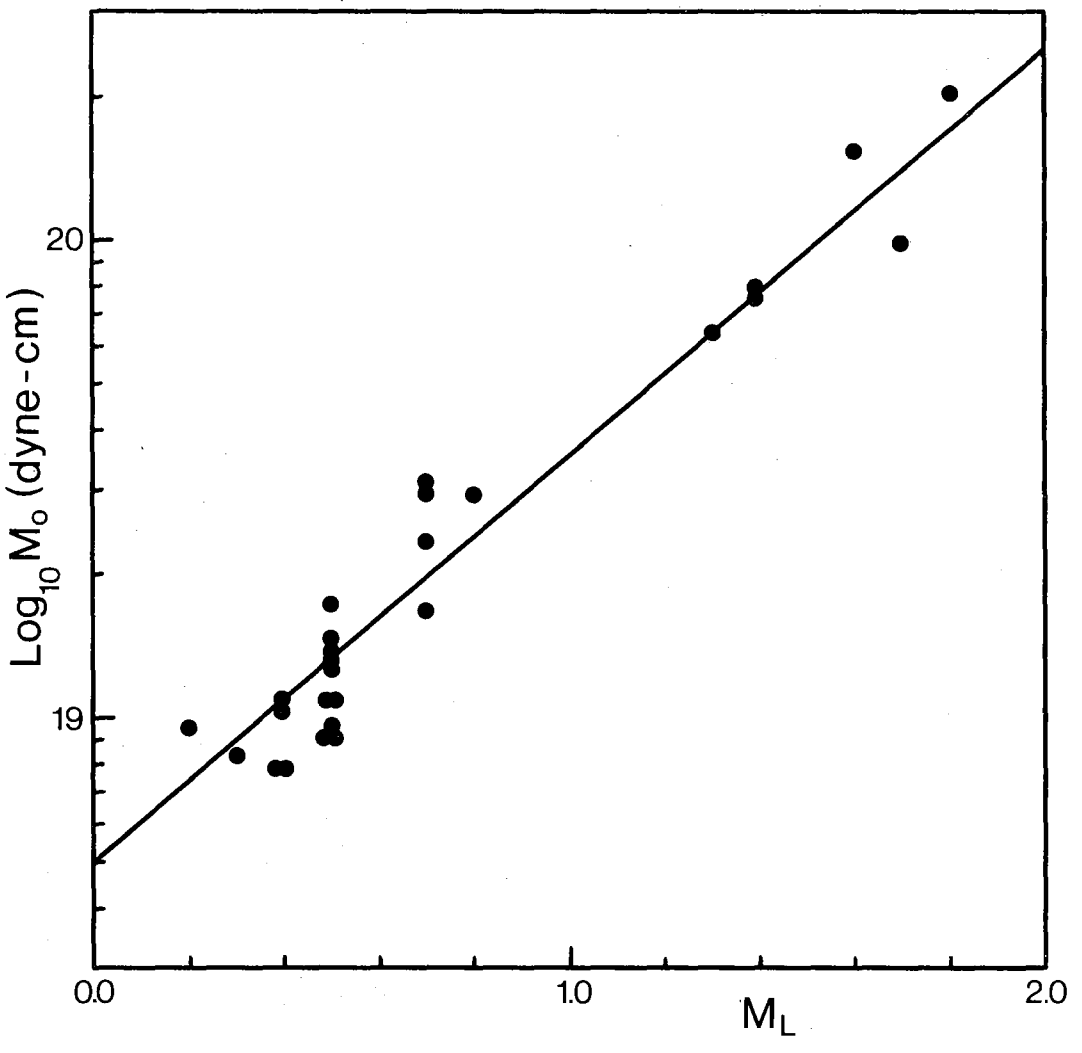

Fig. VI.8.2 M_0/M_L relationship for the Melϕy earthquakes. The straight line is fitted by eye and satisfies the equation $\log M_0 = 18.7 + 0.85\ M_L$.